PREDICTED DYNAMIC PERFORMANCE OF A POSSIBLE AC LINK BETWEEN SASKPOWER NORTH AND SOUTH SYSTEMS

A Thesis

Submitted to the College of Graduate Studies and Research

in Partial Fulfillment of the Requirements

For the Degree of Master of Science

in the Department of Electrical and Computer Engineering

University of Saskatchewan

Saskatoon, Saskatchewan

By

Qi Zhao

PERMISSION TO USE

I agree that the Library, University of Saskatchewan, may make this thesis freely available for inspection. I further agree that permission for copying of this thesis for scholarly purpose may be granted by the professor or professors who supervised the thesis work recorded herein or, in their absence, by the Head of the Department or the Dean of the College in which the thesis work was done. It is understood that due recognition will be given to me and to the University of Saskatchewan in any use of the material in this thesis. Copying or publication or any other use of this thesis for financial gain without approval by the University of Saskatchewan and my written permission is prohibited.

Request for permission to copy or to make any other use of the material in this thesis in whole or part should be addressed to:

Head of the Department of Electrical and Computer Engineering
University of Saskatchewan
57 Campus Drive
Saskatoon, Saskatchewan S7N 5A9
Canada

ABSTRACT

SaskPower has two separate systems, namely the North and the South systems. The South system contains SaskPower major generation and system load. The North system load is located relatively far from its generation (200 to 300 km). The North system is considered, therefore, to be electrically weaker than the South system. Recently there has been an interest in connecting the two systems to improve the security, stability and reliability of the integrated system. Grid interconnections, however, especially between weak and strong systems, often result in the arising of low-frequency oscillations between the newly connected areas. These oscillations that are termed "inter-area oscillations" exhibit, generally poor damping and can severely restrict system operations by requiring the curtailment of electric power transfers level as an operational measure.

There are two options for SaskPower North and South systems interconnection, namely HVAC and HVDC interconnections (tie-lines). This thesis reports the results of digital time-domain simulation studies carried out to investigate the dynamic performance of a proposed 260 km, 138 kV double-circuit HVAC tie-line incorporating a hybrid three-phase Thyristor-Controlled Series Capacitor (TCSC) compensation scheme that would connect the SaskPower North and South systems. The potential problems that might arise due to such an interconnection, namely power flow control and low-frequency oscillations are studied and quantified and a feasible solution is proposed. In this context, the effectiveness of the TCSC compensation scheme in damping power system oscillations in the tie-line is investigated.

Time-domain simulations were conducted on the benchmark model using the ElectroMagnetic Transients Program (EMTP-RV). The results of the investigations demonstrate that the proposed HVAC link that incorporates a TCSC compensation scheme is effective in mitigating the low-frequency oscillations between the North and South systems for different system contingencies and operating conditions.

ACKNOWLEDGEMENTS

My sincerest gratitude would be expressed to my supervisor, Dr. Sherif O. Faried, for providing me the opportunity to be his master student. In the process of doing my research and the preparation of this thesis, I really appreciate his continuous encouragement, his patience and efforts. Without his help and concern on my research, I would never complete this thesis so smoothly.

I would like to acknowledge Dr. U. Karaagac and Dr. D. Rai for their valuable advice and support during the research. I am also pleased to thank all the professors from the Department of Electrical and Computer Engineering who supervised my courses. I appreciate the Advisory Committee members.

I also appreciate my fellow graduate student, Mr. Linh Pham. Many thanks go to Mr. Linh Pham's helpful suggestions and encouragement during doing the research as a group, so that we can finally accomplish the research project.

Last but not least, I would express my endless gratitude to my parents, Mr. Yongqing Zhao, and Mrs. Cuidi Zhou. They are always standing by my side, and supporting me with selfless help whenever I need them.

TABLE OF CONTENTS

LIST OF FIGURES

LIST OF TABLES

LIST OF SYMBOLS

A	Blade sweep area (m^2)
C	Capacitor in the transmission line
C_f	Wind turbine blade design constant
C_p	Power coefficient of the blade
C_{TCSC}	Fixed capacitor of TCSC
C_s	Capacitor of the RC snubber circuit
d	Direct axis
E_{fd}	Exciter output voltage
E_R	Output voltage of the voltage regulator amplifier
E_{ref}	Reference voltage of the excitation system
E_{SB}	Feedback stabilizing signal of the excitation system
Fixed C	Interconnected transmission lines are series capacitor compensated
e_d, e_q	d- and q- axis stator voltages
e_{fd}	Field voltage
$G_{\delta N5S4}(s)$	Transfer function of a phase-compensation type TCSC supplemental controller with the stabilizing signal of δ_{N5S4}
$G_{\delta N5S6}(s)$	Transfer function of a phase-compensation type TCSC supplemental controller with the stabilizing signal of δ_{N5S6}
H	Inertia constant
i_d, i_q	d- and q- axis stator currents
i_{fd}	Field winding current
i_{1d},	d-axis damper winding current
i_{1q}, i_{2q}	q-axis damper winding currents
IMG	Imaginary part of a complex number
k	Degree of compensation
K_A	Gain of the voltage regulator amplifier
K_E	Exciter gain
K_{FE}	Feedback stabilizing loop gain of the excitation system

K_G	Supplemental controller gain
K_P	Proportional controller gain
K_I	Integral controller gain
L_{TCSC}	Fixed inductor of TCSC
L_{ad}	d-axis magnetizing inductance
L_{aq}	q-axis magnetizing inductance
L_d, L_q	d- and q-axis synchronous inductances
L_{ffd}	self-inductance of the field winding
L_{11d}	self-inductance of the d-axis damper winding
L_{11q}, L_{22q}	self-inductances of the q-axis damper winding
P	Real power
PI	Proportional integral
$P_{Line\ N6\text{-}S7}$	Real power flow in transmission line N_6S_7
$P_{Line\ S2\text{-}S3}$	Real power flow in transmission line S_2S_3
$P_{Line\ S4\text{-}S5}$	Real power flow in transmission line S_4S_5
$P_{Line\ S5\text{-}S3}$	Real power flow in transmission line S_5S_3
$P_{Line\ S7\text{-}S6}$	Real power flow in transmission line S_7S_6
$P_{Tie\text{-}Line}$	Real power flow in the interconnected tie-line
P_m	Mechanical power
Q	Reactive power
q	Quadrature axis
R	Blade length
R_L	Resistance of the series capacitor compensated transmission line
R_a	Armature resistance
R_{fd}	Field winding resistance
R_{1d}	d-axis damper winding resistance
R_{1q}, R_{2q}	q-axis damper winding resistances
r_s	Resistance of the RC snubber circuit
s	Laplace transformation operator
T	Superscript to denote matrix transpose
T_F	Forward thyristor
T_R	Reverse thyristor
T_A, T_E, T_{FE}	Time constants in the excitation system

T_e	Electromagnetic torque
T_m	Supplemental controller low-pass filter time constant
T_{MECH}	Mechanical torque
T_1, T_2, T_3, T_4	lead-lag network time constants
T_w	Washout filter time constant
V_b	Infinite-bus Voltage
V_C	Voltage across the series capacitor of the compensated transmission line
V_L	Voltage across the inductance of the series capacitor compensated transmission line
V_R	Voltage across the resistance of the series capacitor compensated transmission line
V_{RE}	Receiving end voltage
V_{SE}	Sending end voltage
$V_{N1}, V_{N2}, V_{N3}, V_{N4}, V_{N5}$ *and* V_{N6}	System bus voltages of the North System
$V_{S1}, V_{S2}, V_{S3}, V_{S4}, V_{S5}, V_{S6}$ *and* V_{S7}	System bus voltages of the South System
V_t	Generator terminal voltage
V_{td}, V_{tq}	d- and q- axis generator terminal voltages
X_C	Series capacitor reactance
X_L	Inductive reactance of the series capacitor compensated transmission line
X_{-max}, X_{-min}	Maximum and minimum TCSC reactances respectively
X_{order}	Dynamic reactance of TCSC
X_{TCSCo}	Initial net reactance of TCSC
α	Thyristor firing angle
Ψ_d, Ψ_q	d- and q- axis stator flux linkages
Ψ_{fd}	Field winding flux linkage
Ψ_{1d}	d-axis damper winding flux linkage
Ψ_{1q}, Ψ_{2q}	q-axis damper winding flux linkages
δ	Generator power (load) angle
δ_{N5S4}	Generator S_4 load angle measured with respect to generator N_5 load angle
δ_{N5S6}	Generator S_6 load angle measured with respect to generator N_5 load angle

λ	Wind turbine blade tip speed ratio
λ_s, λ_r	Stator and rotor side flux linkages
λ_{qm}, λ_{dm}	q-axis and d-axis magnetizing flux linkages
ω	Angular velocity
ω_m	Mechanical angular velocity (rad/s)
ω_0 (f_0)	Synchronous frequency (377 rad/sec)
ω_{S2N5}	Generator S_2 speed measured with respect to generator N_5 speed
ω_{S4N5}	Generator S_4 speed measured with respect to generator N_5 speed
ω_{S6N5}	Generator S_6 speed measured with respect to generator N_5 speed

LIST OF ABBREVIATIONS AND ACRONYMS

BtB	Back-to-Back
CFAD	Constant Firing Angle Delay
DFIG	Doubly Fed Induction Generator
FACTS	Flexible AC Transmission Systems
GSC	Grid Side Converter
HVDC	High Voltage Direct Current
MPT	Maximum Power Tracking
POD	Power Oscillations Damping
RSC	Rotor Side Converter
SSR	Subsynchronous Resonance
SVR	Synchronous Voltage Reversal
TCSC	Thyristor Controlled Series Capacitor
VSC	Voltage-Sourced Converter

Chapter 1

INTRODUCTION

1.1 General

SaskPower has two separate systems, namely the North and the South systems. The South system contains SaskPower major generation and system load. Recently, there has been an interest in connecting the two systems to improve the security, stability and reliability of the integrated system. The benefits of grid interconnections are conclusive [1]. Some of the major technical benefits, many of which have economic impacts are:

- Improving power system reliability through sharing reserved generating capacity within an interconnected network. Grid interconnections also allow the coordination of planned outages of the generating units and transmission facilities for maintenance such that the overall cost is optimized. This has a direct positive impact on power system reliability.
- Reducing investment in adding new generating capacity since individual systems would be able to share their generating resources.
- Improving the load factor through the diversity of system loads with different daily or seasonal patterns that complement their own.

Grid interconnections, however, often result in the rise of low-frequency oscillations between the newly connected areas. These oscillations that are termed "inter-area oscillations" generally exhibit poor damping [2]. Inter-area oscillations can severely restrict system operations by requiring the curtailment of electric power transfer levels as an operational measure. These oscillations can also lead to widespread system disturbances, e.g., cascading outages of transmission lines and, therefore, system-wide voltage collapse. Figure 1.1 illustrates the real power flow through an interconnection (tie-line) between two large systems during and

after clearing a three-cycle, three-phase fault on a system bus. As it can be seen from this figure, the damping of the tie-line power oscillations is low and results in system instability.

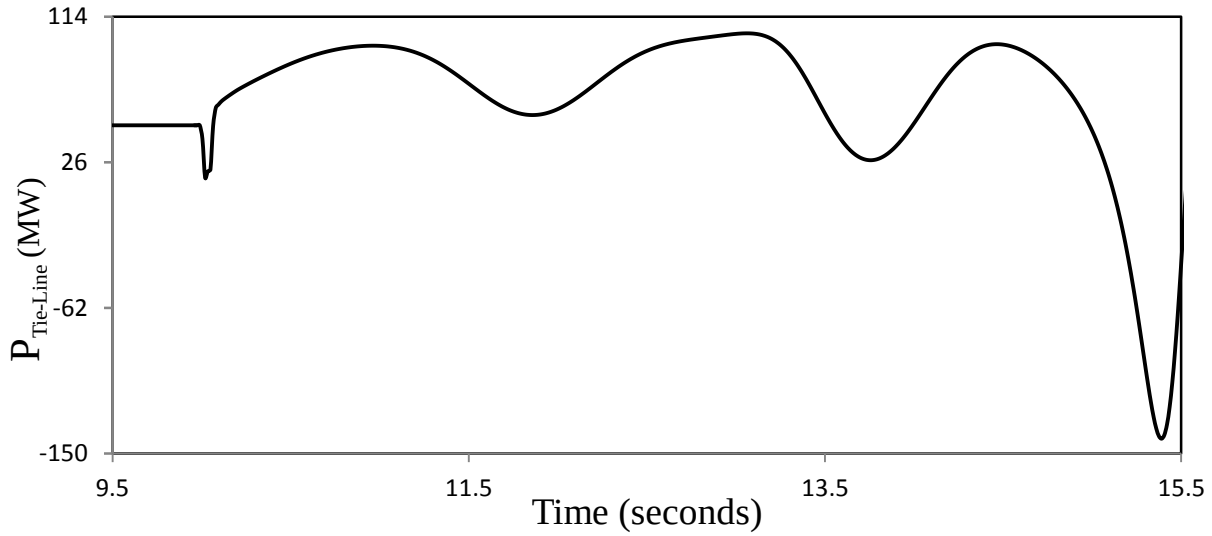

Figure 1.1: A tie-line real power flow during and after clearing a three-cycle, three-phase fault on a system bus.

1.2 SaskPower North and South Systems

Figure 1.2 shows a simple schematic diagram of the SaskPower North and South systems. The North system which is connected to the Manitoba grid by a tie-line for the purpose of power exchange has two hydro generating stations located near Uranium City and Churchill River. The load in the North system is located relatively far from its generation (200 to 300 km). The South system which contains the SaskPower major generation and system load is connected to the Manitoba, Alberta and North Dakota grids by an AC tie-line, a DC back-to-back link and an AC tie-line respectively. The North system is, therefore, considered to be electrically weak compared to the South system.

An interconnection (tie-line) between the SaskPower North and South systems, which would be about 260 km long, could be either a High Voltage Alternating Current (HVAC) or a High Voltage Direct Current (HVDC) interconnection. Each option has its own advantages and disadvantages. An introduction to each option and a comparison between them are presented in the following two sections.

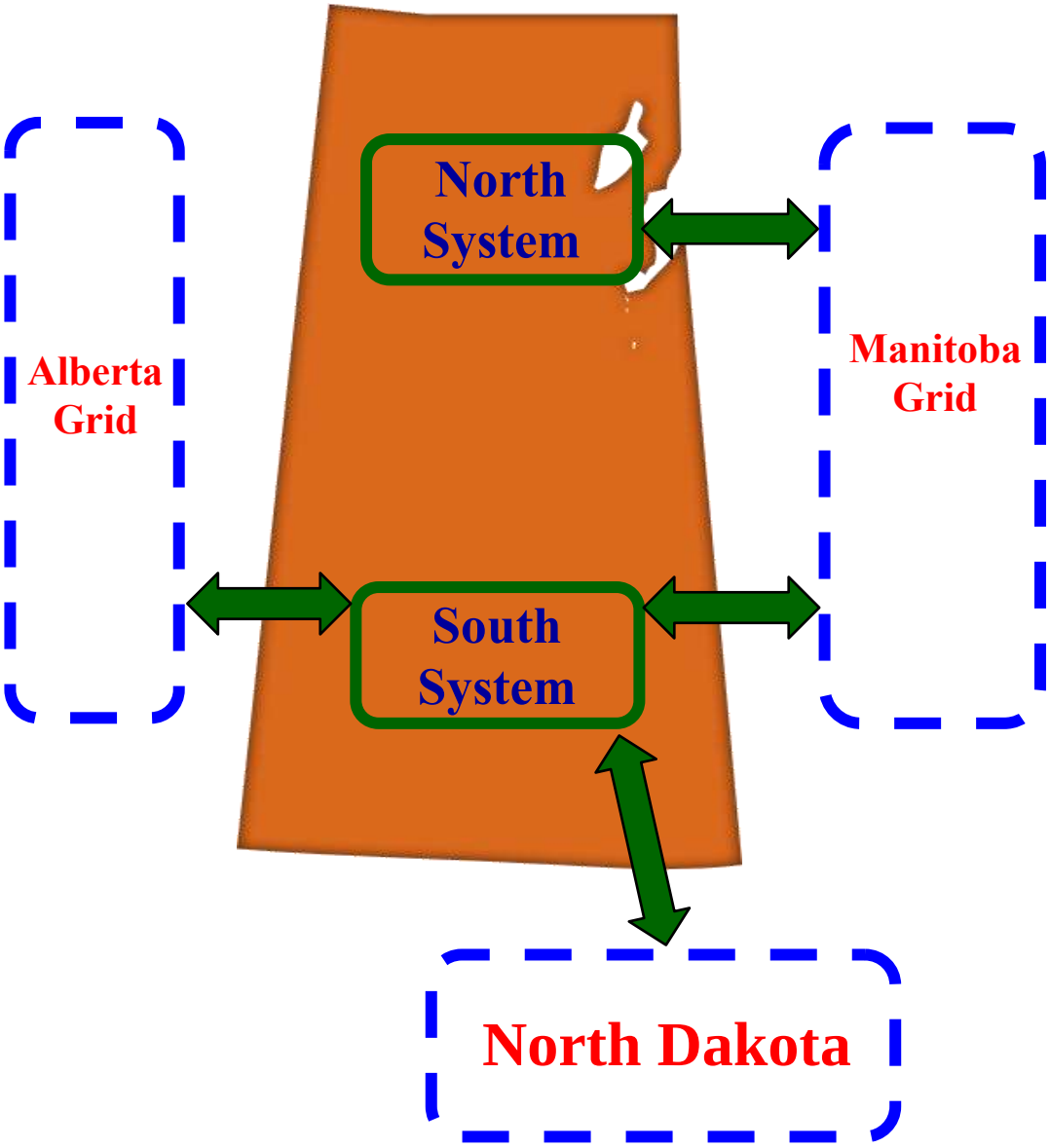

Figure 1.2: SaskPower North and South systems (the two-directional arrows represent power import/export from/to the neighbouring systems).

1.3 Voltage-Sourced Converter HVDC Interconnection

The Voltage-Sourced Converter (VSC) HVDC is a recent HVDC technology that has been installed and operated successfully in many countries around the world. The VSC HVDC technology is designed to transmit power overhead, underground and under water over long distances. This technology extends the economical power range of HVDC transmission down to just a few tens of Megawatts (MW) [3]. In the upper range, the technology now reaches 1,800

MW and ±500 kV [3]. New applications of VSC HVDC include large onshore and offshore wind farm connections, supply to urban load centers and connections to remote "weak" AC systems. The world's first VSC HVDC installation was the Hällsjön project in central Sweden commissioned in March, 1997 [4].

The VSC HVDC consists of two VSCs, one of which operates as a rectifier while the other operates as an inverter. The two converters are connected either back-to-back or joined by a DC cable or a transmission line, depending on the application. The main function of a VSC HVDC link is to transmit a constant DC power from the rectifier station to the inverter station, with high controllability. A simplified diagram of a VSC HVDC transmission system is shown in Figure 1.3 [5]. For transmitting power in the order of 50 to 75 MW between SaskPower North and South systems, a ±110 kV, 260 km VSC HVDC could be used as shown in Figure 1.4.

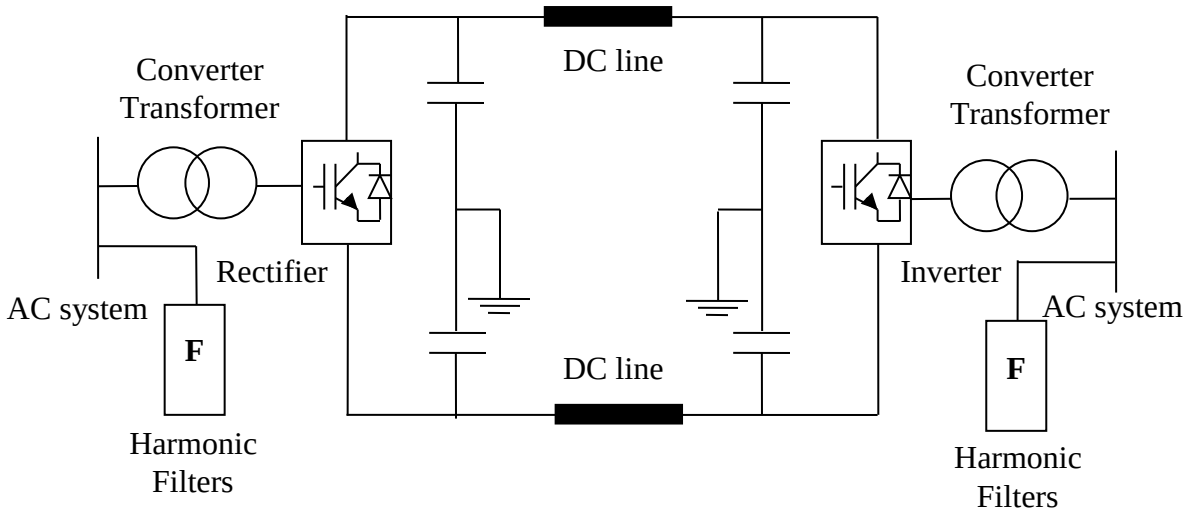

Figure 1.3: A simplified diagram of a VSC HVDC system.

The VSC HVDC has several essential advantages compared to the conventional Current Commutated Converter HVDC (based on thyristors) [6]. They are [7]:

1. Independent control of the active and reactive power output from each terminal.
2. Reduced requirements for harmonic filters.
3. Improvements of the power quality and system stability.
4. Elimination of the requirement for local power generation at the receiving end (inverter terminal).

These features make the VSC HVDC attractive for connection of a weak ac system, island networks, and renewable energy sources, which may be located in remote areas, to a main grid.

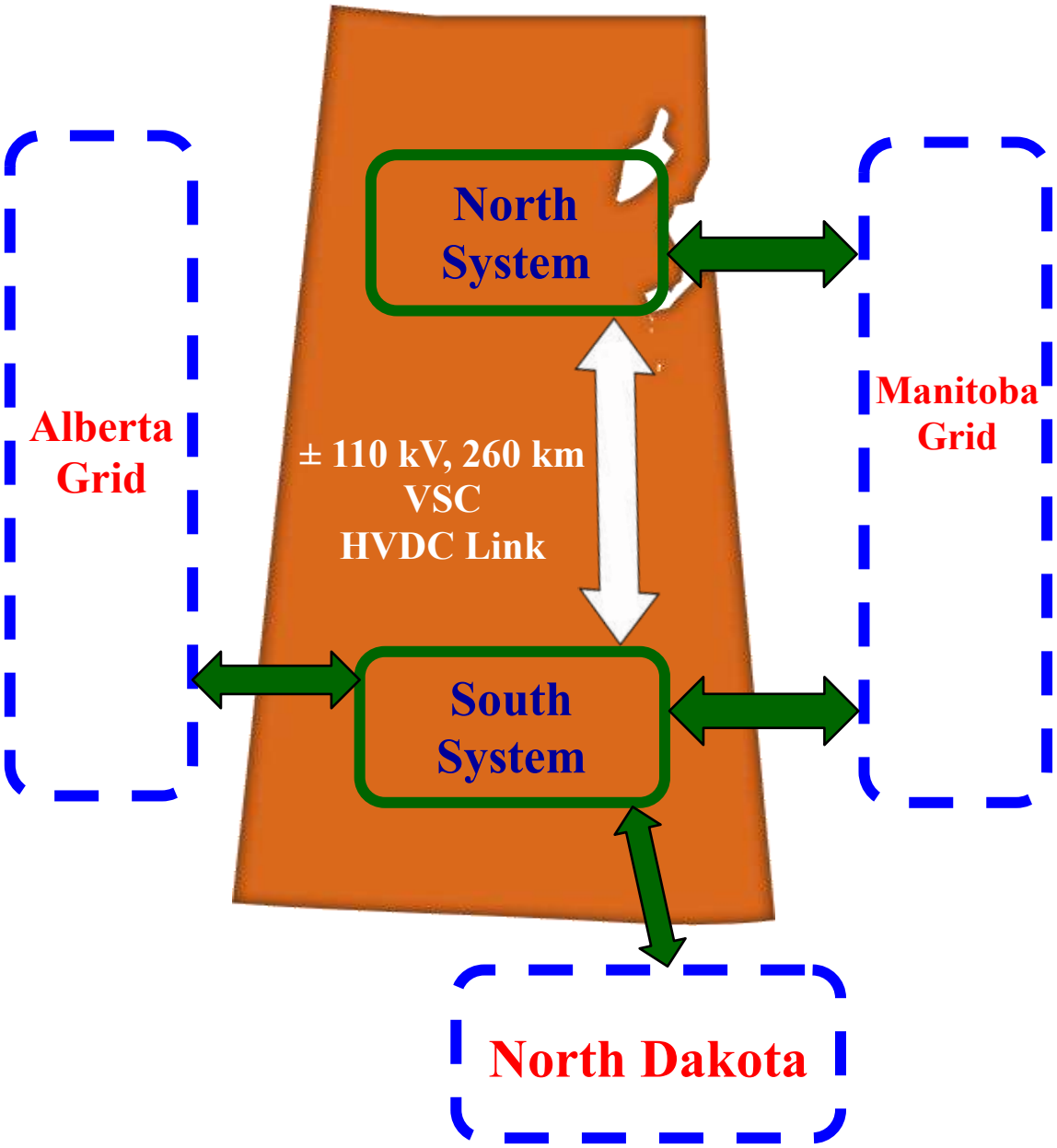

Figure 1.4: The VSC HVDC interconnection option.

1.4 HVAC Interconnection

Compared to the HVDC interconnection, which requires AC/DC/AC conversions, closely coordinated harmonic filtering, controls, and reactive power compensation, an AC link is a more natural method in interconnecting existing AC power systems as AC is the dominant mode of generation, transmission, and distribution. Furthermore, the option of an AC link is technically feasible and economically justified [8]. In the studies conducted in this thesis, it is required to transmit 50 MW from the SaskPower North system to the South system. In this context, a 138 kV, 260 km, double-circuit HVAC transmission tie-line is proposed as shown in Figure 1.5. Due to the long line-length and the possibility of a future need to transmit more power over the interconnection, series capacitive compensation is considered.

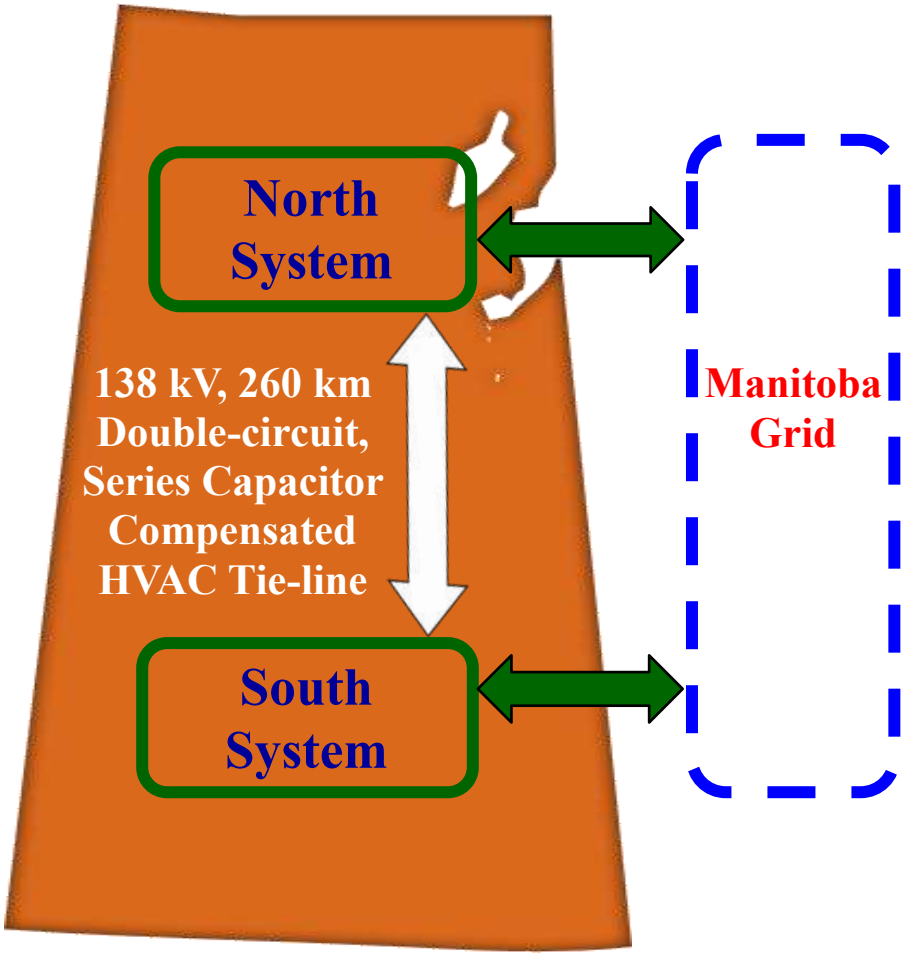

Figure 1.5: The proposed HVAC tie-line.

1.4.1 AC transmission line series compensation

The main purpose of series compensation in a power system is the virtual reduction of line reactance in order to enhance power system stability and increase the capability of transmission corridors [9]. The principle is based on compensating the transmission line reactance by the insertion of a series capacitor. The reactive power generated by the capacitor is proportional to the square of the line current. This means that the series capacitor has a self-regulating effect. When the system load increases, the reactive power generated by the series capacitor increases as well. The response of the series capacitor is automatic, instantaneous and continuous as long as the capacitor current remains within the specified operating constraints. The following are some of the major benefits of incorporating series capacitors in transmission systems:

- Increase in transient stability: a substantial increase in the stability margin is achieved by inserting a series capacitor. The series compensation will improve the situation in two ways: it will decrease the initial generator load angle corresponding to a specific power transfer and it will also shift the power-load angle (P-δ) characteristic upwards. This will lead to expanding the transient stability margin.

- Increase in power transfer: the increase in the power transfer capability as a function of the degree of compensation for a transmission line can be demonstrated using the circuit and the vector diagram displayed in Figure 1.6. The power transfer on the transmission line is given by [10]:

$$P = \frac{|V_{SE}||V_{RE}|}{X_{line} - X_c}\sin\delta = \frac{|V_{SE}||V_{RE}|}{X_{line}(1-k)}\sin\delta \tag{1.1}$$

where k is the degree of compensation defined as

$$k = \frac{X_c}{X_{line}} \tag{1.2}$$

The effect on the power transfer when a constant load angle difference is assumed is shown in Figure 1.7. Practical compensation degree ranges from 20 to 60 percent. Transmission capability increases of more than two times can be obtained in practice.

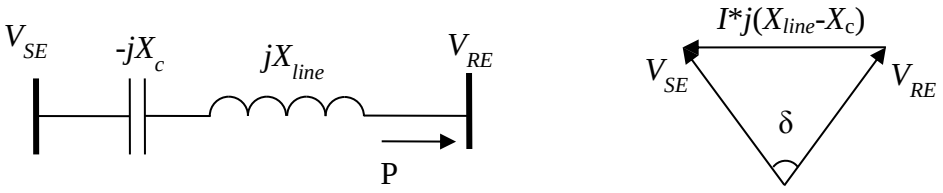

Figure 1.6: Transmission line with a series capacitor.

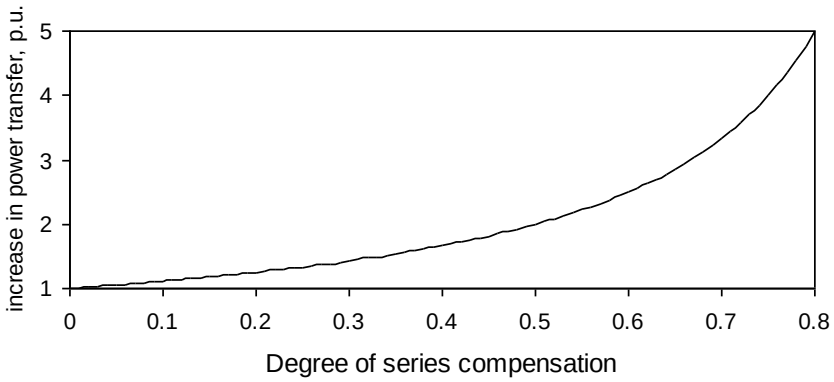

Figure 1.7: Increase in power transfer over a transmission line as a function of the degree of series compensation ($|V_{SE}| = |V_{RE}| = 1\,p.u., X_{line} = 1\,p.u.$).

- A better control of active load sharing between parallel circuits: when two transmission lines are connected in parallel, the natural power sharing between them is dictated by their respective impedances. If the two lines are of different configurations (and consequently of different thermal ratings), their impedances could still be very close. Therefore, the power transmitted in each line will be similar. The voltage drop in both circuits is identical, and therefore, the relationship between the line currents I_{L1} and I_{L2} can be expressed as:

$$I_{L1}Z_{L1} = I_{L2}Z_{L2} \tag{1.3}$$

If overloading the lower thermal rating line, (L_2, Figure 1.8) is to be avoided (i.e., $I_{L2} \leq I_{L2\,max}$), then the full power capacity of the other line, L_1, will never be reached (i.e., $I_{L1} < I_{L1\,max}$). For instance, consider the case when L_1 is a four-conductor bundle (quad) circuit configuration, whereas L_2 has a two-conductor bundle (twin) circuit configuration. If the conductors of these two bundles are identical, then L_1 has twice the rating of L_2. The inductive reactances of the two lines, however, are very close. If a

series capacitor is installed in the higher thermal rating line, both transmission lines can operate at their maximum capacity when the appropriate degree of compensation is provided (50% in this case) [11].

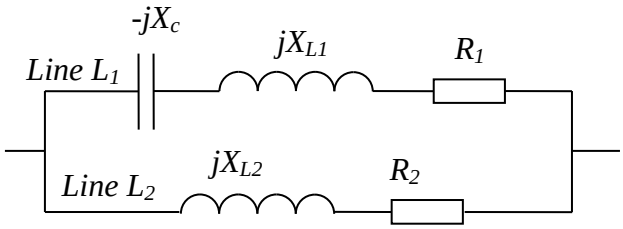

Figure 1.8: Adjusting the power sharing between two parallel lines using a series capacitor.

1.4.2 Potential risks of utilizing series capacitive compensation

One of the factors that hinder increased utilization of series capacitive compensation is the potential risk of Subsynchronous Resonance (SSR) [12]. SSR is a dynamic phenomenon in a power system which has certain special characteristics. The definitions of subsynchronous oscillation and SSR are given by the IEEE as [13]:

> "*Subsynchronous oscillation* is an electric power system condition where the electric network exchanges significant energy with a turbine-generator at one or more of the natural frequencies of the combined system below the synchronous frequency of the system following a disturbance from equilibrium. The above excludes the rigid body modes of the turbine-generator rotors."

> "*Subsynchronous Resonance (SSR)* encompasses the oscillatory attributes of electrical and mechanical variables associated with turbine-generators when coupled to a series capacitor compensated transmission system where the oscillatory energy interchange is lightly damped, undamped, or even negatively damped and growing."

1.5 Inter-Area Oscillations

When two power systems (two areas) are connected via a tie-line as shown in Figure 1.9, two types of low-frequency oscillations could be observed. The first type is known as local-

modes of oscillation. It involves a generator (or a group of generators) in one area oscillating against another generator (or another group of generators) in the "*same"* area. Figure 1.10 illustrates an example of a local mode of oscillations in area 1 between G_{11} - G_{12} and G_{13}. The second type is known as inter-area-modes of oscillation. It involves the generators in Area 1 oscillating as a coherent generator against the generators in Area 2 that are also oscillating as a coherent generator. Figure 1.11 illustrates an example of the inter-area mode of oscillations between Areas 1 and 2. The frequency of inter-area oscillations which depends on the strength of the system and on the moment of inertia of the generator rotors lies in the range of 0.1 Hz to 2.5 Hz [14]. The consequences of inter-area oscillations can be excessive wear of mechanical actuators of the machine controllers, fatigue of the generator shaft system, system instability or even major system blackouts.

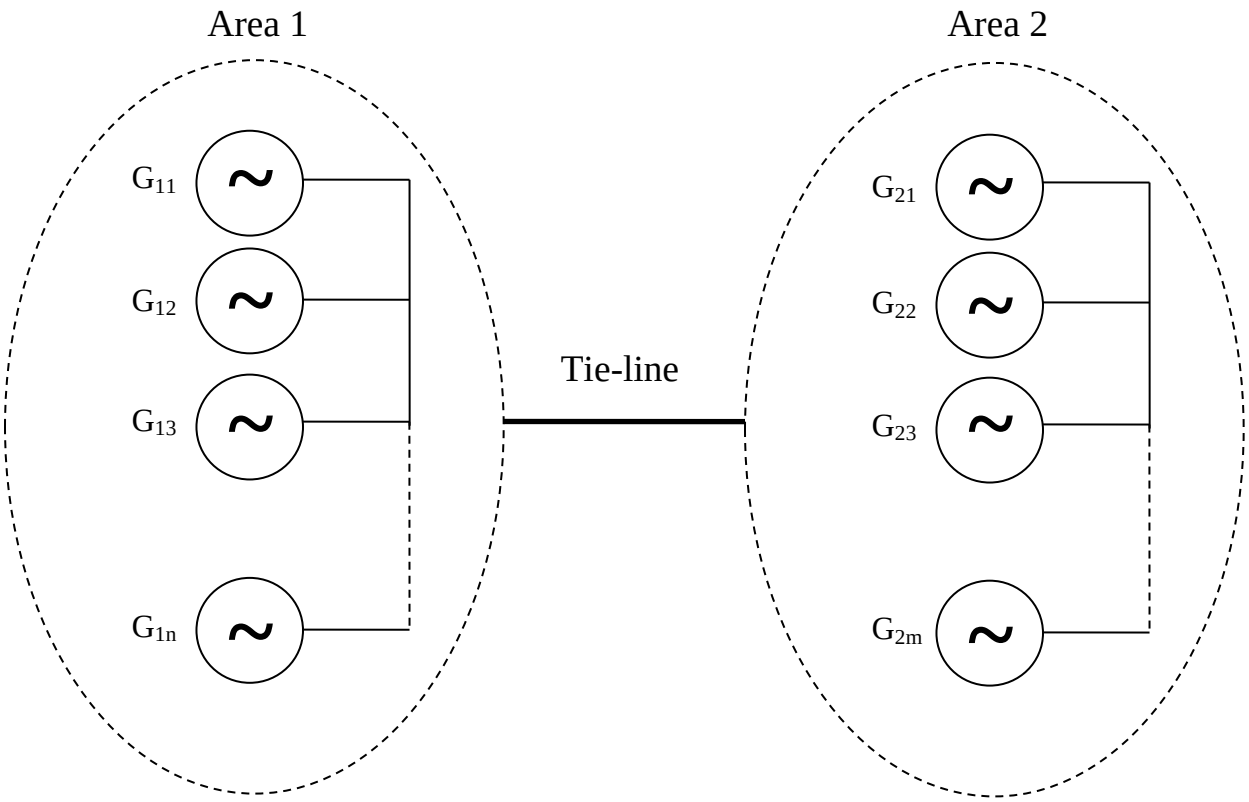

Figure 1.9: A simplified interconnected two-area system.

Local modes of oscillation are primarily influenced and determined by the local states. Inter-area oscillations are more difficult to study and investigate because they need the complete interconnected system to study and their characteristics are determined by the global states of the

entire power system. Since this research work involves an interconnection (tie-line) between the SaskPower North and South systems, inter-area oscillations are a major concern.

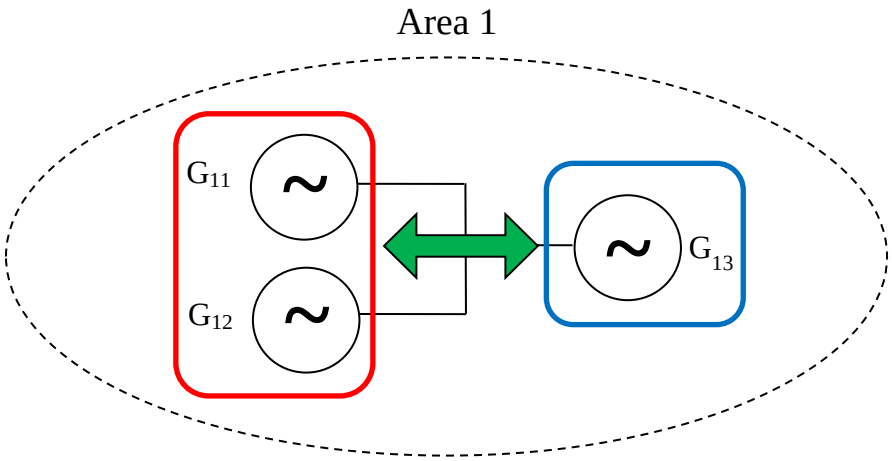

Figure 1.10: A local oscillation mode in Area 1.

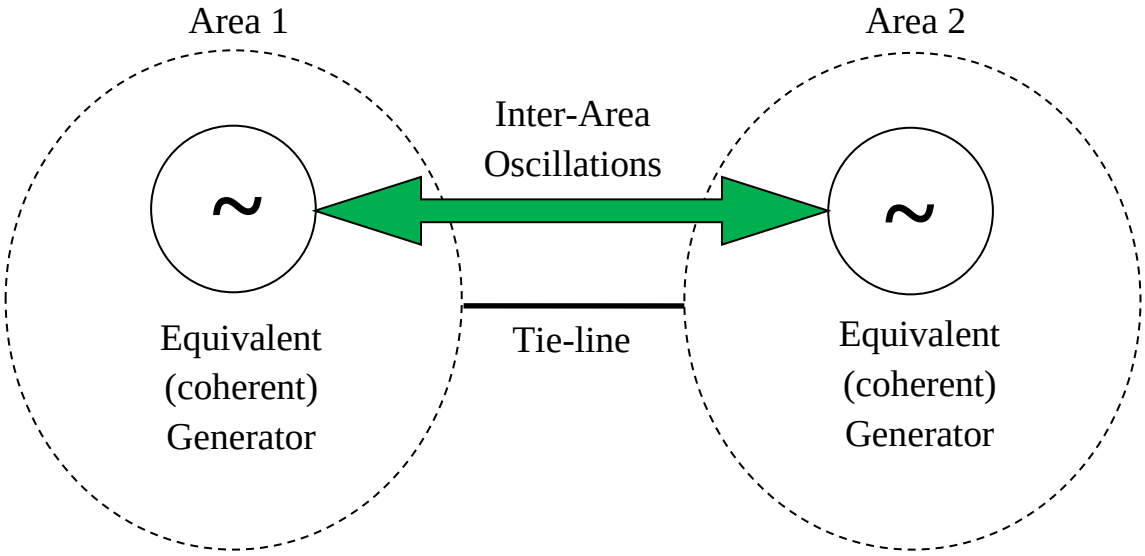

Figure 1.11: An inter-area oscillation mode between Areas 1 and 2.

1.6 Flexible AC Transmission Systems

The discussed advantages of series capacitive compensation can be achieved without the risk of SSR phenomenon if series Flexible AC Transmission Systems (FACTS) devices are used instead of series capacitors. These devices are also able to provide sufficient and fast damping of power system oscillations.

FACTS controllers are power electronic based controllers which can rapidly influence transmission system voltages, currents, impedances and/or phase angles [15], [16]. These controllers have the flexibility of controlling both real and reactive power, which can provide an excellent capability for improving power system dynamics. The FACTS technology provides an unprecedented way for controlling transmission grids and increasing transmission capacity.

The FACTS controllers may be based on thyristor devices with no gate turn-off (only with gate turn-on), or with power devices with gate turn-off capability. In general, the principal controllers with gate turn-off devices are based on dc to ac converters, which can exchange active and/or reactive power with the ac system. In the studies conducted in this thesis, a series FACTS controller based on thyristor switches is considered. This FACTS controller, displayed in Figure 1.12, is called a Thyristor Controlled Series Capacitor (TCSC) [15], [16]. In this context, the hybrid TCSC compensation scheme shown in Figure 1.13 is proposed to be installed in the AC interconnection. In such a scheme, series capacitive compensation is created in each phase using a TCSC in series with a fixed capacitor (C_c). It is worth noting here that such a hybrid TCSC compensation scheme has been installed and operated successfully by utilities in several countries. One example of these installations is the Brazilian North-South interconnection (a 500 kV, 1020 km transmission line with a rated transmitted power of 1300 MW), where a hybrid three-phase TCSC connects the North and South systems [17], [18]. Such a hybrid three-phase TCSC, displayed in Figure 1.14, consists of five fixed capacitors (distributed equally along the line length) and two TCSC modules (located at the sending and receiving terminals). The degree of compensation of the interconnection is 66% (1100 Mvar capacitive), where the fixed capacitors provide 54% and each TCSC module provides 6%. The task of the TCSC modules is purely to damp the low-frequency, inter-area power oscillations between the two systems. These oscillations would otherwise provide a hazard to the stability of the interconnected system. The TCSC and the hybrid three-phase TCSC employed by several utilities for power flow control and damping low-frequency and SSR oscillations, have shown superior performance through field tests, and analytical and simulation studies [19]-[32].

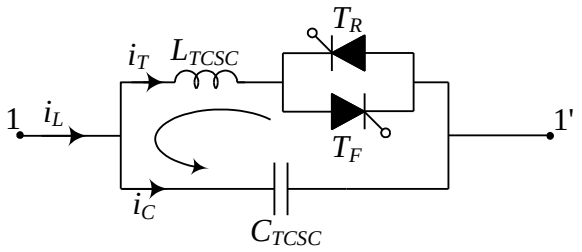

Figure 1.12: A schematic diagram of the TCSC.

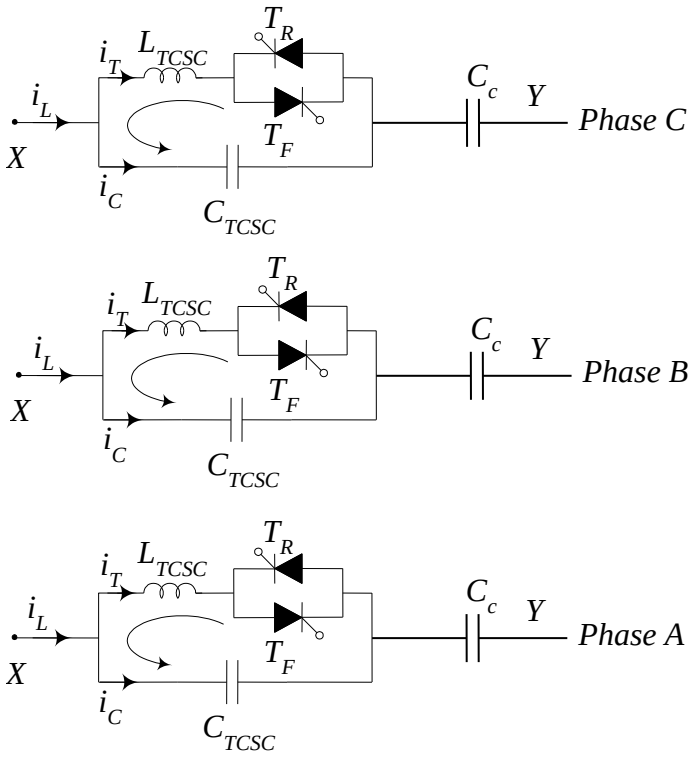

Figure 1.13: Schematic diagram of a hybrid TCSC compensation scheme.

1.7 Research Objective and Scope of the Thesis

The main objective of this research work is to investigate the dynamic performance of a proposed 138 kV, 260 km double-circuit tie-line incorporating a hybrid TCSC compensation scheme that would connect the SaskPower North and South systems. The potential problems that might arise due to such an interconnection, namely power flow control and low-frequency oscillations have been studied and quantified and a proposed feasible solution should be established. In this context, the effectiveness of a Power Oscillation Damping (POD) controller

incorporated in a hybrid TCSC compensation scheme to damp power system oscillations in the tie-line is investigated.

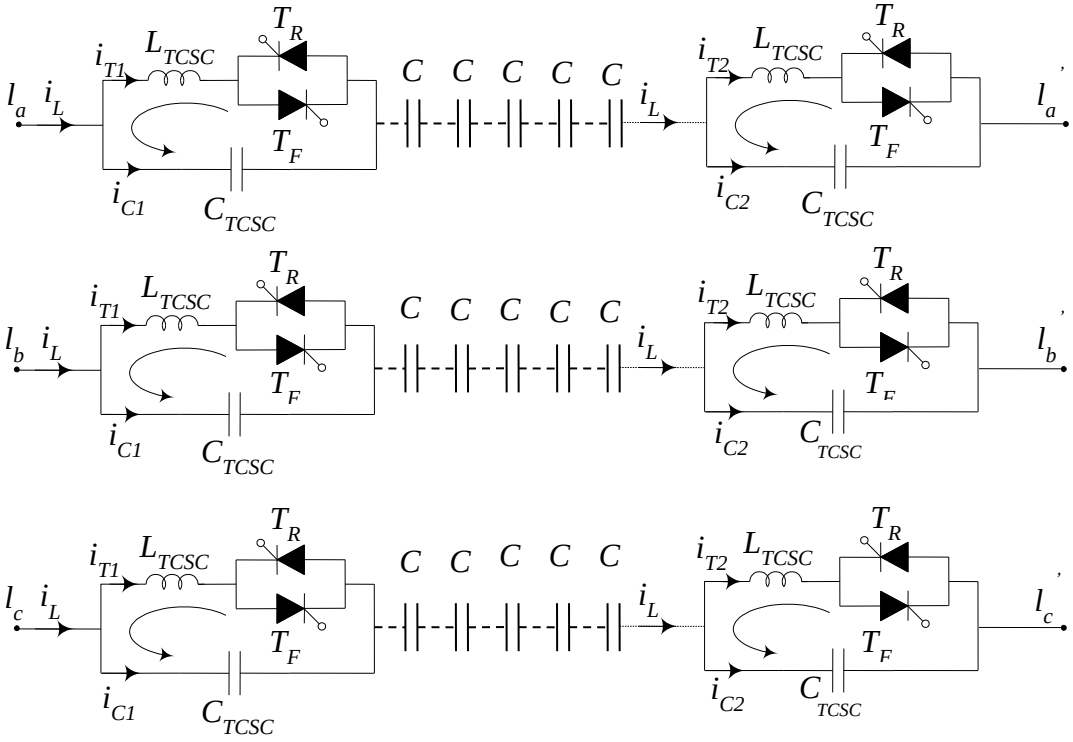

Figure 1.14: A three-line diagram of a hybrid three-phase TCSC.

The research work involves the following three major tasks in order to meet its objective.

- Developing adequate models for the SaskPower North and South systems suitable for studying the dynamic performance of the AC interconnection with its hybrid three-phase-TCSC compensation scheme.

- Studying the power flows of the SaskPower North and South systems before and after incorporating the interconnection and identifying any major loop flow problems (e.g., overloaded transmission lines) in the interconnected system.

- Conducting dynamic stability studies on the interconnected system using time-domain simulations to examine the performance of the TCSC supplemental controllers in damping the system low-frequency oscillations.

The thesis is organized in five chapters, a list of references section and an appendix.

Chapter 1 introduces the fundamental benefits and the problems arising from grid interconnections and series capacitive compensation. A brief introduction to the SaskPower North and South systems and the objectives of the research are also presented in this chapter.

Chapter 2 describes the system used for the investigations conducted in this thesis, and the detailed dynamic models of the individual components are presented. The results of digital time-domain simulations in a case study of the system during a three-phase fault are presented at the end of this chapter.

In Chapter 3, a comprehensive description of the TCSC, its three modes of operation, as well as the analysis of its net reactance are presented. Modeling the hybrid TCSC compensation scheme in the ElectroMagnetic Transient Program (EMTP-RV) is also discussed in this chapter. The load flow profiles of the SaskPower North and South systems as well as the interconnected North and South systems (with an AC interconnection incorporating a hybrid TCSC compensation scheme) are examined and important conclusions are drawn.

In Chapter 4, the effectiveness of the supplemental controller of the hybrid TCSC compensation scheme in damping power system oscillations is investigated using time-domain simulation case studies.

Chapter 5 summarizes the research described in this thesis and presents some conclusions.

The data of the systems under investigations are given in Appendix A.

Chapter 2

POWER SYSTEM MODELING FOR LARGE DISTURBANCE STUDIES

2.1 Introduction

This chapter discusses the mathematical models of various components in the system under study and models of SaskPower North and South systems suitable for studying the dynamic performance of the HVAC interconnection. The results of digital time-domain simulations of a case study of the integrated system incorporating the HVAC interconnection during a three-phase fault are also presented at the end of this chapter.

2.2 Power System Modeling

The nonlinear differential equations of the system under study are derived by developing individual mathematical models which represent various components in the system, namely the synchronous generator, the excitation system, the transmission line, the system load, the Doubly Fed Induction Generator (DFIG) wind turbine and the Back-to-Back (BtB) dc capacitor link. The whole system differential equations can be formed by knowing the mutual interaction among these models.

2.2.1 Modeling the synchronous machine

In a conventional synchronous machine, the stator circuit, consisting of a three-phase winding, produces a sinusoidal space distributed magnetomotive force. The rotor of the machine carries the field (excitation) winding which is excited by a dc voltage. The electrical damping due to the eddy currents in the solid rotor and, if present, the damper winding is represented by three equivalent damper circuits; one on the direct axis (d-axis) and the other two on the

quadrature axis (q-axis). The performance of the synchronous machine can be described by the equations given below in the d-q reference frame (Figure 2.1) [10]. In these equations, the convention is adopted for the signs of voltages and currents that *v* is the impressed voltage at the terminals and the direction of positive current *i* corresponds to generation. The sign of the currents in the equivalent damper windings is taken to be positive when they flow in a direction similar to that of the positive field current [33].

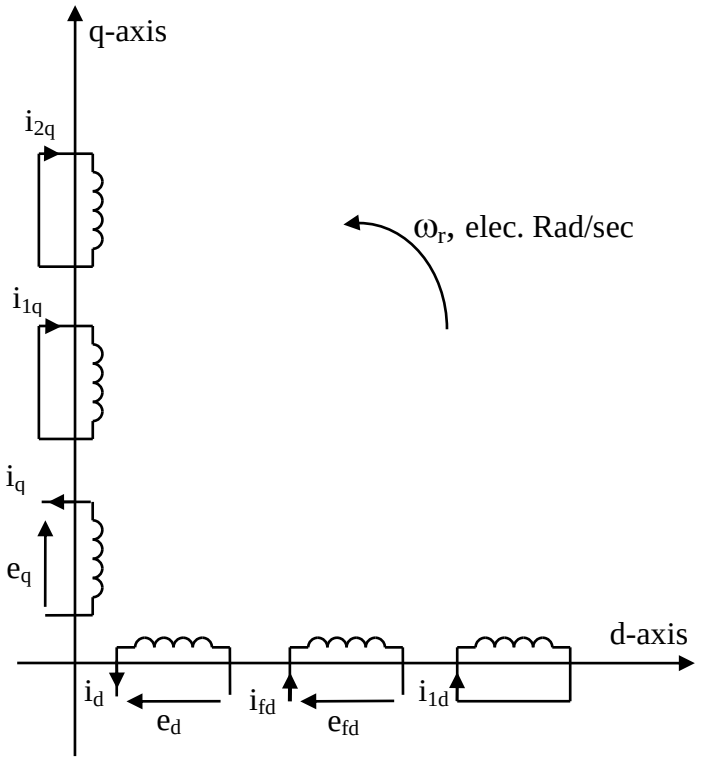

Figure 2.1: Modeling the synchronous machine in the d-q reference frame.

With time *t* expressed in seconds, the angular velocity ω expressed in rad/s (ω_0 = 377 *rad/sec*) and the other quantities expressed in per unit, the stator equations become:

$$e_d = \frac{1}{\omega_0}\frac{d\Psi_d}{dt} - \frac{\omega}{\omega_0}\Psi_q - R_a i_d \tag{2.1}$$

$$e_q = \frac{1}{\omega_0}\frac{d\Psi_q}{dt} + \frac{\omega}{\omega_0}\Psi_d - R_a i_q \tag{2.2}$$

The rotor equations:

$$e_{fd} = \frac{1}{\omega_0}\frac{d\Psi_{fd}}{dt} + R_{fd} i_{fd} \tag{2.3}$$

$$0 = \frac{1}{\omega_0}\frac{d\Psi_{1d}}{dt} + R_{1d}i_{1d} \tag{2.4}$$

$$0 = \frac{1}{\omega_0}\frac{d\Psi_{1q}}{dt} + R_{1q}i_{1q} \tag{2.5}$$

$$0 = \frac{1}{\omega_0}\frac{d\Psi_{2q}}{dt} + R_{2q}i_{2q} \tag{2.6}$$

The stator flux linkage equations:

$$\Psi_d = -L_d i_d + L_{ad} i_{fd} + L_{ad} i_{1d} \tag{2.7}$$

$$\Psi_q = -L_q i_q + L_{aq} i_{1q} + L_{aq} i_{2q} \tag{2.8}$$

The rotor flux linkage equations:

$$\Psi_{fd} = L_{ffd} i_{fd} + L_{ad} i_{1d} - L_{ad} i_d \tag{2.9}$$

$$\Psi_{1d} = L_{ad} i_{fd} + L_{11d} i_{1d} - L_{ad} i_d \tag{2.10}$$

$$\Psi_{1q} = L_{11q} i_{1q} + L_{aq} i_{2q} - L_{aq} i_q \tag{2.11}$$

$$\Psi_{2q} = L_{aq} i_{1q} + L_{22q} i_{2q} - L_{aq} i_q \tag{2.12}$$

The electromegnetic torque equation:

$$T_e = \Psi_d i_q - \Psi_q i_d \tag{2.13}$$

The overall differential equations which describe the transient performance of the synchronous machine are given by the following matrix equation:

$$\left[\frac{dX_{syn}}{dt}\right] = \left[At_{syn}\right]\left[X_{syn}\right] + \left[Bt_{syn}\right]\begin{bmatrix} V_{td} \\ V_{tq} \\ e_{fd} \end{bmatrix} \tag{2.14}$$

where

$$[X_{syn}] = [i_d \quad i_q \quad i_{fd} \quad i_{1q} \quad i_{1d} \quad i_{2q}]^T$$

$$[At_{syn}] = [L]^{-1}[Qt]$$

$$[Bt_{syn}] = [L]^{-1}[Rt]$$

$$[L] = \begin{bmatrix} -L_d & 0 & L_{ad} & 0 & L_{ad} & 0 \\ 0 & -L_q & 0 & L_{aq} & 0 & L_{aq} \\ -L_{ad} & 0 & L_{ffd} & 0 & L_{ad} & 0 \\ 0 & -L_{aq} & 0 & L_{11q} & 0 & L_{aq} \\ -L_{aq} & 0 & L_{ad} & 0 & L_{11d} & 0 \\ 0 & -L_{aq} & 0 & L_{aq} & 0 & L_{22q} \end{bmatrix} \tag{2.15}$$

$$[Qt] = \begin{bmatrix} \omega_0 R_a & -\omega L_q & 0 & \omega L_{aq} & 0 & \omega L_{aq} \\ \omega L_d & \omega_0 R_a & -\omega L_{ad} & 0 & -\omega L_{ad} & 0 \\ 0 & 0 & -\omega_0 R_{fd} & 0 & 0 & 0 \\ 0 & 0 & 0 & -\omega_0 R_{1q} & 0 & 0 \\ 0 & 0 & 0 & 0 & -\omega_0 R_{1d} & 0 \\ 0 & 0 & 0 & 0 & 0 & -\omega_0 R_{2q} \end{bmatrix}$$

$$[Rt] = \begin{bmatrix} \omega_0 & 0 & 0 \\ 0 & \omega_0 & 0 \\ 0 & 0 & \omega_0 \\ 0 & 0 & 0 \\ 0 & 0 & 0 \\ 0 & 0 & 0 \end{bmatrix}$$

here, the superscript ^{T} means matrix transpose.

The synchronous machine swing equation can be written as:

$$\frac{2H}{\omega_o}\frac{d\omega}{dt} = T_{MECH} - T_e \tag{2.16}$$

$$\frac{d\delta}{dt} = \omega - \omega_o \tag{2.17}$$

In the above two equations (2.16 and 2.17), ω is in radians per second, the inertia constant H is in seconds, and the load angle δ is in radians, ω_0 is the synchronous frequency (377 rad/sec) and the mechanical and electrical torques T_{MECH} and T_e are in per unit.

In developing the equations of multi-machine systems, the equations of each synchronous machine expressed in its own d-q reference frame which rotates with its rotor must be expressed in a common reference frame. Usually, a reference frame rotating at synchronous speed is used as the common reference. Axis transformation equations are used to transform between the individual machine (d-q) reference frames and the common (R-I) reference frames [10].

2.2.2 Modeling the transmission line

A series capacitor-compensated transmission line can be represented by the *RLC* circuit shown in Figure 2.2 [34]. In the voltage phasor diagram shown in Figure 2.3, the rotor angle δ is the angle (in elec. rad) by which the q-axis leads the reference voltage V_b. The differential equations for the circuit elements, after applying Park's transformation [34], can be expressed in the d-q reference frame by the following matrix expressions.

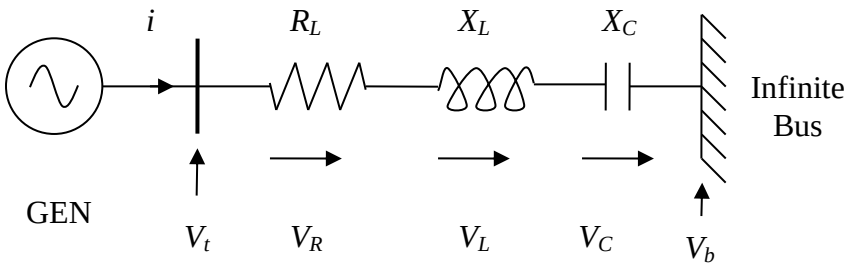

Figure 2.2: A series capacitor-compensated transmission line.

The voltage across the resistance:

$$\begin{bmatrix} V_{Rd} \\ V_{Rq} \end{bmatrix} = \begin{bmatrix} R_L & 0 \\ 0 & R_L \end{bmatrix} \begin{bmatrix} i_d \\ i_q \end{bmatrix} \tag{2.18}$$

The voltage across the inductance:

$$\begin{bmatrix} V_{Ld} \\ V_{Lq} \end{bmatrix} = \begin{bmatrix} 0 & -\frac{\omega}{\omega_0} X_L \\ \frac{\omega}{\omega_0} X_L & 0 \end{bmatrix} \begin{bmatrix} i_d \\ i_q \end{bmatrix} + \begin{bmatrix} \frac{X_L}{\omega_0} & 0 \\ 0 & \frac{X_L}{\omega_0} \end{bmatrix} \begin{bmatrix} \frac{di_d}{dt} \\ \frac{di_q}{dt} \end{bmatrix} \tag{2.19}$$

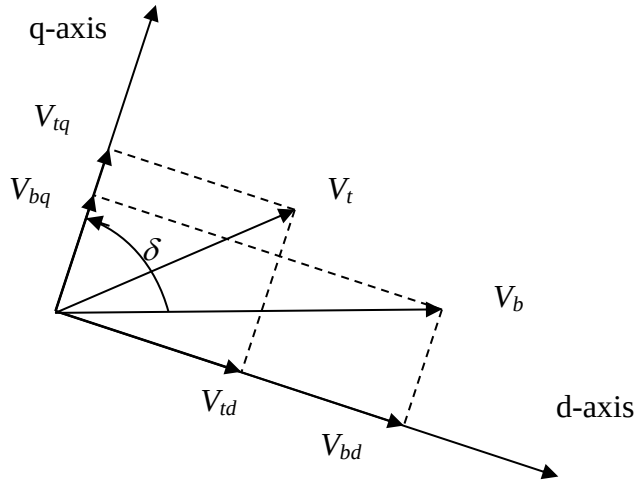

Figure 2.3: Voltage phasor diagram.

The voltage across the capacitor:

$$\begin{bmatrix} \frac{dV_{Cd}}{dt} \\ \frac{dV_{Cq}}{dt} \end{bmatrix} = \begin{bmatrix} \omega_0 X_C & 0 \\ 0 & \omega_0 X_C \end{bmatrix} \begin{bmatrix} i_d \\ i_q \end{bmatrix} + \begin{bmatrix} 0 & \omega \\ -\omega & 0 \end{bmatrix} \begin{bmatrix} V_{Cd} \\ V_{Cq} \end{bmatrix} \tag{2.20}$$

The overall equations of the transmission line can be written as

$$\begin{bmatrix} \frac{dV_{Cd}}{dt} \\ \frac{dV_{Cq}}{dt} \\ V_{td} \\ V_{tq} \end{bmatrix} = [Att] \begin{bmatrix} V_{Cd} \\ V_{Cq} \end{bmatrix} + [Rt1] \begin{bmatrix} \frac{di_d}{dt} \\ \frac{di_q}{dt} \end{bmatrix} + [Rt2] \begin{bmatrix} i_d \\ i_q \end{bmatrix} + [Btt][V_b] \tag{2.21}$$

where

$$[Att] = \begin{bmatrix} 0 & \omega \\ -\omega & 0 \\ 1 & 0 \\ 0 & 1 \end{bmatrix}$$

$$[Rt1] = \begin{bmatrix} 0 & 0 \\ 0 & 0 \\ \frac{X_L}{\omega_0} & 0 \\ 0 & \frac{X_L}{\omega_0} \end{bmatrix}$$

$$[Rt2] = \begin{bmatrix} \omega_0 X_C & 0 \\ 0 & \omega_0 X_C \\ R_L & -\frac{\omega}{\omega_0} X_L \\ \frac{\omega}{\omega_0} X_L & R_L \end{bmatrix} \tag{2.22}$$

$$[Btt] = \begin{bmatrix} 0 \\ 0 \\ \sin\delta \\ \cos\delta \end{bmatrix}$$

In the case of an uncompensated transmission line, the impedance X_C in Equations 2.20 and 2.22 is set to zero.

2.2.3 Modeling the excitation system

The block diagram of the excitation system is displayed in Figure 2.4, and the corresponding data are given in Appendix A [34].

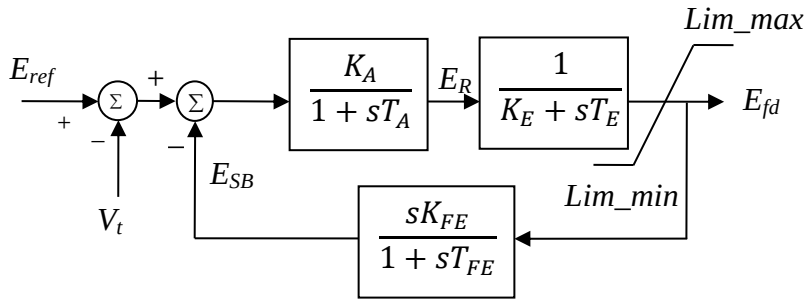

Figure 2.4: Block diagram of the excitation system.

Utilizing the relationship between the excitation system output voltage and the field voltage given by $E_{fd} = \frac{L_{ad}}{R_{fd}} e_{fd}$, the state-space equation of the excitation system can be derived from its block diagram and is given by

$$\left[\frac{dX_v}{dt}\right] = [At_v][X_v] + [Bt_v]\begin{bmatrix} V_t \\ E_{ref} \end{bmatrix} \tag{2.23}$$

where

$$[X_v] = \begin{bmatrix} e_{fd} & E_R & E_{SB} \end{bmatrix}^T$$

$$[At_v] = \begin{bmatrix} -\frac{K_E}{T_E} & \frac{1}{T_E}\frac{R_{fd}}{L_{ad}} & 0 \\ 0 & -\frac{1}{T_A} & -\frac{K_A}{T_A} \\ -\frac{K_E K_F}{T_E T_F}\frac{L_{ad}}{R_{fd}} & \frac{K_F}{T_F T_E} & -\frac{1}{T_F} \end{bmatrix} \tag{2.24}$$

$$[Bt_v] = \begin{bmatrix} 0 & 0 \\ -\frac{K_A}{T_A} & \frac{K_A}{T_A} \\ 0 & 0 \end{bmatrix}$$

2.2.4 Modeling the transformer

The three-phase transformer is constructed by using three single-phase transformers connected in Delta (low-voltage side)/ Y grounded (high-voltage side). The transformer leakage and magnetizing reactances as well as the winding resistances and core loss are represented in the model.

2.2.5 Modeling system loads

The system loads are modeled in these studies by constant impedances. The formula used in calculating the load impedances is given by [35]:

$$Z_{Load} = \frac{|V_{Load}|^2}{P_{Load} - jQ_{Load}} \tag{2.25}$$

where

Z_{Load} = load impedance.

V_{Load} = load voltage.

P_{Load} = load real power.

Q_{Load} = load reactive power.

2.2.6 Modeling the DFIG wind turbine

The basic configuration of a DFIG wind turbine is displayed in Figure 2.5, where the stator of the induction machine is directly connected to the grid while BtB partial-scale power converter (25% to 30% of the generator rating) connects the slip ring terminals to the grid [37]. The BtB converter consists of two voltage-sourced converters (Rotor-Side Converter (RSC) and Grid-Side Converter (GSC)) and a common dc bus. The mathematical model of the DFIG wind turbine can be summarized as follows [36] – [41]:

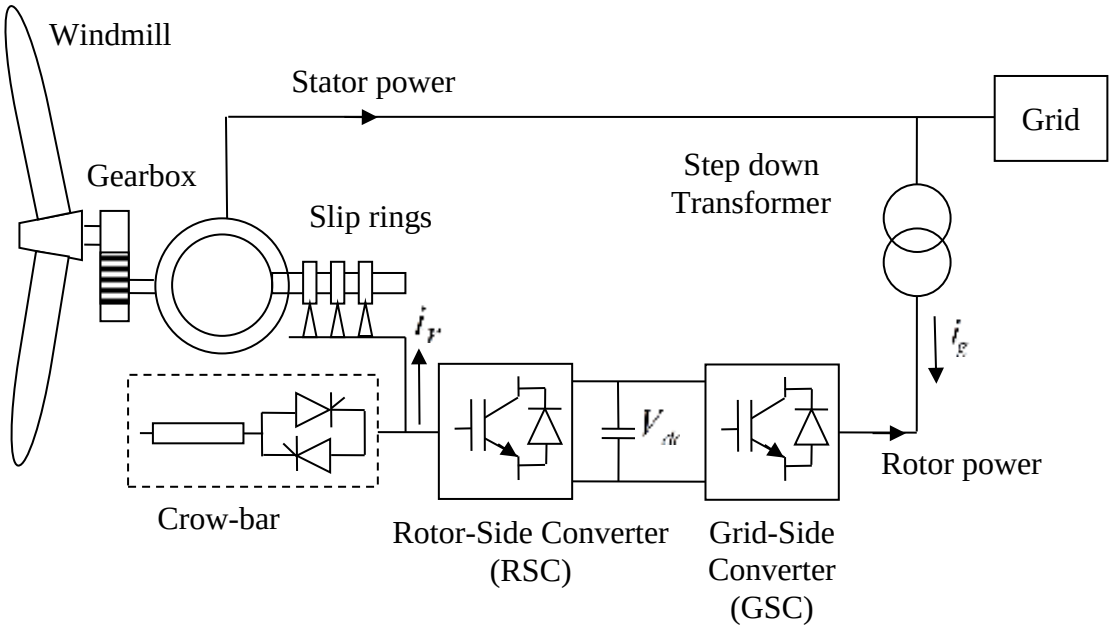

Figure 2.5: Schematic diagram of a DFIG wind turbine.

The dynamic output mechanical torque of the wind turbine is expressed as

$$T_m = \frac{1}{2}\rho A R C_P V_\omega^2 / \lambda \tag{2.26}$$

where ρ is the air density (kgm^{-3}), A is the blade sweep area (m^2), R is the blade length (m), and V_ω is the wind speed (m/s) [39]-[40]. C_P is the power coefficient of the blade which is a function of the blade pitch angle θ and the tip speed ratio λ according to the following equation:

$$C_P = \frac{1}{2}\left(\frac{RC_f}{\lambda} - 0.022\theta - 2\right) e^{-0.255\frac{RC_f}{\lambda}} \tag{2.27}$$

where C_f is the wind turbine blade design constant and the tip speed ratio λ is given by

$$\lambda = \frac{\omega_m R}{V_\omega} \tag{2.28}$$

where ω_m is the mechanical angular velocity (rad/s).

The power, rotating speed, and wind speed relationship is illustrated in Figure 2.6 [40].

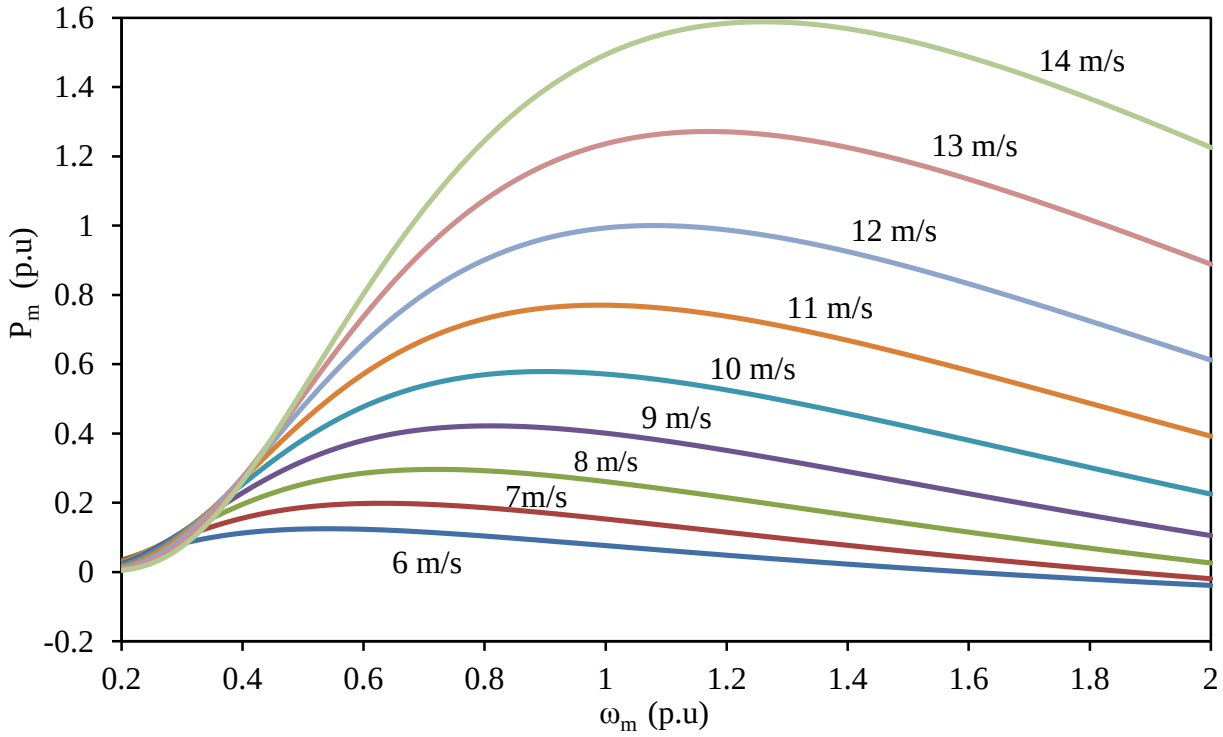

Figure 2.6: Mechanical power, rotor speed and wind speed relationships.

Figure 2.7 shows the equivalent circuit of a DFIG in the synchronous *qd* reference frame, where the *q*-axis leads the *d*-axis by 90˚. The stator and rotor voltage equations in *qd* reference frame can be obtained as follows:

$$\begin{cases} V_s = r_s I_s + j\omega_s \lambda_s + \frac{d\lambda_s}{dt} \\ V_r = r_r + j(\omega_s - \omega_r)\lambda_r + \frac{d\lambda_r}{dt} \end{cases} \tag{2.29}$$

where $V_s = v_{qs} - jv_{ds}$ and $V_r = v_{qr} - jv_{dr}$. The flux linkage expressions are given as follows:

$$\begin{cases} \lambda_s = L_s I_s + M I_r \\ \lambda_r = L_r I_r + M I_s \end{cases} \tag{2.30}$$

where $L_s = L_{ls} + M$, $L_r = L_{lr} + M$, $\lambda_s = \lambda_{qs} - j\lambda_{ds}$, $\lambda_r = \lambda_{qr} - j\lambda_{dr}$, $I_s = i_{qs} - ji_{ds}$, and $I_r = i_{qr} - ji_{dr}$.

From Equations 2.29 and 2.30, a set of differential equations with stator and rotor currents as state variables, stator and rotor voltages as inputs can be established. While the rotor voltages are determined by the RSC control scheme, the stator voltages are determined by the network interface.

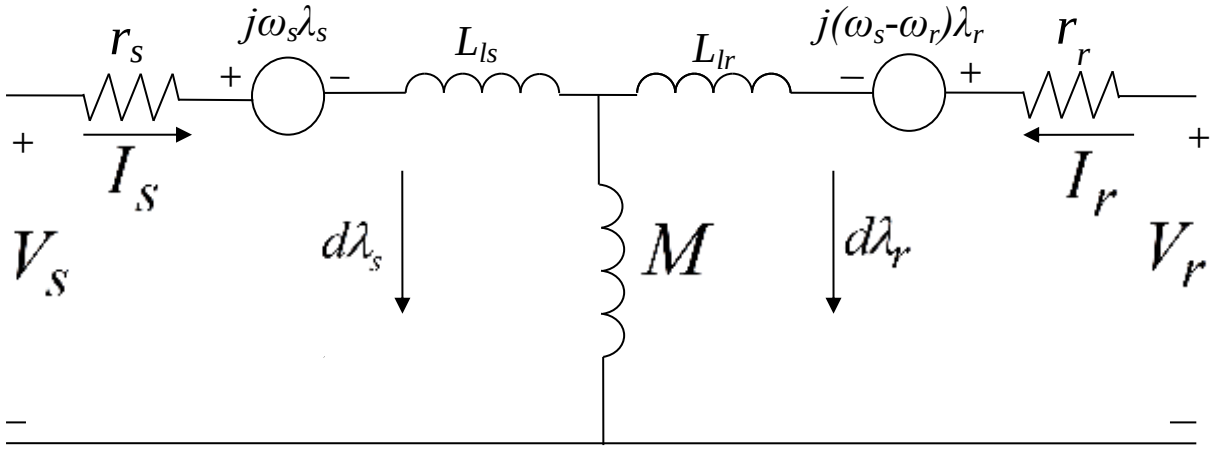

Figure 2.7: Equivalent circuit of the DFIG.

The electromagnetic torque T_e can be expressed as follows:

$$T_e = \lambda_{qm} i_{dr} - \lambda_{dm} i_{qr} \tag{2.31}$$

where λ_{qm} and λ_{dm} are, respectively, the *q*- and *d*- axes magnetizing flux linkages, defined as

$$\begin{cases} \lambda_{qm} = \lambda_{qs} - i_{qs} L_{ls} \\ \lambda_{dm} = \lambda_{ds} - i_{ds} L_{ls} \end{cases} \tag{2.32}$$

2.2.7 Modeling the BtB dc capacitor link

The dynamics of the BtB dc capacitor link can be described with the help of the equivalent circuit displayed in Figure 2.8 as [40]

$$C v_{dc} \frac{dv_{dc}}{dt} = P_r - P_g \tag{2.33}$$

where

$$\begin{cases} P_r = K_1(v_{qr} i_{qr} + v_{dr} i_{dr}) \\ P_g = K_2(v_{qg} i_{qg} + v_{dg} i_{dg}) \end{cases} \tag{2.34}$$

In Equation 2.34, K_1 and K_2 are constants, P_r, P_g are the active powers of the RSC and the GSC respectively, v_{qr}, v_{dr} are the quadrature- and direct- axes RSC voltage respectively and v_{qg}, v_{dg} are the quadrature- and direct- axes GSC voltage respectively.

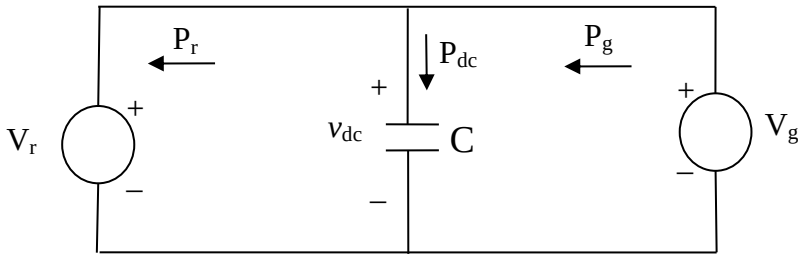

Figure 2.8: Equivalent circuit for the BtB dc capacitor link.

The frequency converters are modeled by a fundamental frequency approach, which is appropriate and sufficient for power system dynamic studies. Assuming an ideal DC-link voltage and an ideal pulse-width modulation [42], the relation between AC- and DC- voltages can be expressed as follows

$$|U_{AC}| = K_0 P_m U_{DC} \tag{2.35}$$

P_m, which donates the pulse-width-modulation index, is limited ($0 < P_m \leq 1$) to avoid saturation effects. The factor K_0 depends on the modulation method, e.g. rectangular or sinusoidal modulation. In the case of sinusoidal modulation, which is standard in power applications, the factor K_0 is defined as

$$K_0 = \frac{\sqrt{3}}{2\sqrt{2}} \tag{2.36}$$

The DC-link Capacitor provides an intermediate energy storage, which decouples the generator-side converter and the grid-side converter. The size of the DC-link Capacitor is selected based on a trade-off between voltage ripples, lifetime and fast control of the DC-link [43], [44].

The control of the DFIG wind turbine is achieved by controlling the RSC and GSC utilizing vector control techniques. Vector control allows decoupled control of both the real and reactive power. The idea is to use a rotating reference frame based on an AC flux or voltage and then to project the currents on this rotating frame. Such projections are usually referred to as the *d*- and *q*- components of their respective currents. For flux-based rotating frames, changes in the *q*- component leads to real power changes, while changes in the *d*- component leads to reactive power changes. In voltage-based rotating frames (90˚ ahead of flux-based frames), the effect is the opposite.

Figure 2.9 shows a general control scheme for the DFIG BtB converters [45]-[47]. In such a scheme, the RSC operates in the stator flux reference while the GSC operates in the stator voltage reference frame. The *q*-axis current of the RSC is used to control the real power while the *d*-axis current is used for reactive power control. On the other hand, the *d*-axis current for the GSC is used to control the dc link voltage to a constant level while the *q*-axis current is used for reactive power control.

As illustrated in Figure 2.9, both RSC and GSC are controlled by a two-stage controller. The first stage consists of very fast current controllers regulating the rotor currents to references values that are specified by slower power controllers (Stage-2). In normal operation, the aim of the RSC is to control independently the real and reactive power on the grid while the GSC has to maintain the dc link capacitor at a set value regardless of the magnitude and direction of the rotor power and to guarantee converter operation with unity power factor (zero reactive power). The reference $P_{grid-Ref}$ for the real power is given by the maximum power tracking point (MPT) lookup table as a function of the optimal generator speed. The reference $Q_{grid-Ref}$ for the reactive power of the RSC can be set to a certain value or to zero according to whether or not the DFIG is required to contribute with reactive power. The reactive power reference for the GSC, $Q_{GSC-Ref}$ is "usually" set to zero. This means that the GSC exchanges only real power with the

grid and, therefore, the transmission of reactive power controllability of the GSC can be useful during the process of voltage reestablishment after clearing a system fault. The reference signal V_{dc-Ref} is set to a constant value that depends on the size of the converter, the stator/rotor voltage ratio and the modulation factor of the power converter [47].

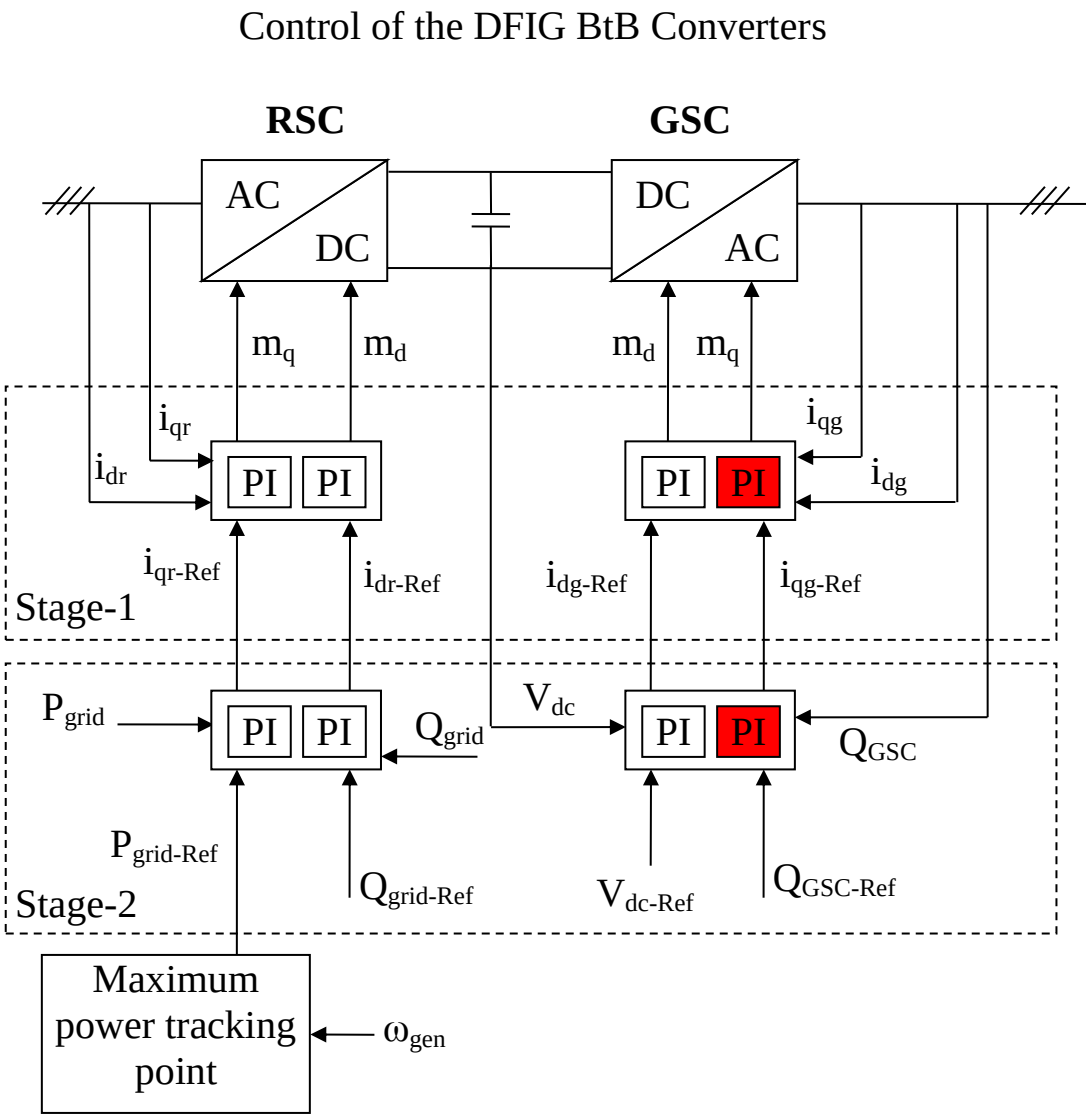

Figure 2.9: Schematic diagram of a general control scheme of the DFIG BtB converters.

2.3 Modeling the SaskPower North and South Systems for Dynamic Studies of the Integrated System

The two hydro generating stations in the SaskPower North system, G_{N1} and G_{N5} are rated at 25 MVA and 231.6 MVA respectively. Between these two generating stations which are 650 km apart are two load centers at buses N_2 and N_3. The Manitoba grid is connected to the SaskPower North system at bus N_6 as shown in Figure 2.10. Transmission lines voltage is 138 kV.

In the studies conducted in this thesis, only the northern part of the SaskPower South system is modeled. This is due to the fact that such a northern part which has a high density of generation could represent reasonably the SaskPower South system as the dynamic studies are focused on the tie-line performance. Therefore, modeling the entire SaskPower South system is unnecessary. As it can be seen from Figure 2.10, there are four generating stations in the modeled SaskPower South system; G_{S1}, G_{S2}, G_{S4} and G_{S6} with rated capacity of 192 MVA, 147.1 MVA, 192 MVA and 231.6 MVA respectively. There are also two load centers located at buses S_3 and S_5 that are connected with a 200 km, 220 kV transmission line. A DFIG-based wind farm comprising 50 × 1.5 MW DFIG wind turbines is also connected to the SaskPower South system at bus S_4. The assigned wind speed is 11 m/s and power output of the wind farm is 75 MW. Transmission line voltages in SaskPower South system are 138 and 220 kV.

The data of the modeled SaskPower North and South systems are given in Appendix A [48]. Moreover, since generators are required to operate above minimum levels, some loads are added to some generator buses. The electrical parameters of the 138 and 220 kV transmission lines are typical transmission lines data [48]. The modeled SaskPower integrated system incorporating an AC tie-line is shown in Figure 2.11. In order to carry out the time-domain simulation studies, the two large systems representing Manitoba grid connections, shown in Figure 2.10, are replaced with a single large system and a virtual transmission line between buses N_6 and S_7.

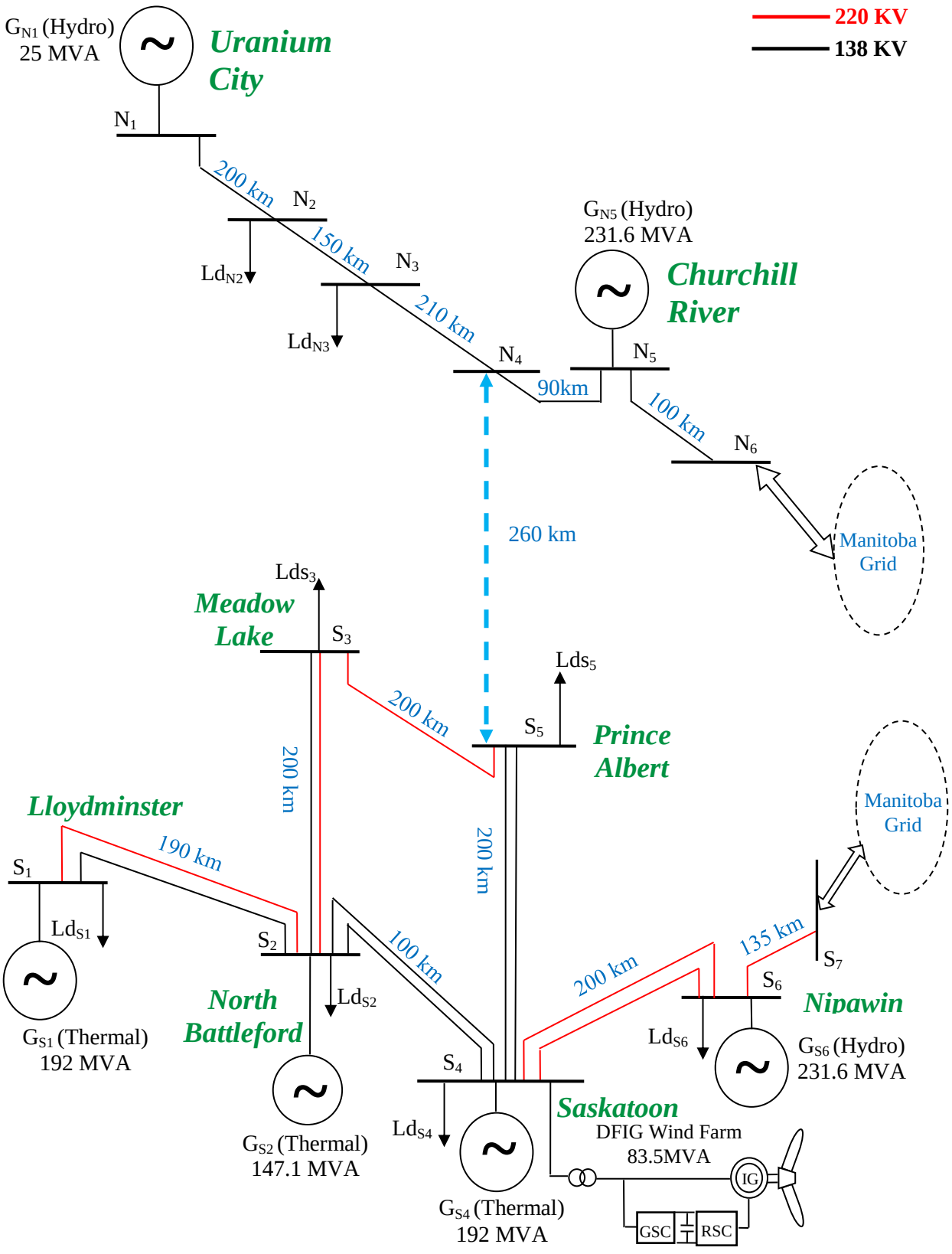

Figure 2.10: Modeling the SaskPower North and South systems.

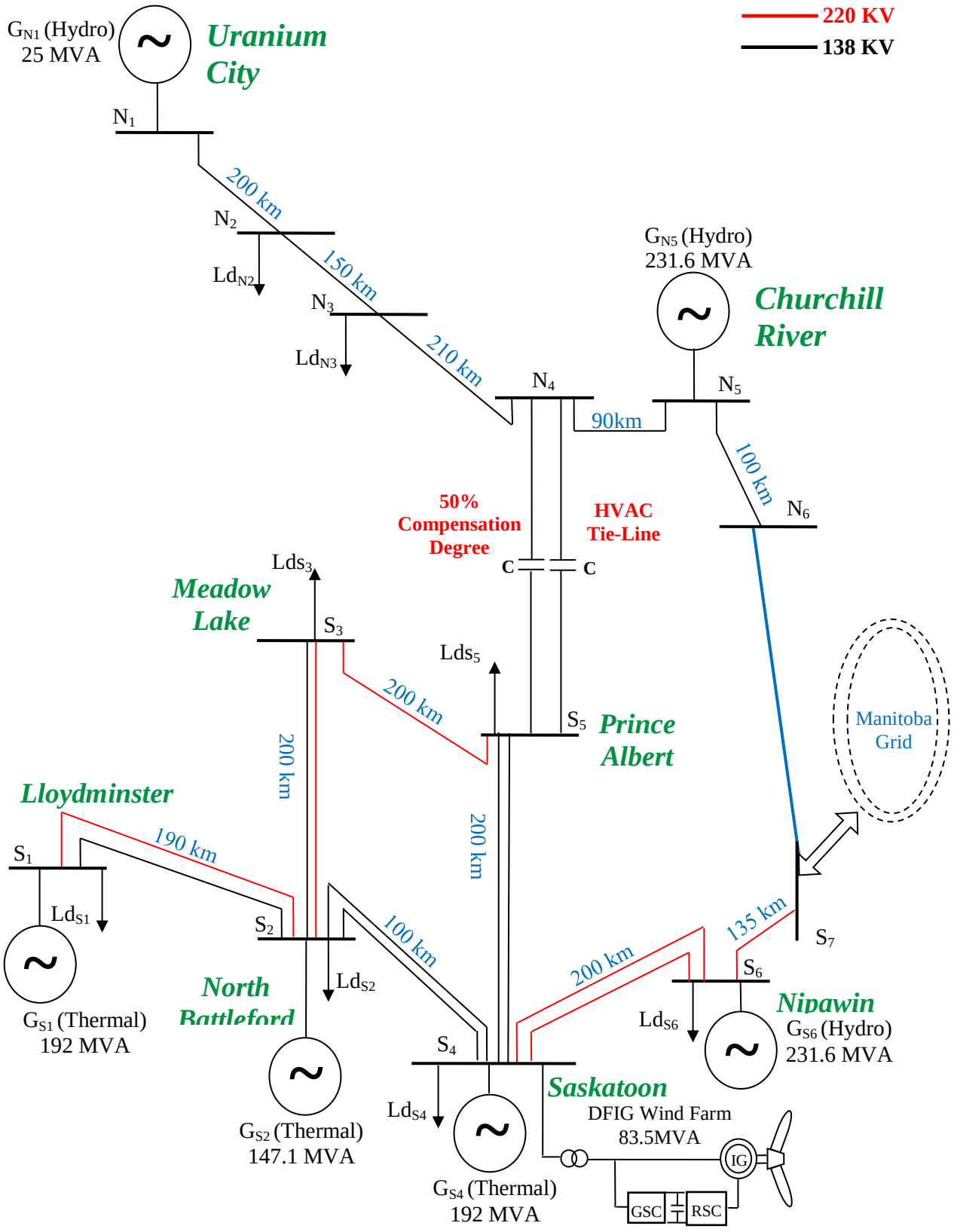

Figure 2.11: SaskPower integrated system incorporating a series capacitor compensated (50% compensation degree) tie-line.

2.4 A Sample Case Study

In the studies conducted in this thesis, the ElectroMagnetic Transient Program (EMTP-RV) is used for modeling the various system components and producing the time-domain simulation results. Due to the initialization process in the EMTP-RV, the time-domain simulation results are displayed at a starting time of either 9 or 9.5 seconds and system faults are assumed to occur at t = 10 seconds.

Figure 2.12 illustrates the transient time responses of the SaskPower integrated system incorporating a 260 km, 138 kV series capacitor compensated (50% compensation degree) double-circuit tie-line during and after clearing a three-cycle three-phase fault on the virtual transmission line N_6-S_7 (between buses N_6 and S_7). In order to get an insight on the impact of series capacitive compensation on the system dynamics, the transient time responses of the system for the case of an uncompensated tie-line are also shown in Figure 2.12. The physical explanation of tripping the virtual transmission line N_6-S_7, shown in Figure 2.11, is that the SaskPower North system has lost its interconnection with the Manitoba grid (Figure 2.10). The following observations can be made from examing Figure 2.12:

1. As expected, the real power transmitted from the North system to the South system through the tie-line, before the fault (i.e. at steady state) is around 50 MW.

2. In the case of the uncompensated tie-line, the transmission line real power flows, system bus voltages, generator speed and load angle deviations experience severe low-frequency oscillations after fault clearing. Failing to reach a new steady-state condition, the system loses its stability as it can be seen from the sustained oscillations (with a frequency of 4.76 Hz starting at t = 16.36 seconds).

3. In the case of the series capacitive compensated tie-line, the system performance is much better than that of the uncompensated case. Nevertheless, the low-frequency oscillations of most of the system variables are “slowly” growing indicating a system instability.

4. The DFIG-based wind farm is stable after fault clearing delivering its rated power of 75 MW.

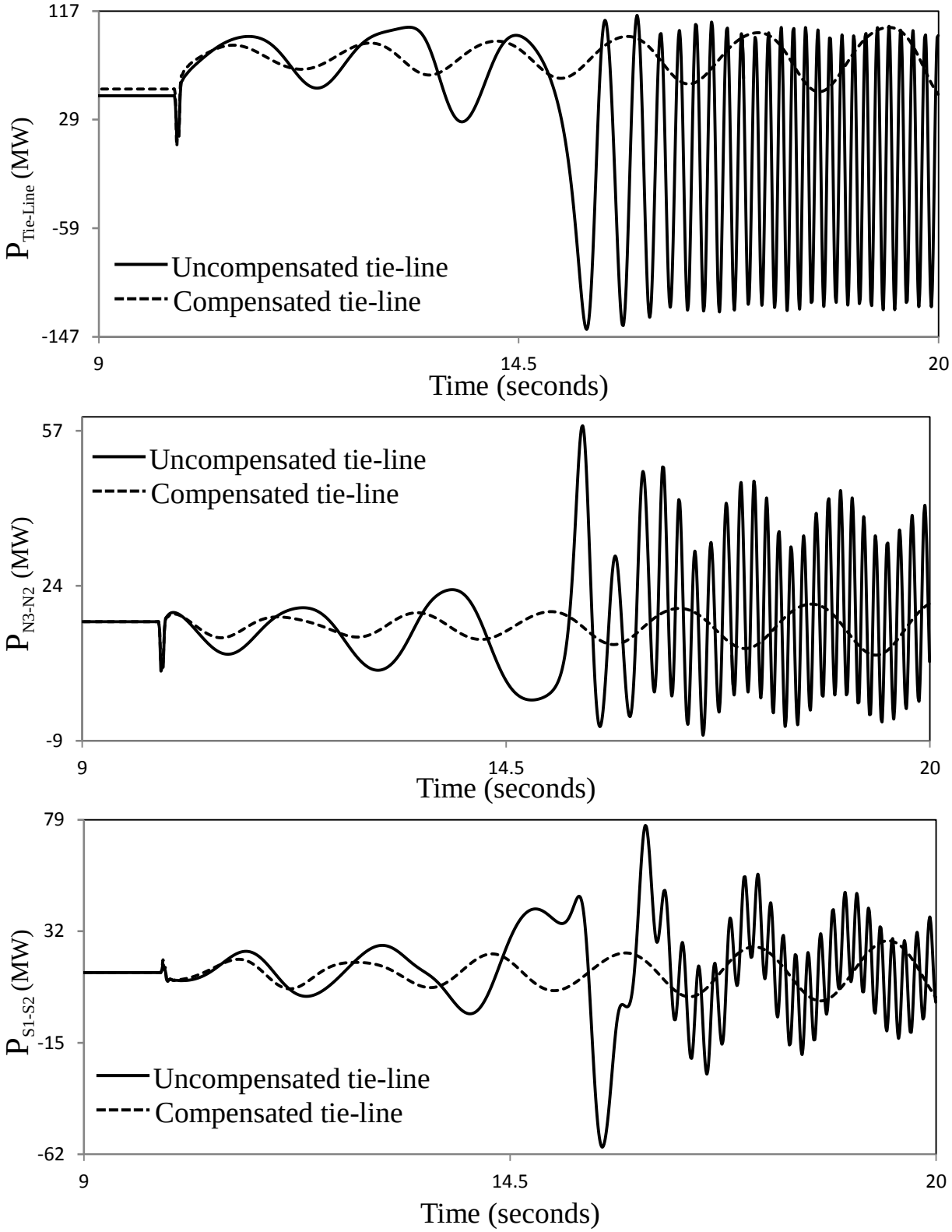

Figure 2.12: Transient time responses of the power system during and after clearing a three-cycle, three-phase fault on the virtual transmission line N_6-S_7 (with the 260 km, 138 kV double-circuit tie-line).

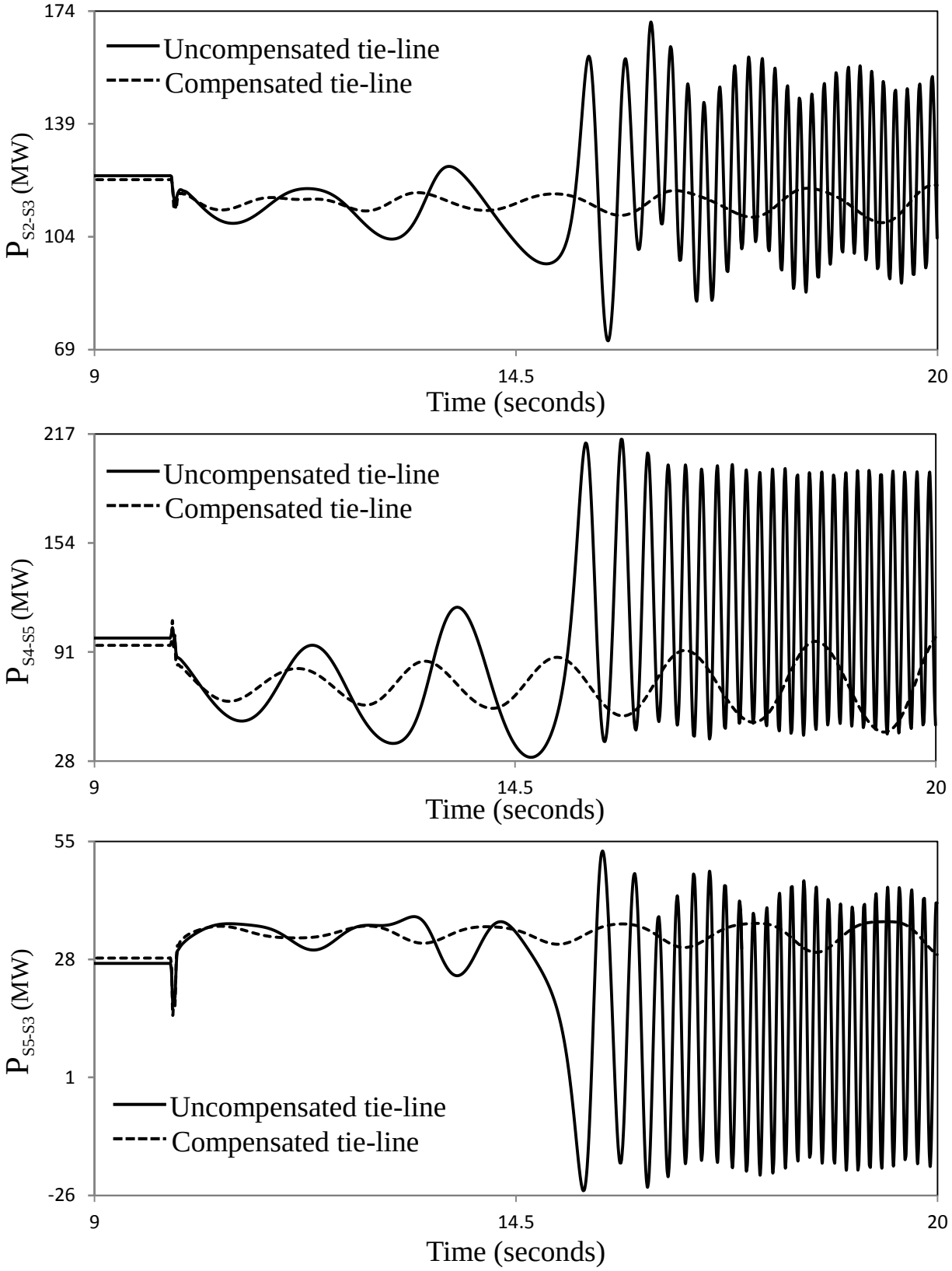

Figure 2.12: Continued.

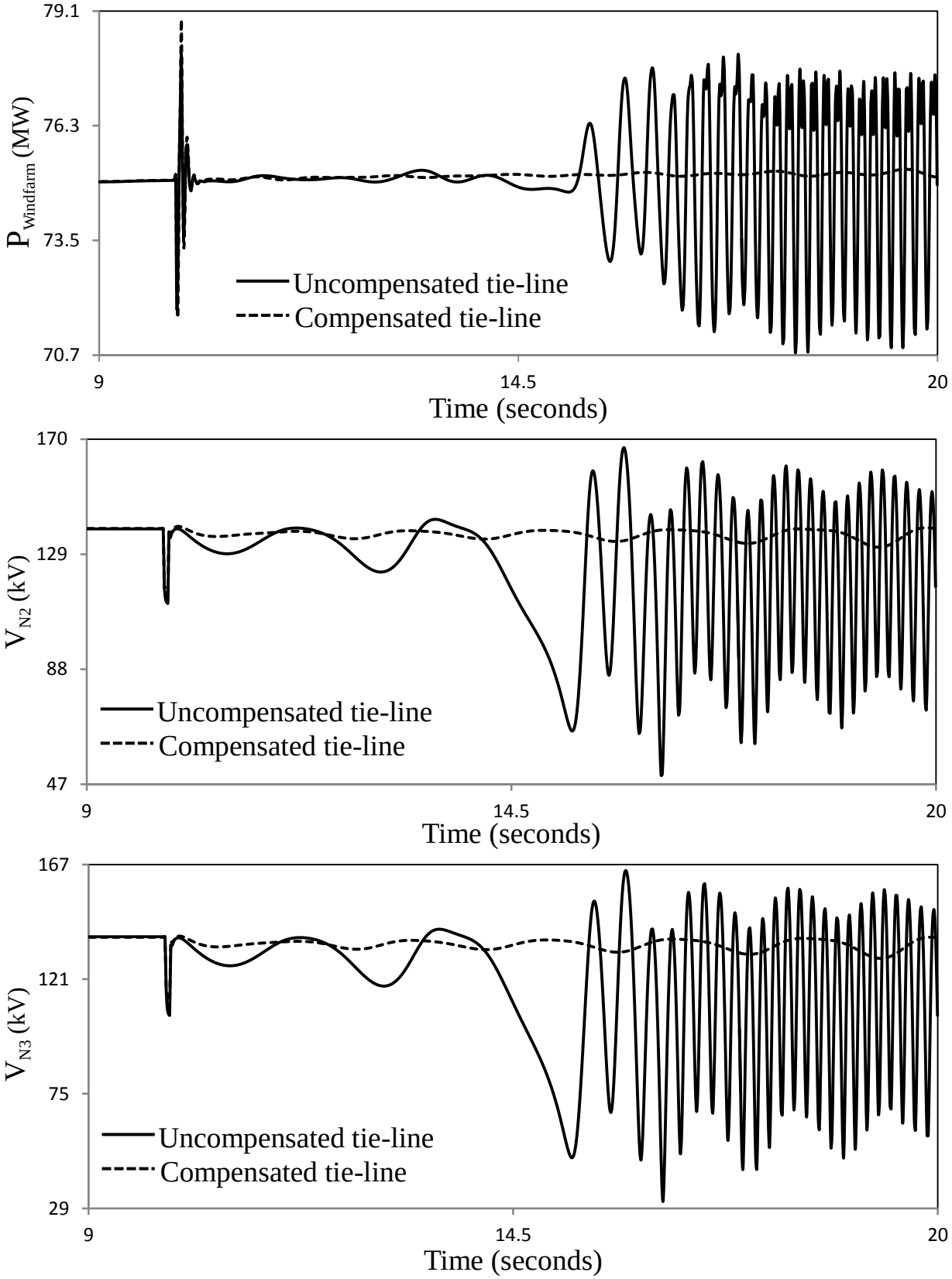

Figure 2.12: Continued.

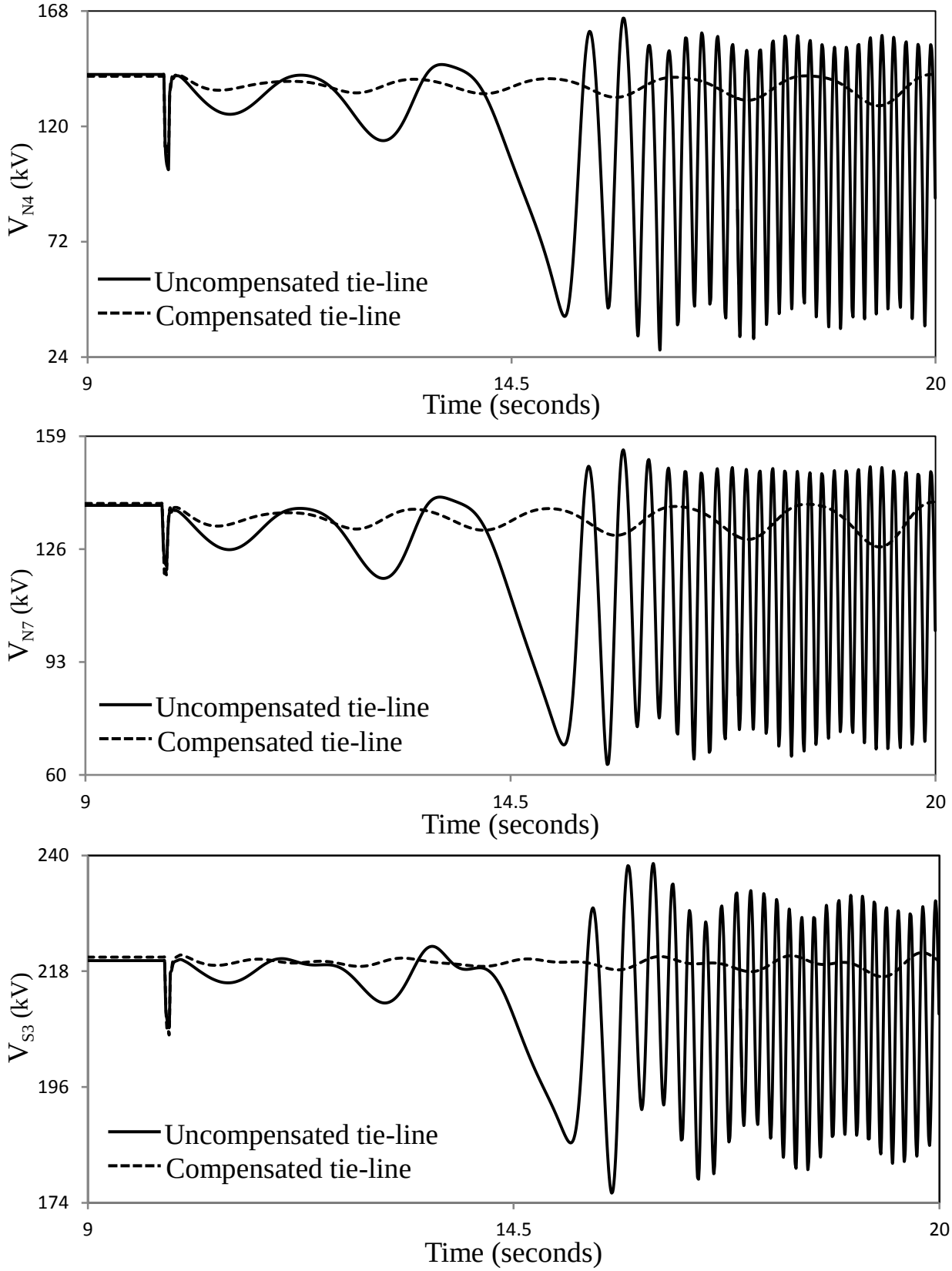

Figure 2.12: Continued.

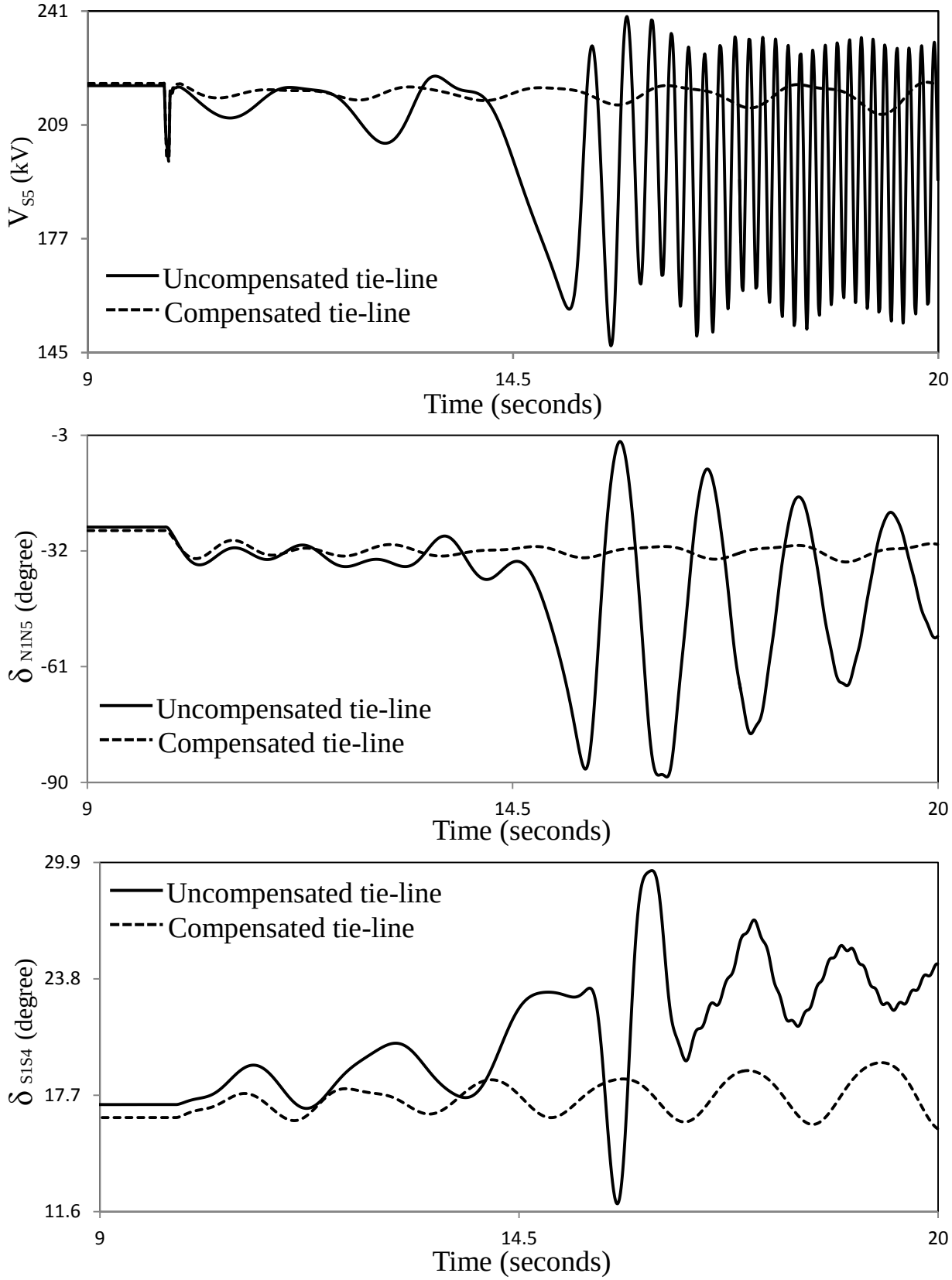

Figure 2.12: Continued.

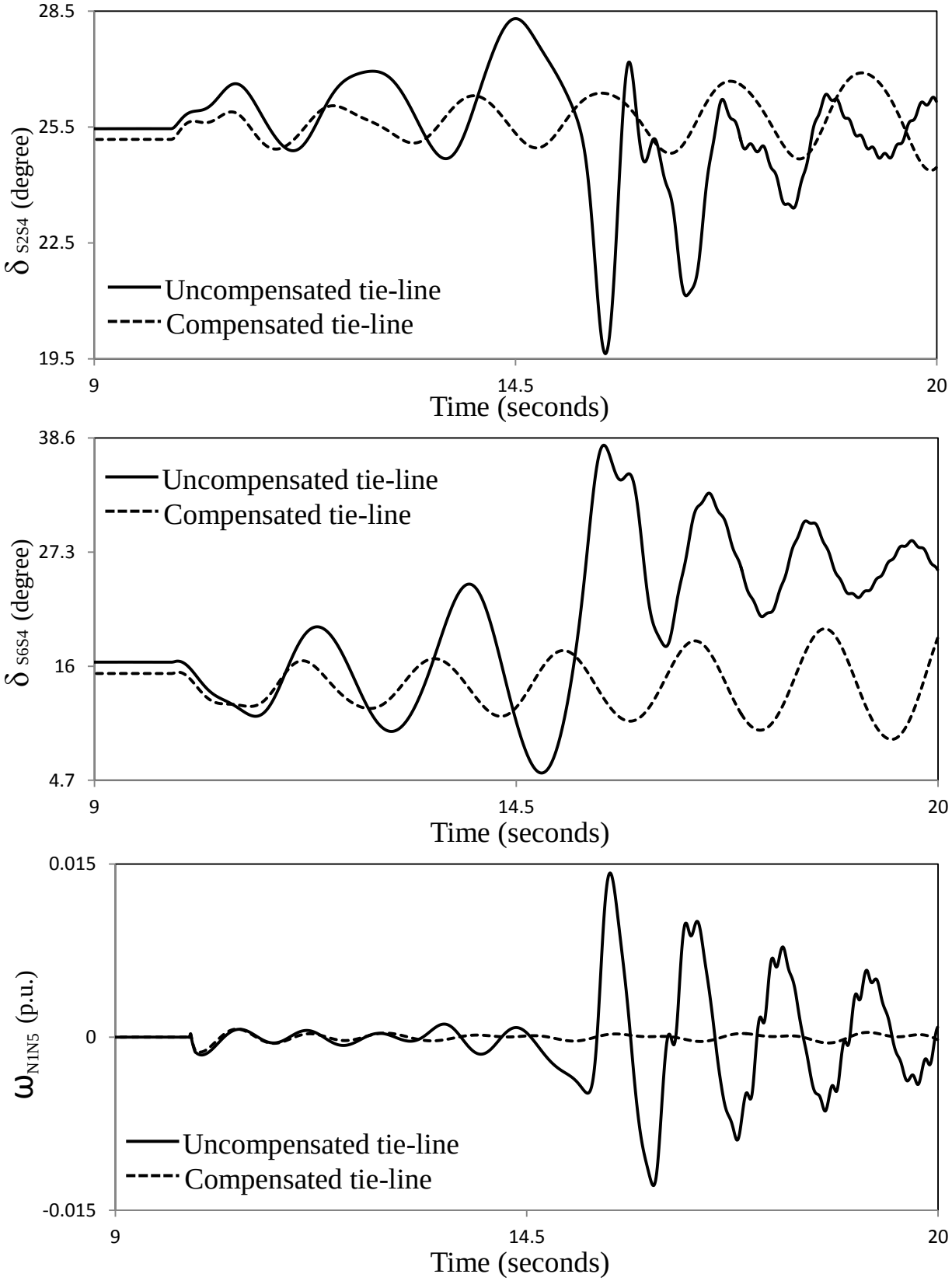

Figure 2.12: Continued.

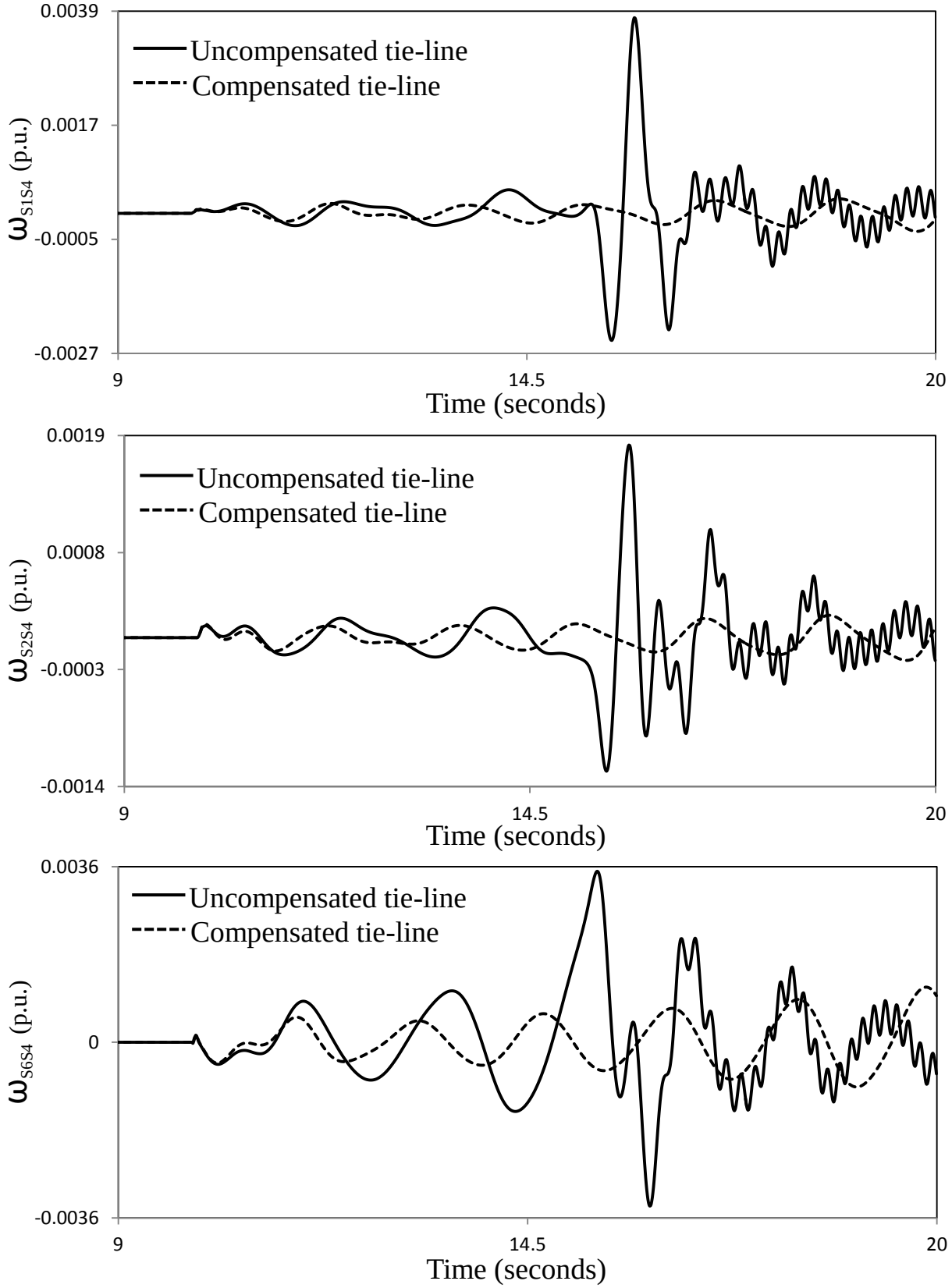

Figure 2.12: Continued.

2.5 Summary

In this chapter, the mathematical models of various components of the system under study are presented. A detailed description of the SaskPower North and South system models suitable for studying the dynamic performance of the HVAC interconnection is also presented. The results of digital time-domain simulations of a case study of the integrated system incorporating the HVAC interconnection during a three-phase fault are also presented.

Chapter 3

THE HYBRID THREE-PHASE THYRISTOR CONTROLLED SERIES CAPACITOR AND SYSTEM LOAD FLOW STUDIES

3.1 Introduction

In this chapter, the description and the basic principles of a TCSC as well as the derivation of its mathematical model are discussed. Modeling the TCSC in the ElectroMagnetic Transient Program (EMTP-RV) is also described. The load flow studies conducted on the SaskPower North and South systems as well as of the integrated system incorporating the HVAC 138 kV double-circuit tie-line and a hybrid TCSC compensation scheme are presented.

3.2 Thyristor Controlled Series Capacitor

The TCSC shown in Figure 3.1 consists of a number of series connected modules. In each module, the capacitor bank is provided with a parallel thyristor controlled inductor that circulates current pulses which add in phase with the line current. This boosts the capacitor voltage beyond the level that would be obtained by the line current alone. A Zinc oxide varistor is included in each module for secure overvoltage protection of the TCSC. Each thyristor is triggered once per cycle and has a conduction interval which is shorter than a half-cycle of the rated frequency. If the additional voltage created by the circulating current pulses is controlled to be proportional to the line current, the transmission system will perceive the TCSC as having a virtually increased reactance beyond the physical reactance of the capacitor. This feature which is referred to “vernier control” can be used for short-time transient control. The upper limit for vernier operation is a function of the line current magnitude and time spent at the operating point. Moreover, this scheme can provide an accurate setting of the compensation degree with a high

resolution as well as a subsynchronous resonance immune series compensation even at high compensation degrees [26] [49].

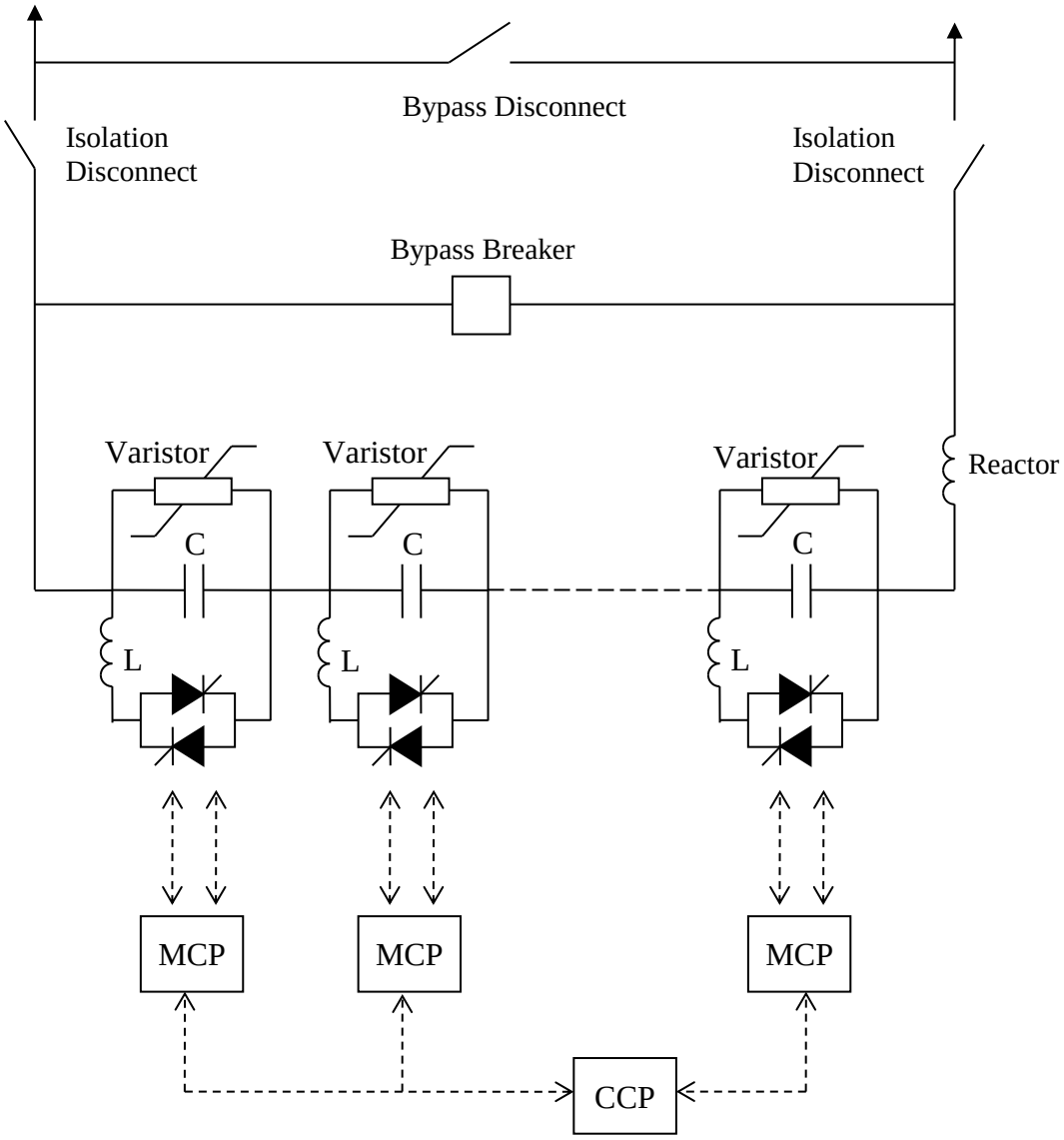

Figure 3.1: A multi-module TCSC.

The control and protection of TCSC are partitioned in two levels; common and module. Commands for both control and protective operations flow from the common level to the module level. Status information is sent back from each module level. The design concept is to permit

any module or combination of modules to be out of service while still being able to operate the remaining modules to benefit the power system.

The common-level protection detects problems affecting all modules, and as such, generally requires bypassing all modules with the bypass breaker. The module-level protection detects problems affecting a single-module and as such, may only initiate protective actions within the affected module. The thyristor switches allow for bypassing individual modules by continuous gating the thyristors, and this is an effective protective action for many potential internal failures (e.g., capacitor failure). However, for some serious problems within a module (e.g., varistor failure), protective actions may involve bypassing all modules with the bypass breaker.

3.3 Operation of the TCSC

3.3.1 Basic principles [50]

A simple understanding of TCSC functioning can be realized by analyzing the behavior of the circuit shown in Figure 3.2 which consists of a variable inductor connected in parallel with a fixed capacitor. The equivalent impedance, Z_{eq}, of this LC combination is expressed as:

$$Z_{eq} = -j\frac{1}{\omega C - \frac{1}{\omega L}} \tag{3.1}$$

The impedance of the capacitor alone, however, is given by $X_c = -j\frac{1}{\omega C}$.

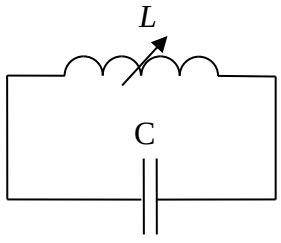

Figure 3.2: A variable inductor connected in parallel with a fixed capacitor.

If $\omega C - \left(\frac{1}{\omega L}\right) > 0$ or, in other words, $\omega L > \frac{1}{\omega C}$, the reactance of the fixed capacitor is less than that of the parallel-connected variable reactor and that this combination provides a

variable-capacitive reactance are both implied. Moreover, this inductor increases the equivalent-capacitive reactance of the LC combination above that of the fixed capacitor.

If $\omega C - \frac{1}{\omega L} = 0$, a resonance develops that results in an infinite-capacitive impedance. If, however, $\omega C - \frac{1}{\omega L} < 0$, the LC combination provides inductance above the value of the fixed inductor. This situation corresponds to the inductive-vernier mode of the TCSC operation.

In the variable-capacitive mode of the TCSC, as the inductive reactance of the variable inductor is increased, the equivalent-capacitive reactance is gradually decreased. The minimum equivalent-capacitive reactance is obtained for extremely large inductive reactance or when the variable inductor is open-circuited, in which the value is equal to the reactance of the fixed capacitor itself.

The behavior of the TCSC is similar to that of the parallel LC combination. The difference is that the LC-combination analysis is based on the presence of pure sinusoidal voltage and current in the circuit, whereas in the TCSC, the voltage and current are not sinusoidal because of the thyristor switchings. The analysis in this case is presented in Section 3.4.

3.3.2 Modes of TCSC operation

There are three modes of TCSC operation:

1. Bypassed-Thyristor Mode: the thyristors are made to fully conduct resulting in a continuous sinusoid of flow current through the thyristor valves (Figure 3.3 (a)). The TCSC module behaves like a parallel capacitor-inductor combination. The net current through the module, however, is inductive, for the susceptance of the reactor is chosen to be greater than that of the capacitor.

2. Blocked-Thyristor Mode: the firing pulses of the thyristor valves are blocked. The TCSC module is reduced to a fixed capacitor (Figure 3.3 (b)).

3. Partially Conducting Thyristor or Vernier Mode: This mode allows the TCSC to behave either as a continuously controllable capacitive reactance or as a continuously

controllable inductive reactance. It is achieved by varying the thyristor-pair firing angle in an appropriate range. In practice, the TCSC operates only in the *capacitive-vernier-control* mode. In such a mode, the thyristors are fired when the capacitor voltage and the capacitor current have opposite polarity. This condition causes the reactor current to have a direction opposite to that of the capacitor current, thereby, resulting in a loop-current flow in the TCSC controller. The loop current increases the voltage across the fixed capacitor, effectively enhancing the equivalent capacitive reactance and the series compensation level for the same value of line current. To preclude resonance, the firing angle α of the forward facing thyristor, as measured from the positive reaching a zero crossing of the capacitor voltage, is constrained in the range $\alpha_{min} \leq \alpha \leq 180°$. This constraint provides a continuous vernier of the TCSC module reactance. The loop current increases as α is decreased from 180° to α_{min}. The maximum TCSC reactance permissible with $\alpha = \alpha_{min}$ is typically two-and-half to three times the capacitor reactance at fundamental frequency.

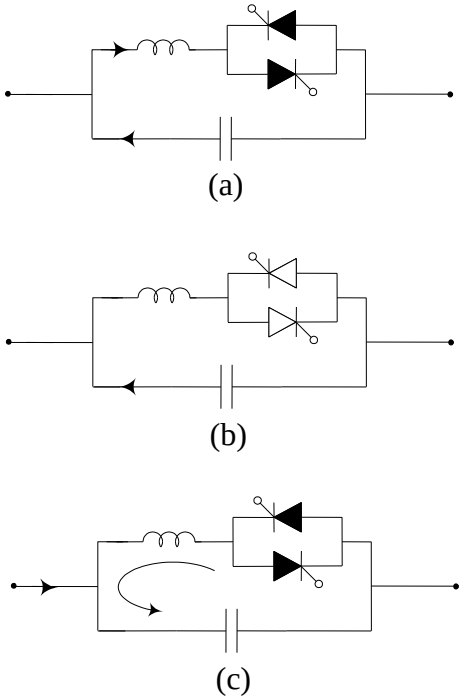

Figure 3.3: TCSC modes of operation: (a) Bypassed-Thyristor Mode, (b) Blocked Thyristor Mode, (c) Vernier Mode.

3.4 Analysis of the TCSC

The following "approximate" analysis of TCSC operation in the vernier-control mode is performed based on the simplified TCSC circuit shown in Figure 3.4 [50]. Transmission line current is assumed to be the independent-input-variable and is modeled as an external current source, $i_s(t)$. Moreover, it is assumed that the line current is sinusoidal, as field tests have demonstrated that very few harmonics exist in the line current [19].

The current through the fixed-series capacitor, *C*, is expressed as

$$C\frac{dv_c}{dt} = i_s(t) - i_T(t).u \tag{3.2}$$

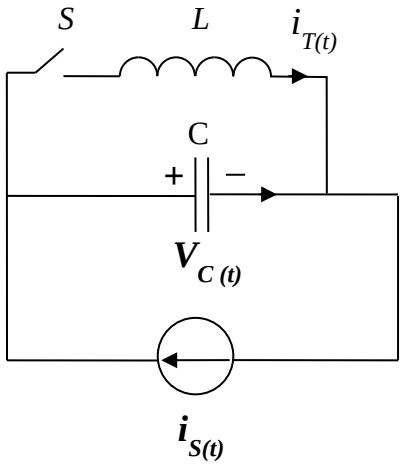

Figure 3.4: A simplified TCSC circuit.

The switching variable *u* is equal to 1 when the thyristor valves are conducting (switch S is closed). When the thyristor valves are blocked (switch S is open), *u*=0. The thyristor current, $i_T(t)$, can be described as

$$L\frac{di_T}{dt} = v_c.u \tag{3.3}$$

Let the line current, $i_s(t)$ be represented by

$$i_s(t) = I_m cos\omega t \tag{3.4}$$

Equations (3.3) and (3.4) can be solved with the knowledge of the instants of switching. In equidistant firing-pulse control, for balanced TCSC operation, the thyristors are switched on twice in each cycle of the line current at instants t_1 and t_3 given by

$$t_1 = -\frac{\beta}{\omega} \tag{3.5}$$

$$t_3 = \frac{\pi-\beta}{\omega} \tag{3.6}$$

where β is the angle of advance (before the forward voltage becomes zero). Or,

$$\beta = \pi - \alpha, \qquad 0 < \beta < \beta_{max} \tag{3.7}$$

The firing angle α is generated using a reference signal that can be in phase with the capacitor voltage. The thyristor switch S turns off at the instant t_2 and t_4 defined as:

$$t_2 = t_1 + \frac{\sigma}{\omega} \tag{3.8}$$

$$t_4 = t_3 + \frac{\sigma}{\omega} \tag{3.9}$$

where σ is the conduction angle and,

$$\sigma = 2\beta \tag{3.10}$$

Solving the TCSC equations (3.2 to 3.4) results in the steady-state thyristor current i_T, as:

$$i_T(t) = \frac{k^2}{k^2-1} I_m \left[cos\omega t - \frac{cos\beta}{cosk\beta} cos\omega_r t\right]; \qquad -\beta \leq \omega t \leq \beta \tag{3.11}$$

where

$$\omega_r = \frac{1}{\sqrt{LC}} \tag{3.12}$$

$$k = \frac{\omega_r}{\omega} = \sqrt{\frac{1}{\omega L}\frac{1}{\omega C}} = \sqrt{\frac{X_C}{X_L}} \tag{3.13}$$

and X_C is the nominal reactance of the fixed capacitor only. The steady-state capacitor voltage at the instant $\omega t = -\beta$ is expressed by:

$$v_{C1} = \frac{IMGX_C}{k^2-1}(\sin\beta - k\cos\beta\tan k\beta) \tag{3.14}$$

At $\omega t = \beta$, $i_T = 0$, and the capacitor voltage is given by:

$$v_C(t)|_{t=\frac{\beta}{\omega}} = v_{C2} = -v_{C1} \tag{3.15}$$

The capacitor voltage is finally obtained as:

$$v_C(t) = \frac{IMG\ X_C}{k^2-1}\left[-sin\omega t + k\frac{cos\beta}{cosk\beta}sin\omega_r t\right]; \qquad -\beta \le \omega t \le \beta \tag{3.16}$$

$$v_C(t) = v_{C2} + IMG\ X_C(sin\omega t - sin\beta); \qquad \beta \le \omega t \le \pi - \beta \tag{3.17}$$

Because the nonsinusoidal capacitor voltage, v_C, has odd symmetry about the axis $\omega t = 0$, the fundamental component, V_{CF}, is obtained as:

$$V_{CF} = \frac{4}{\pi}\int_0^{\pi/2} v_C(t) sin\ \omega t\ d(\omega t) \tag{3.18}$$

The equivalent TCSC reactance is computed as the ratio of V_{CF} to I_m:

$$X_{TCSC} = \frac{V_{CF}}{I_m} = X_C - \frac{X_C^2}{(X_C - X_L)}\frac{2\beta + sin2\beta}{\pi} + \frac{4X_C^2}{(X_C - X_L)}\frac{cos^2\beta}{(k^2-1)}\frac{(ktank\beta - tan\beta)}{\pi} \tag{3.19}$$

The net reactance of the TCSC in per unit of X_C, denoted by $X_{net}(= X_{TCSC}/X_C$, sometimes called the boost factor) can be expressed as:

$$X_{net} = 1 - \frac{X_C}{(X_C - X_L)}\frac{\sigma + sin\sigma}{\pi} + \frac{4X_C}{(X_C - X_L)}\frac{cos^2 0.5\sigma}{(k^2-1)}\frac{(ktan0.5k\sigma - tan0.5\sigma)}{\pi} \tag{3.20}$$

Because the TCSC is used mainly as a capacitive device, the convention is to define positive reactance as capacitive and negative reactance as inductive. As an example, $X_{net} = +2$ implies that the thyristor are fired so that the resulting circulating current in the fixed capacitor-thyristor controlled reactor loop causes a 60-Hz voltage of $2X_C I_{line}$ p.u. to appear across the fixed capacitor, which lags the line current by 90 °.

The traditional boost control method (constant firing angle delay (CFAD)) controls the firing angle $\beta = \pi - \alpha$ of the thyristor. A rather non-linear relationship exists between the boost factor *kB* and the steady state conduction angle $\sigma = 2\beta$, making *kB* very sensitive to the instant of triggering when the TCSC operates at a high boost factor. Further, at transients, a complicated dynamic characteristic governs the relationship between the firing angle and the conduction angle. Instead of controlling the thyristor firing angle, another control scheme, named "Synchronous Voltage Reversal" (SVR), is being used. It aims to control the instant when the capacitor voltage crosses zero [51], [52]. This eliminates the non-linearity in the boost

control and results in that the TCSC apparent impedance at subsynchronous frequencies appears as inductive. Furthermore, at low boost factors, SVR controlled TCSC can provide much better SSR damping than conventional CFAD control [53]. In the studies conducted in this thesis, the SVR control is used.

3.5 The Hybrid Three-Phase-TCSC Compensation Scheme

Figure 3.5 shows a three-phase hybrid series capacitive compensation. In such a scheme, the series capacitive compensation in each phase is created, cost effectively, using a TCSC in series with a fixed capacitor (C_C). Thus, the phase balance is maintained at the power frequency as well as at any other frequency. This can be expressed mathematically as follows:

1) At the power frequency, the series reactance between buses X and Y, in Figure 3.5, in phases a, b, and c are given by:

$$X_a = X_b = X_c = \frac{1}{j\omega_0 C_C} - jX_{TCSC_0} \tag{3.21}$$

where $-jX_{TCSC_0}$ is the effective capacitive reactance of the TCSC at the power frequency.

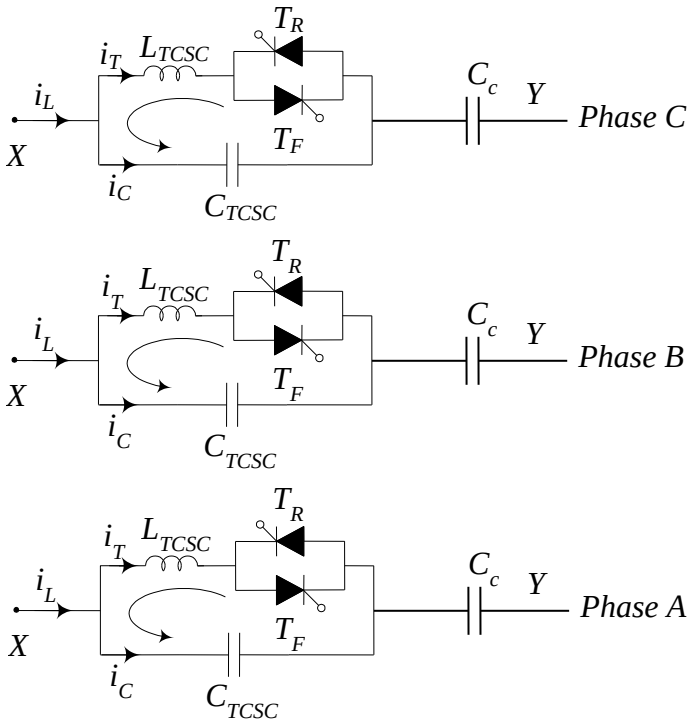

Figure 3.5: A hybrid three-phase-TCSC compensation scheme.

2) During any other frequency, f_e, including subsynchronous frequencies,

$$X_a = X_b = X_c = \frac{1}{j\omega_e C_C} - jX_{TCSC_0} - j\Delta X_{TCSC} \quad (3.22)$$

The first terms in Equations (3.21) and (3.22) are different because of the difference in frequency. The third term in Equation (3.22) represents the change in the effective capacitive reactance of the TCSC due to the action of the TCSC supplement controller.

3.6 Modeling the Three-Phase-TCSC in the EMTP-RV

The three-phase TCSC is modeled in the EMTP-RV as a single module using ideal thyristor pairs and RC snubber circuits as shown in Figure 3.6 [54], [55]. A Phase Locked Loop (PLL) is used to extract phase information of fundamental frequency line current, which will be used to synchronize TCSC operation. The thyristor gating control is based on the Synchronous Voltage Reversal (SVR) technique [51] - [53]. The TCSC impedance is measured in terms of a boost factor *kB*, which is the ratio of the apparent reactance of the TCSC seen from the line to the physical reactance of the TCSC capacitor bank. A positive value of *kB* is considered for capacitive operation. A low-pass filter based estimation algorithm is used to estimate the voltage and the current phasors. A boost measurement block performs complex impedance calculations for the boost factor of the TCSC as $\boldsymbol{kB = Imag\left\{\hat{V}_C / \hat{I}_C\right\}/X_{CTCSC}}$, where $\hat{V}_C$ and $\hat{I}_C$ are the estimated phase voltage and current and $\boldsymbol{X_{CTCSC}}$ is the capacitive reactance of the TCSC capacitor branch at the fundamental frequency. A proportional-integral (PI) control based boost level controller is implemented to control the TCSC boost level to the desired value by adjusting the instant of the expected capacitor voltage zero crossing. The integral part of the controller helps in removing the steady state errors. The controller parameters were determined by performing repeated time domain simulations for the different operating conditions. This algorithm uses the difference between the actual boost level and the reference boost level (*err*) shown in Figure 3.6 as an objective function. The algorithm starts with arbitrary initial values for the control parameters and calculates the values of the objective function each time. The control parameters are incremented for the next iteration and the procedure is repeated until the objective function approaches a minimum value (below a threshold value). The procedure

described above is widely applied by industry for tuning of the controller parameters. The multiple simulations run based tuning procedure similar to the above was reported in [56], [57].

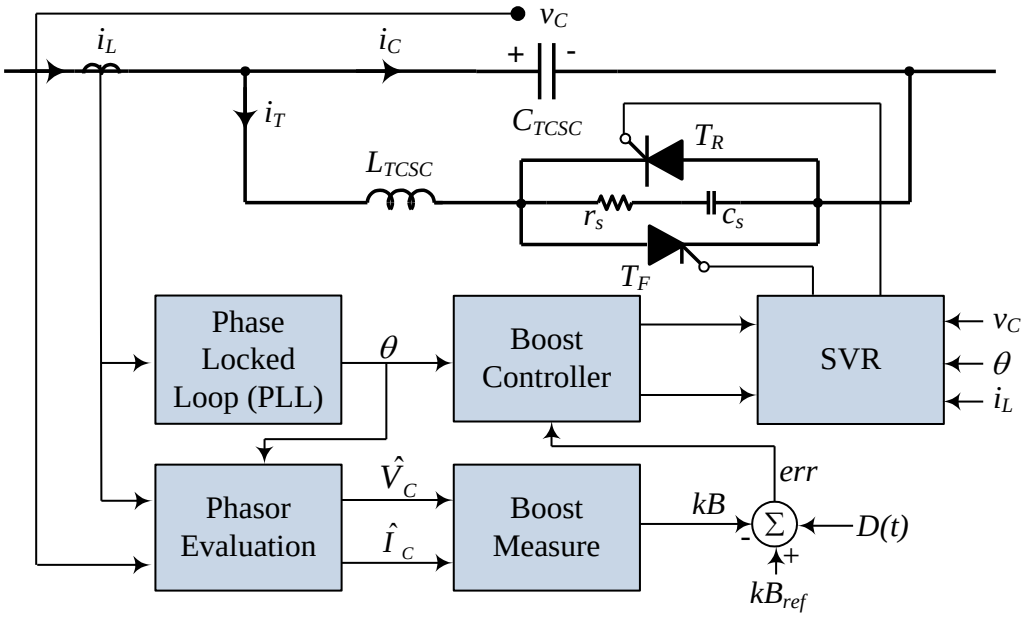

Figure 3.6: Block diagram of a TCSC controller.

In Figure 3.6, kB_{ref} is the TCSC boost level set point and *D(t)* is the supplementary control signal for damping low-frequency oscillations. The Synchronous Voltage Reversal block solves for angle γ from the non-linear relation, $u_{CZ} = X_0 i_{LM}[\lambda\gamma - \tan(\lambda\gamma)]$, where u_{CZ} is the estimated capacitor voltage at the desired instant when the capacitor voltage zero crossing occurs, i_{LM} is the measured value of the line current i_L, X_0 is the TCSC capacitor reactance at the TCSC resonance frequency, λ is the ratio between the TCSC resonance frequency and the system fundamental frequency, and γ is the angle difference between the firing time and the voltage zero-crossing. The value of γ is used to calculate the exact firing instants of the individual thyristors. The non-linear relationship between the boost factor and the thyristor firing angle α is shown in Figure 3.7.

The most striking feature of the TCSC is that it behaves like an inductor at subsynchronous frequencies. This prevents the occurrence of a series resonance within a certain critical frequency band. On the other hand, the TCSC behaves like a capacitor at the power frequency. The transition of the virtual reactance of the TCSC from inductive to capacitive

outside the subsynchronous frequency band is achieved by means of a reactance controller (like the SVR technique), providing a controllable capacitive reactance around the power frequency as shown in Figure 3.8 [58]. The details of the SVR algorithm are given in [51], [52].

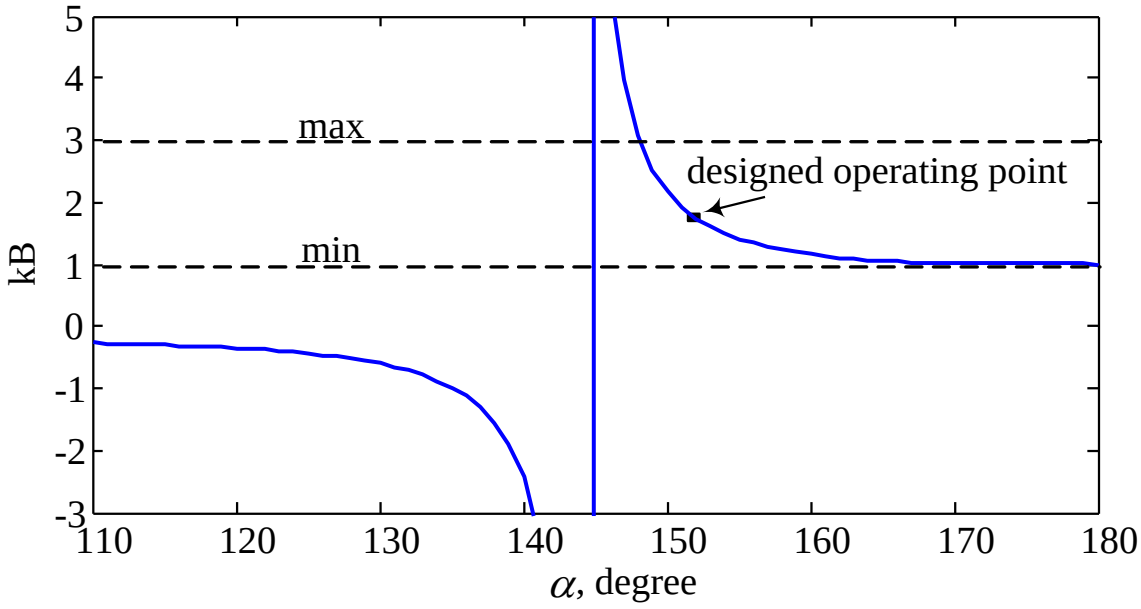

Figure 3.7: TCSC boost factor as a function of the thyristor firing angle α.

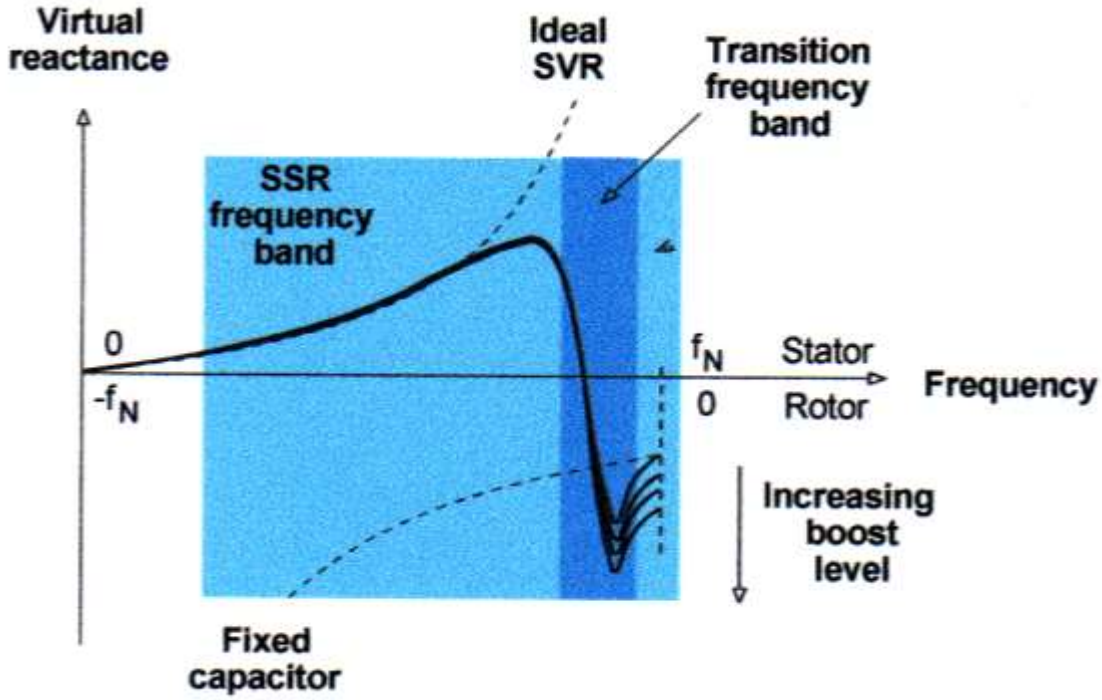

Figure 3.8: Effect of the SVR technique on the virtual reactance of the TCSC.

3.7 System Load Flow Studies

As mentioned earlier in Chapters 1 and 2, it is planned to transmit 50 MW from the SaskPower North system to its South system through a "new" 260 km, 138 kV tie-line. With this new tie-line, it is required to still be able to keep the imported/exported power from Manitoba grid to a minimum.

The results of the load flow studies (the bus voltages and the real power flows) for the SaskPower North and South systems are shown in Figures 3.9 and 3.10 respectively. It can be seen from these figures that the North and South systems are exporting 0.1 MW and 0.09 MW respectively to the Manitoba grid. It can also be seen from Figure 3.9 that after the interconnection with the SaskPower South system, the 50 MW which will be transmitted to the South system is supplied mainly from generator G_{N5} (231.6 MVA rating).

Figure 3.11 shows the results of the load flow studies (the bus voltages and the real power flows) for the SaskPower integrated system incorporating a 260 km, 138 kV uncompensated double-circuit AC tie-line. It can be seen from this figure that the new line results in changing the loop power flow profile as the power exported from the North system to the Manitoba grid is increased to 40 MW, and the South system is now importing 38.94 MW although the net power exchange with the Manitoba grid still at a minimum level.

Figure 3.12 shows the results of the load flow studies (the bus voltages and the real power flows) for the SaskPower integrated system incorporating a 260 km, 138 kV AC tie-line with a hybrid three-phase-TCSC compensation scheme. The comparison between this figure and Figures 3.9 and 3.10 shows that, generally, the TCSC compensated tie-line does not result in significant changes in the loop power flow profiles of the SaskPower North and South systems. Another point that could be observed from Figure 3.12 is that the net power exchange with the Manitoba grid is still maintained at a minimum level (almost zero).

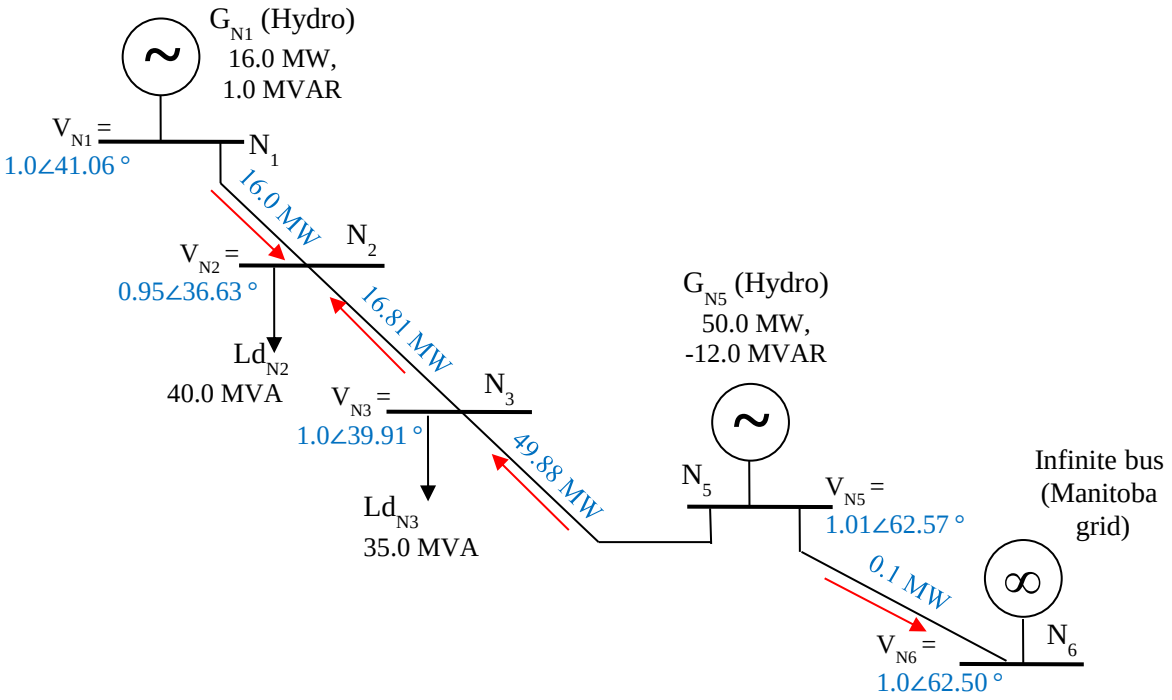

Figure 3.9: SaskPower North system load flow results.

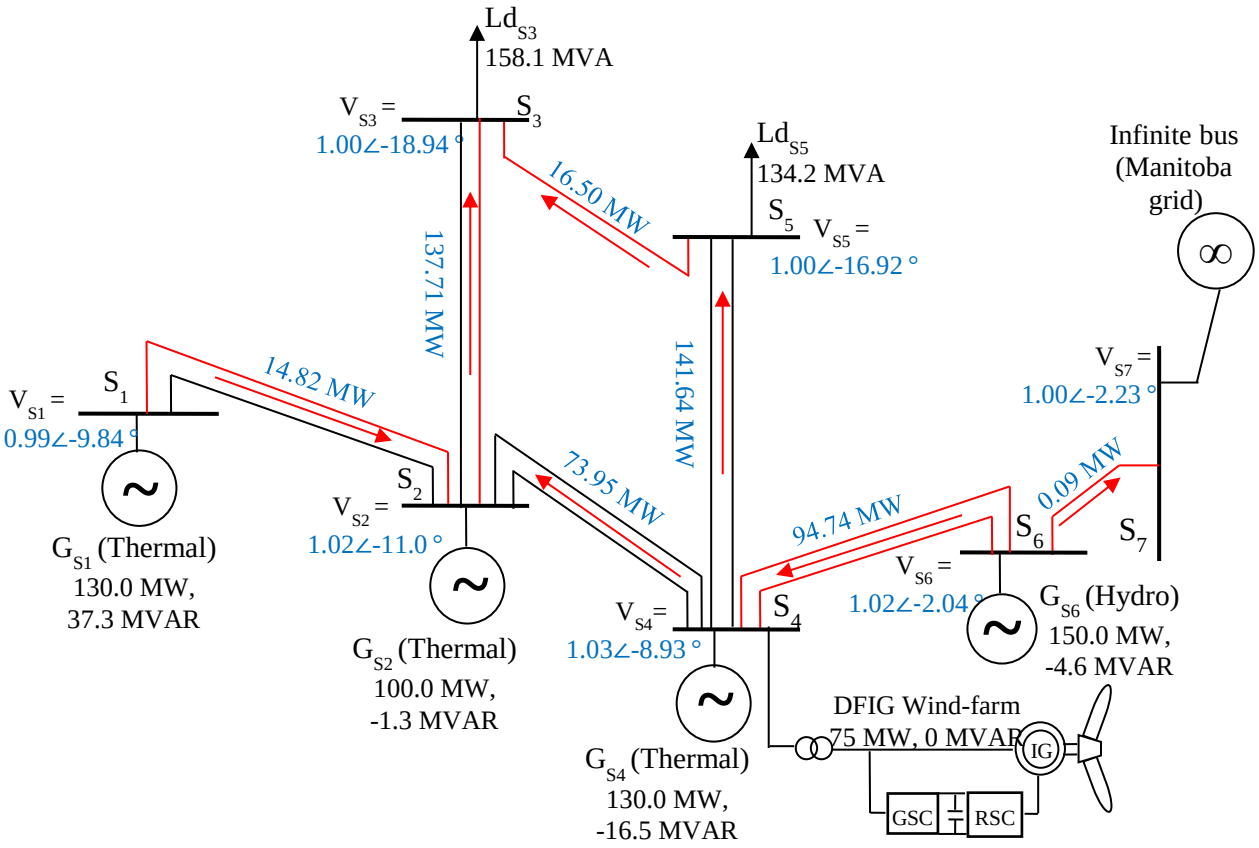

Figure 3.10: The modeled SaskPower South system load flow results.

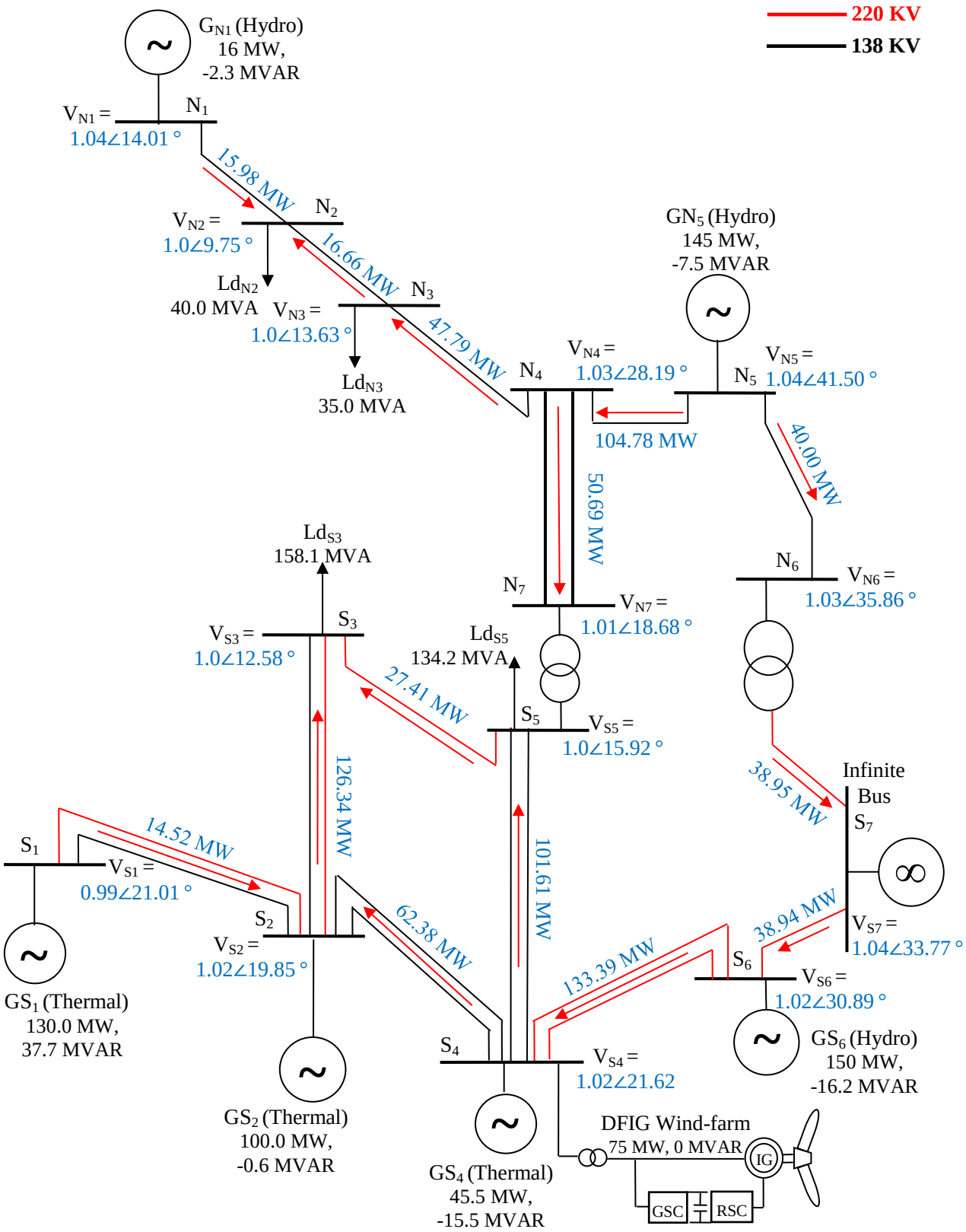

Figure 3.11: Load flow results of SaskPower integrated system incorporating a HVAC interconnection.

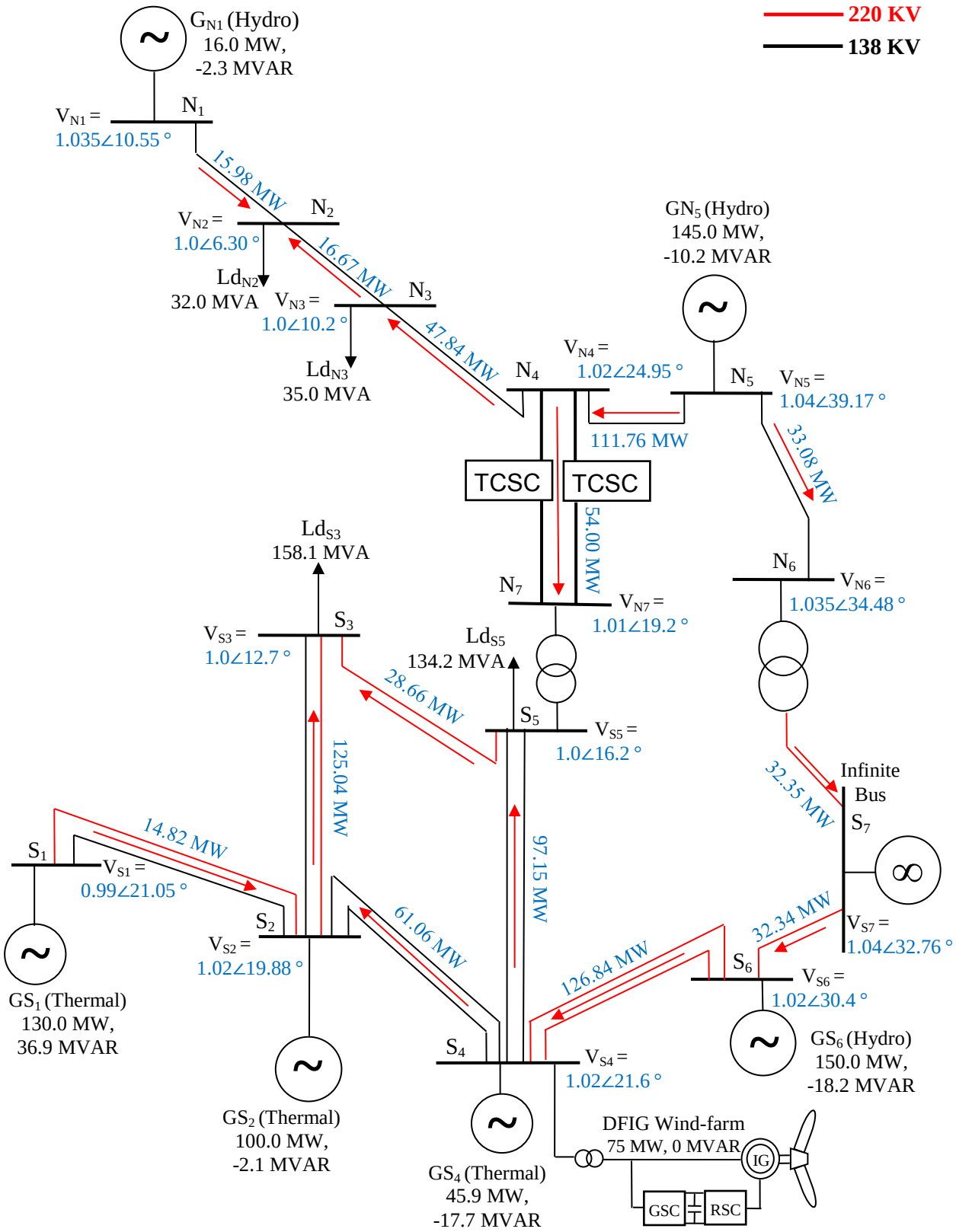

Figure 3.12: Load flow results of SaskPower integrated system incorporating a hybrid three-phase-TCSC compensated tie-line.

3.8 Summary

This chapter presents the description, basic principles and the derivation of the mathematical model of a TCSC. A hybrid series capacitive compensation scheme consisting of a TCSC in series with a fixed capacitor is also introduced. This compensation scheme is incorporated in the AC tie-line connecting the SaskPower North and South systems. The effectiveness of the scheme in damping power system oscillations is investigated in the next chapter.

Chapter 4

DYNAMIC PERFORMANCE OF THE HYBRID THREE-PHASE-TCSC COMPENSATION SCHEME

4.1 Introduction

The control offered by the TCSC is an "impedance" type control, i.e. the inserted voltage is proportional to the line current. This type of control normally is best suited to applications in power flow corridors, where a well-defined phase angle difference exists between the ends of the transmission line to be compensated and controlled. As a result, transient stability improvement and the increase in the maximum real power transmitted can be achieved. A TCSC could also be used, however, to provide additional damping to the electromechanical (0.5 - 2 Hz) power oscillations as it provides fast speed of response and executes any switching pattern without restrictions that may apply for mechanical breakers.

In this chapter, the effectiveness of the hybrid three-phase TCSC compensation scheme in damping power system oscillations is investigated. In this regard, attention is focused on the damping of the real power flow on the tie-line. For this purpose, the scheme is assumed to be installed in the 260 km, 138 kV double-circuit tie-line between buses N_4 and N_7 (Figure 3.12) where the TCSC is providing 50% of the total capacitive compensation ($X_{CC} = X_{TCSC}$). Several time-domain simulation case studies of three-cycle, three-phase faults at different locations are carried out. The performance of the TCSC compensation scheme in each case study is compared to the corresponding case with only fixed capacitor compensation.

4.2 TCSC Power Oscillation Damping Controller

As the real power flow in a transmission line is proportional to the inverse of the total reactance, power oscillation damping can be achieved by properly modulating the TCSC

reactance. The TCSC can be made to dynamically vary the series-compensation level in response to the controller-input signal so that the resulting changes in the power flow enhance the system damping. The traditional type of controller for Power Oscillation Damping (POD) purposes uses cascade-connected wash-out filters and linear lead-lag compensators to generate the desired reactance modulation signal. The purpose of the wash-out filters is to eliminate the average and extract the oscillating part of the input signal. The lead-lag compensators provide the desired phase shift at the oscillation frequency. Such a controller is illustrated in Figure 4.1 [59], [60]. In some situations, a simple controller consists of only the wash-out filters can have a better performance than that of the lead-lag controller. Such a controller, shown in Figure 4.2 can be regarded as a proportional type controller.

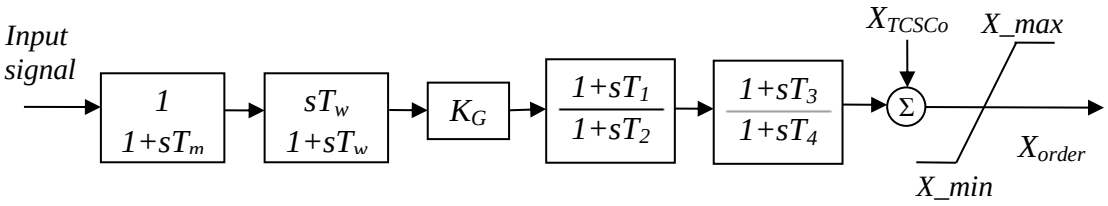

Figure 4.1: Structure of a lead-lag POD controller.

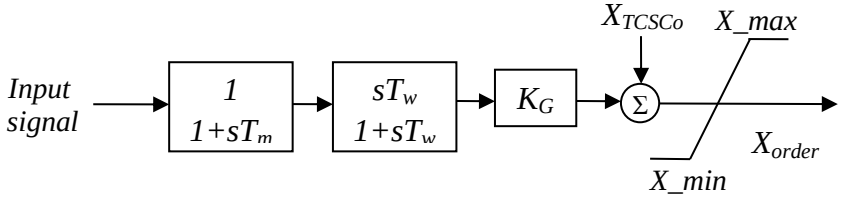

Figure 4.2: Structure of a simple POD controller.

The selection of the appropriate input (stabilizing) signal is an important issue in the design of an effective and robust controller. The selected input signal must yield correct control action when a severe fault occurs in the system. As an example, it was reported in [61] that if the real power is used as the input signal of a pure derivative controller, the output control signal may cause negative damping effects in the presence of disturbances involving large changes in the generator power angles.

The input signals could be local (e.g. real power flows) or remote (e.g. load angles or speed deviations of remote generators). If a wide-area network of Synchronized Phasor

Measurement Units (PMU) is available, then the remote signals can be downloaded at the controller in real time without delay [62] – [66]. In the studies conducted in this thesis, it is assumed the availability of a wide-area network of PMU units where the supplemental controller input (stabilizing) signals can be downloaded at the controllers in real time without delay [63] – [66]. In this regards, the generator load angles, measured with respect to the load angle of a reference generator (δ_{N5S4} and δ_{N5S6}) are selected as the supplemental controller stabilizing signals for the TCSC. The selection of these stabilizing signals δ_{N5S4} and δ_{N5S6} for the TCSC supplemental control is based on the detailed studies reported in [33] that conclude such kind of stabilizing signal is the best one among other signals (relative speeds and transmission line real power flow).

In the studies conducted in this thesis, the TCSC supplemental control parameters are determined by performing multiple time domain simulations with the aim of improving the transient responses of the system. It is worth emphasizing that the obtained controller parameters are not optimal and better parameters could be obtained by other control design techniques such as adaptive control, fuzzy logic and neural network techniques. The design of a controller using any of these techniques is out of scope of this thesis.

4.3 Case Study I: Temporary Three-Phase Fault with a Duration of 0.05 Seconds on the Virtual Transmission Line N_6-S_7 near Bus N_6

The fault location is shown in Figure 4.3. Generator G_{N5} load angle, measured with respect to generator G_{S4} load angle (δ_{N5S4}) is selected as the TCSC supplemental control stabilizing signal as it provides a noticeable improvement in the damping of the power system oscillations. Selected transmission line real power flows, generator load angles and speeds (measured with respect to generator G_{N5} load angle and speed) and system bus voltages during and after the fault clearing are illustrated in Figures 4.4 to 4.7 respectively. The transfer function of the TCSC supplemental control is given by

$$G_{\delta_{N5S4}}(s) = 0.1\,\frac{10}{(s+10)}\,\frac{0.7S}{(0.7s+1)}\,\frac{(1+0.766S)}{(1+0.4S)} \tag{4.1}$$

The following observations are made from Figures 4.4 to 4.7:

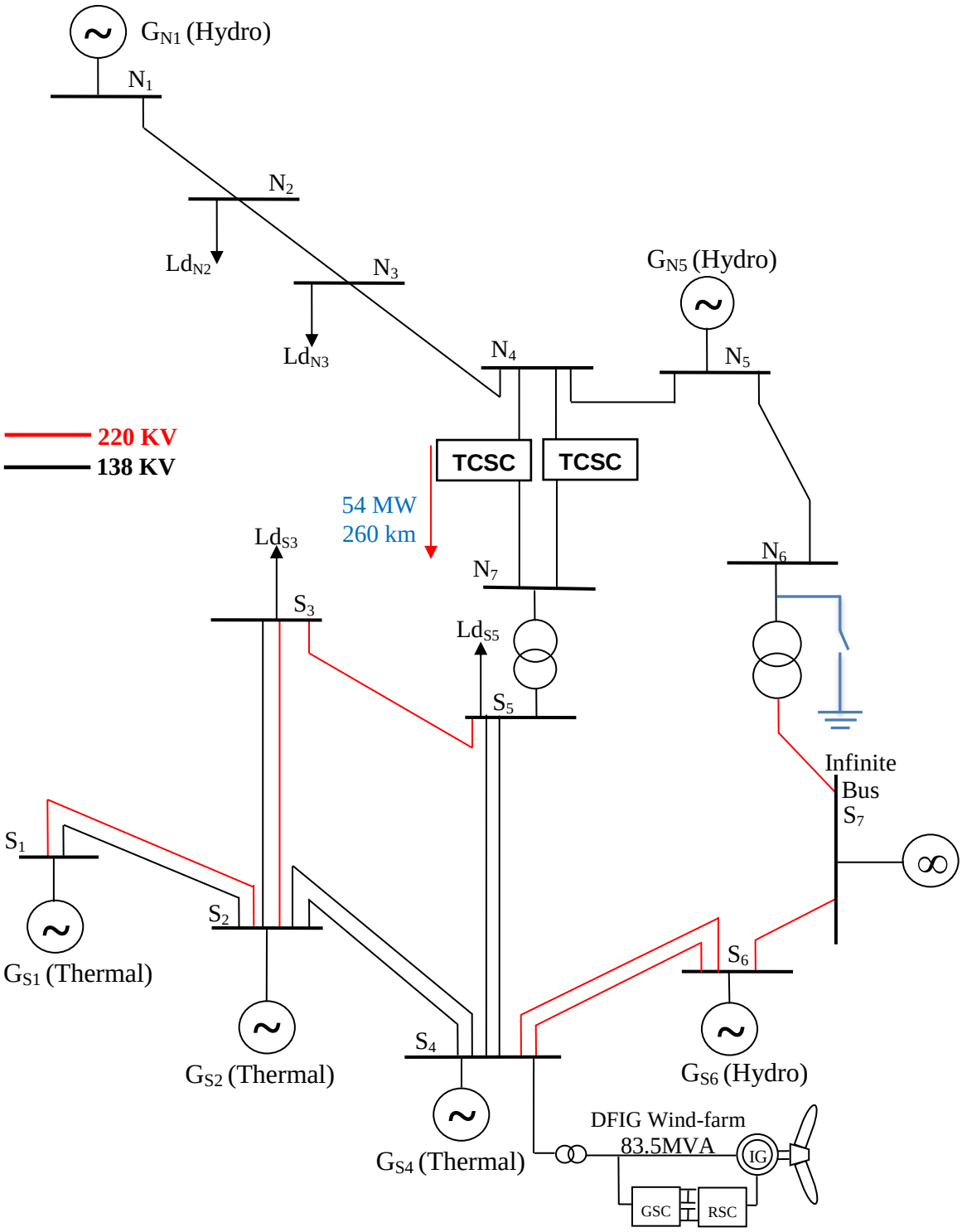

Figure 4.3: Case Study I: temporary three-phase fault with a duration of 0.05 seconds on the virtual transmission line N_6-S_7 near bus N_6.

- In the case of fixed capacitor compensation, the system is first swing stable but the post-contingency oscillations are not well-damped especially in the generator relative load angles and speeds.

- The TCSC supplemental controller reduces the first and subsequent swings of the tie-line real power flow as well as of the generator load angles and speeds and provides a better damping than in the case of fixed capacitor compensation.

- In the case of the TCSC compensation scheme, Figure 4.7 shows that the oscillations in the voltages of buses N_6 and S_7 are relatively smaller than in the case of fixed capacitor compensation. Moreover, the TCSC supplemental controller provides faster damping of these oscillations.

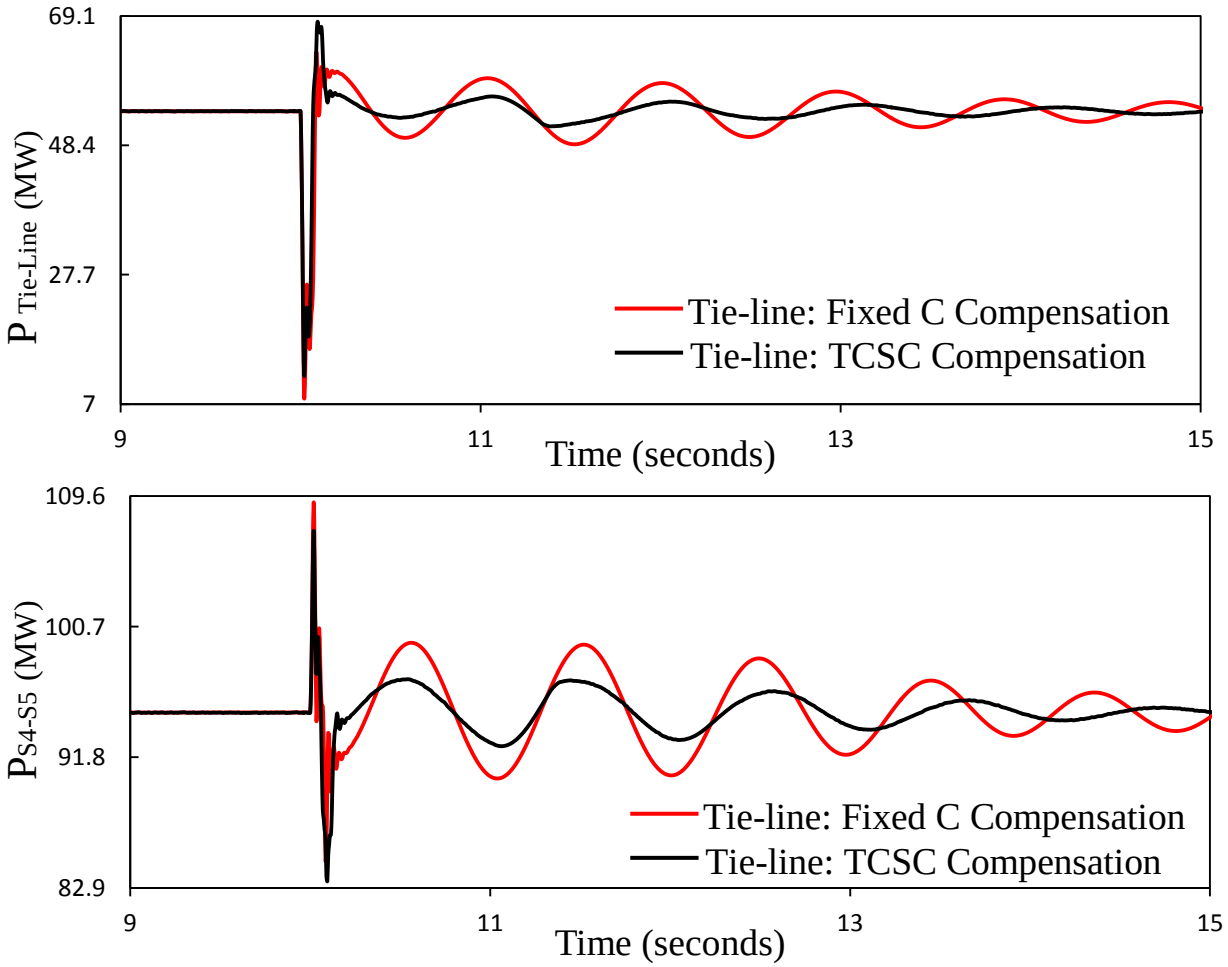

Figure 4.4: Real power flows on the tie-line and other transmission lines during and after clearing a temporary three-phase fault with a duration of 0.05 seconds on the virtual transmission line N_6-S_7 (case study I).

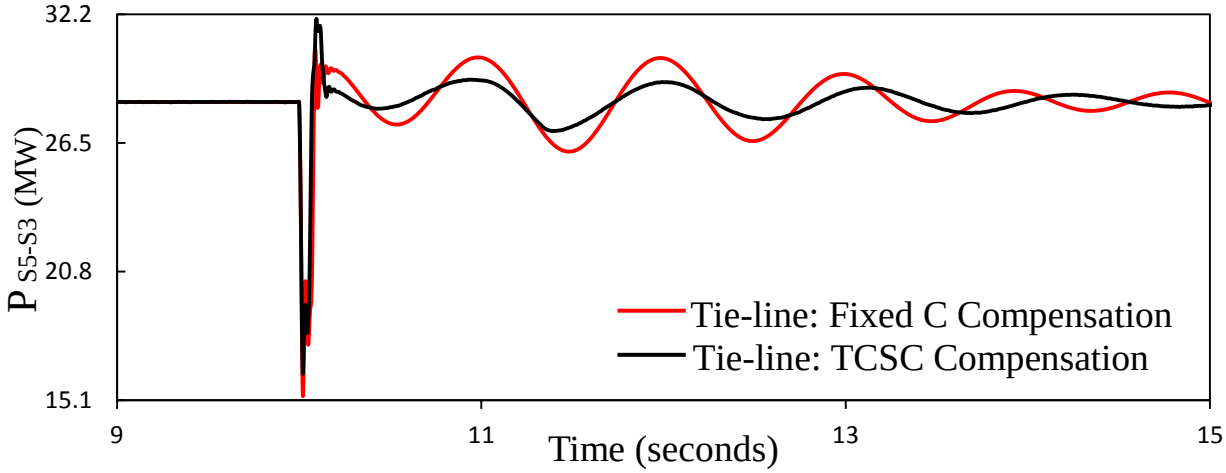

Figure 4.4: Continued.

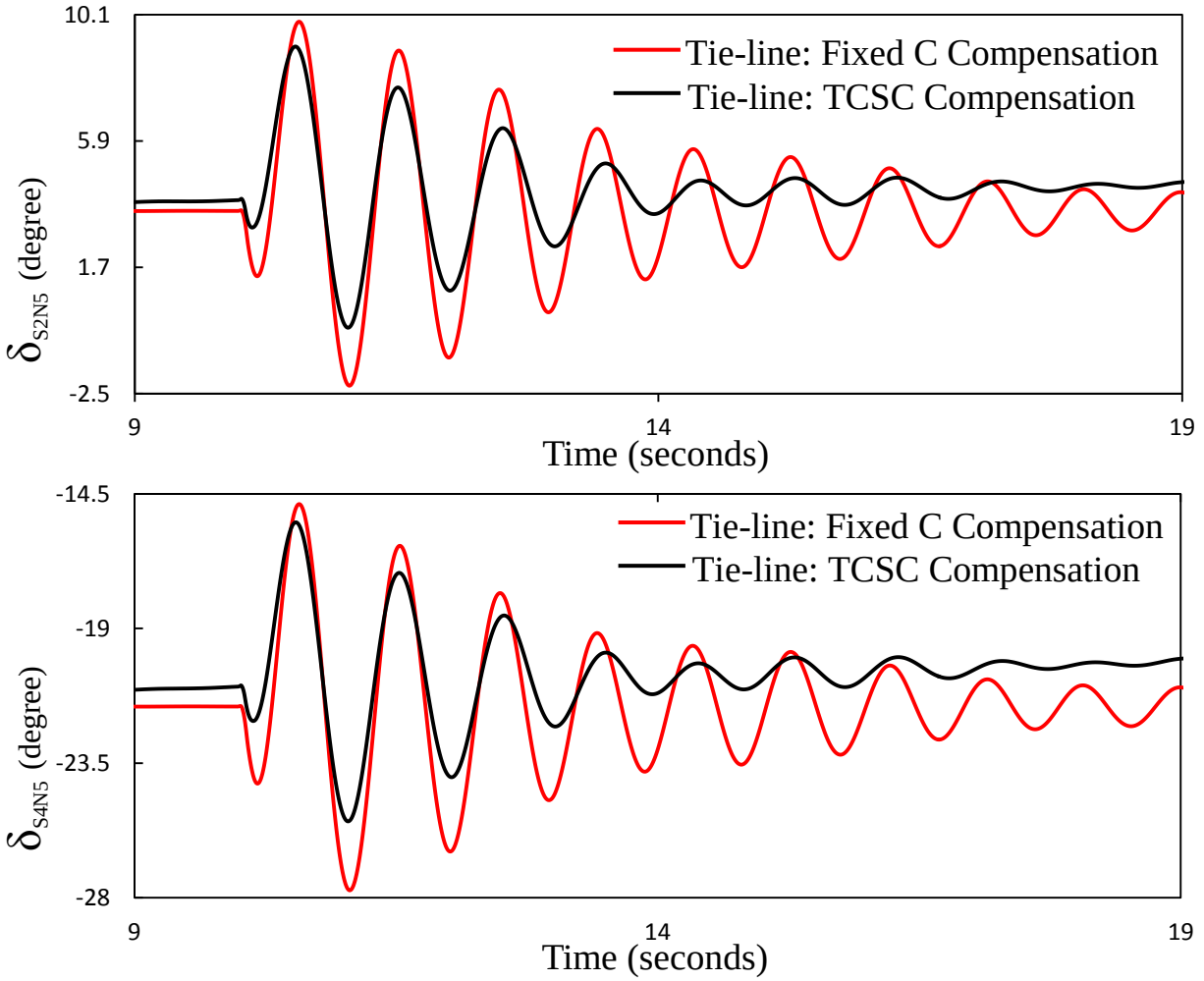

Figure 4.5: Generator load angles, measured with respect to generator G_{N5} load angle, during and after clearing a temporary three-phase fault with a duration of 0.05 seconds on the virtual transmission line N_6-S_7 (case study I).

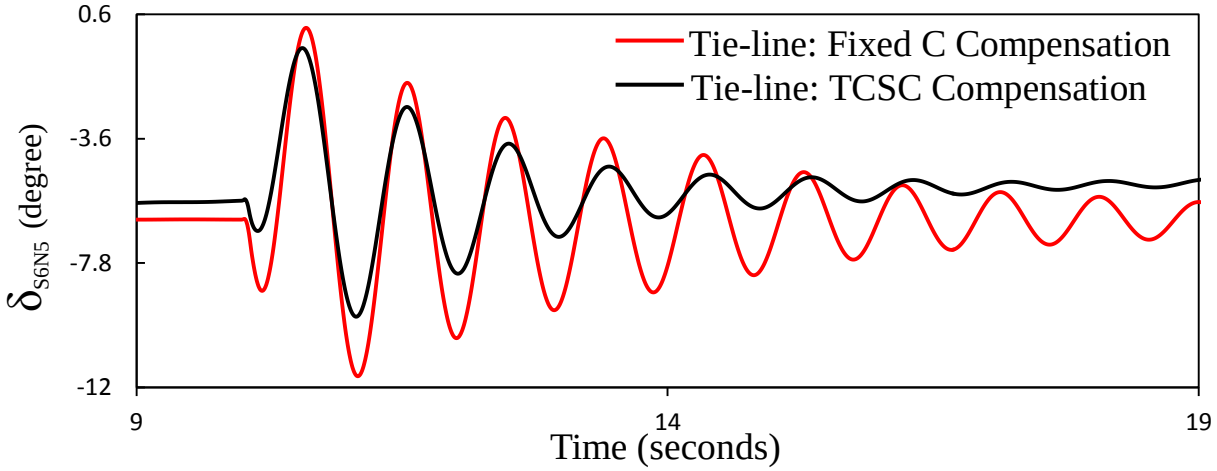

Figure 4.5: Continued.

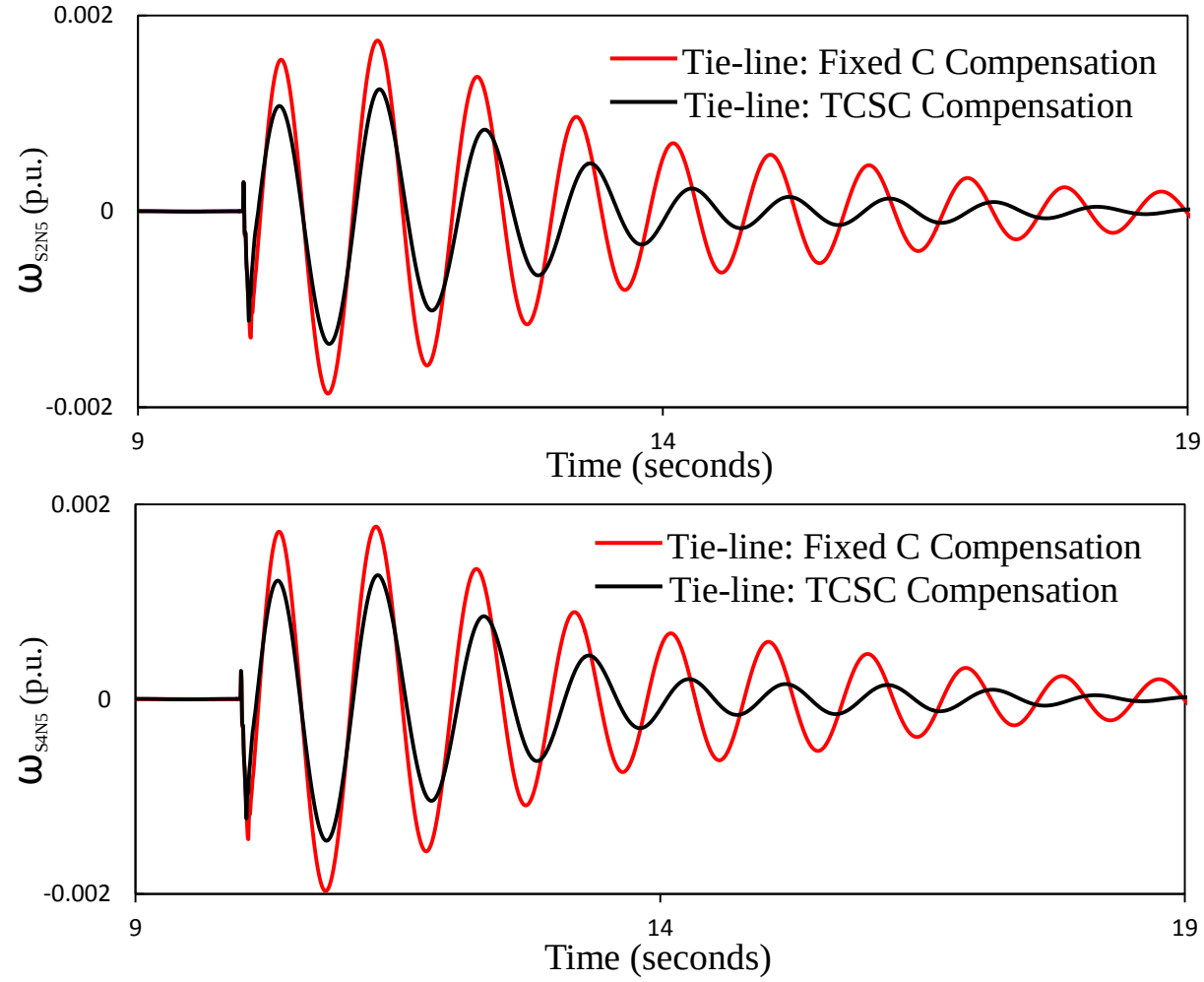

Figure 4.6: Generator speeds, measured with respect to generator G_{N5} speed, during and after clearing a temporary three-phase fault with a duration of 0.05 seconds on the virtual transmission line N_6-S_7 (case study I).

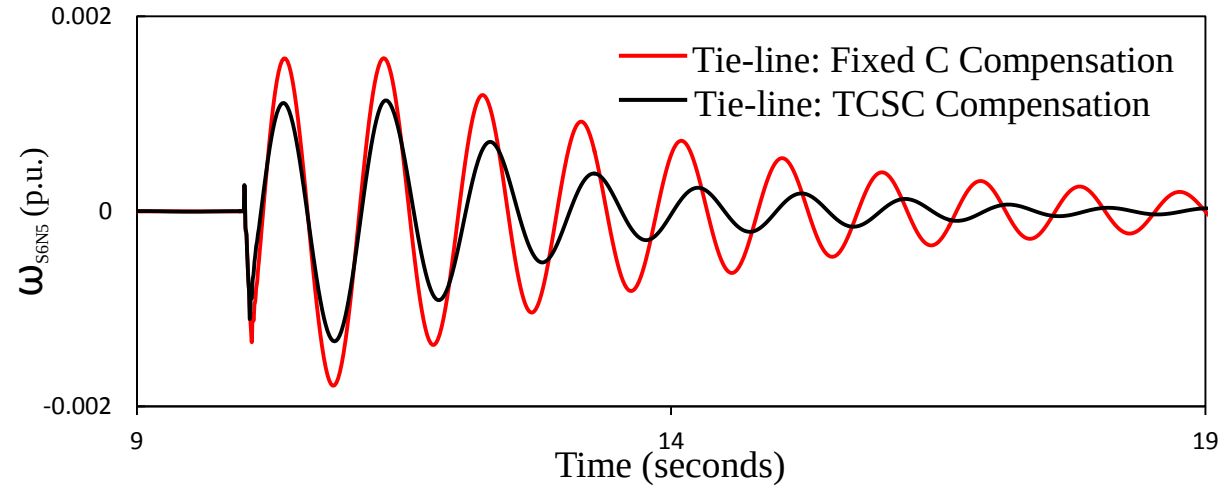

Figure 4.6: Continued.

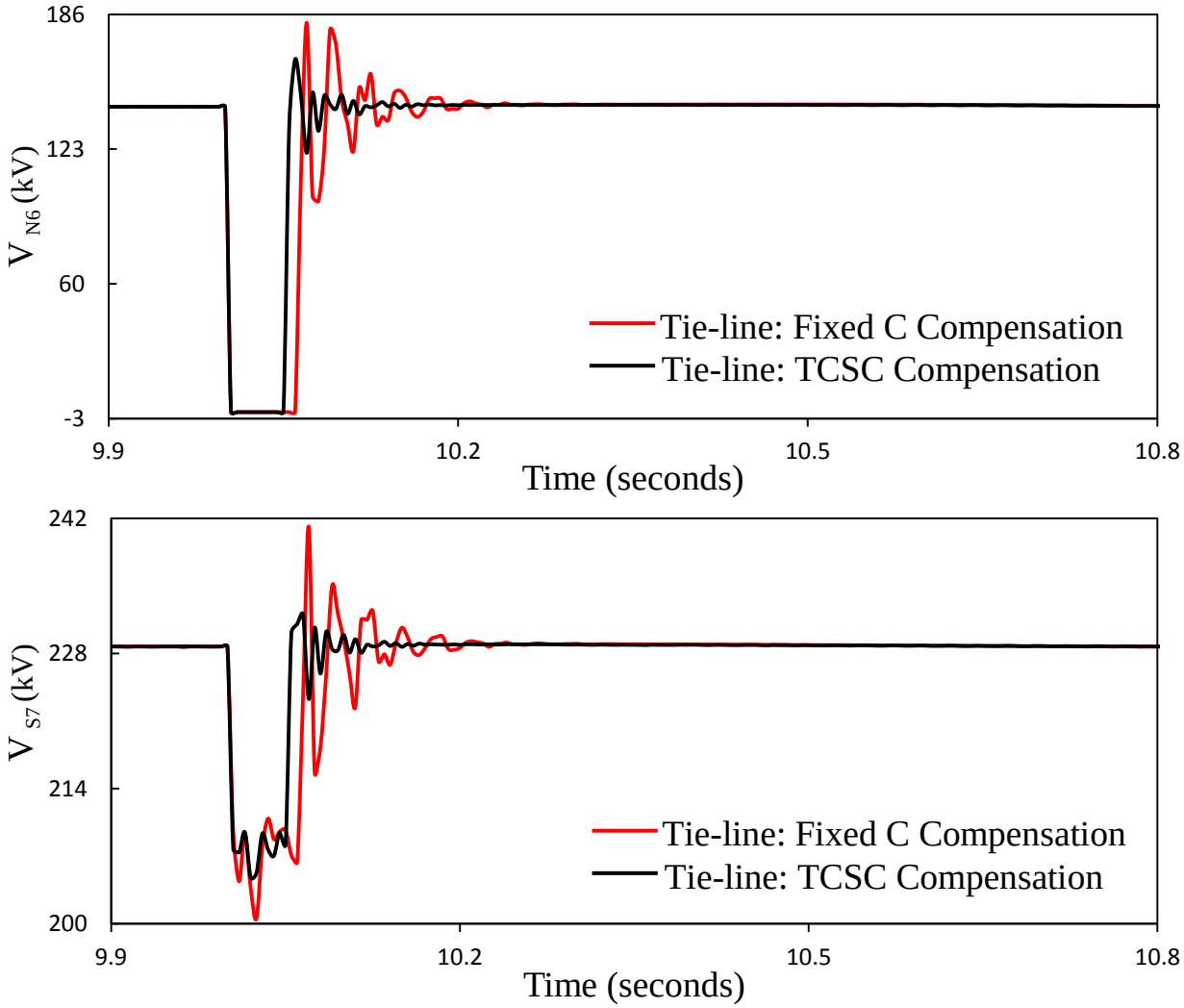

Figure 4.7: Bus voltage responses during and after clearing a temporary three-phase fault with a duration of 0.05 seconds on the virtual transmission line N_6-S_7 (case study I).

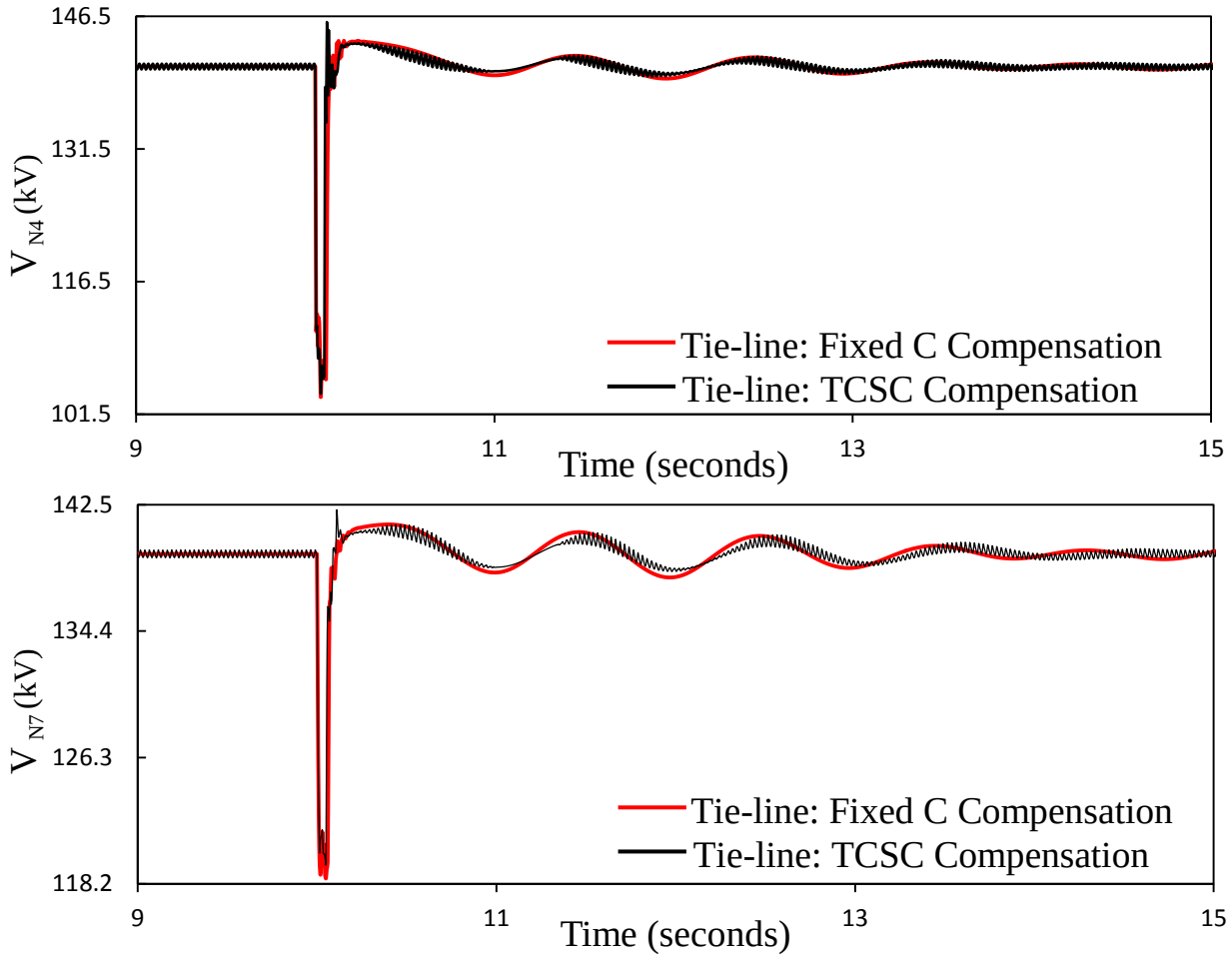

Figure 4.7: Continued.

4.4 Case Study II: Temporary Three-Phase Fault with a Duration of 0.05 Seconds on the Transmission Line S_6-S_7 near Bus S_6

The fault location is shown in Figure 4.8. In this case, generator G_{N5} load angle, measured with respect to generator G_{S4} load angle (δ_{N5S4}) is selected as the TCSC supplemental control stabilizing signal as it provides a noticeable improvement in the damping of the power system oscillations. Selected transmission line real power flows, generator load angles and speeds (measured with respect to generator G_{N5} load angle and speed) and system bus voltages during and after the fault clearing are illustrated in Figures 4.9 to 4.12 respectively. The transfer function of the TCSC supplemental control is given by

$$G_{\delta_{N5S4}}(S) = 0.051 \frac{10}{(S+10)} \frac{0.8S}{(0.8S+1)} \frac{1+3.14S}{1+0.75S} \tag{4.2}$$

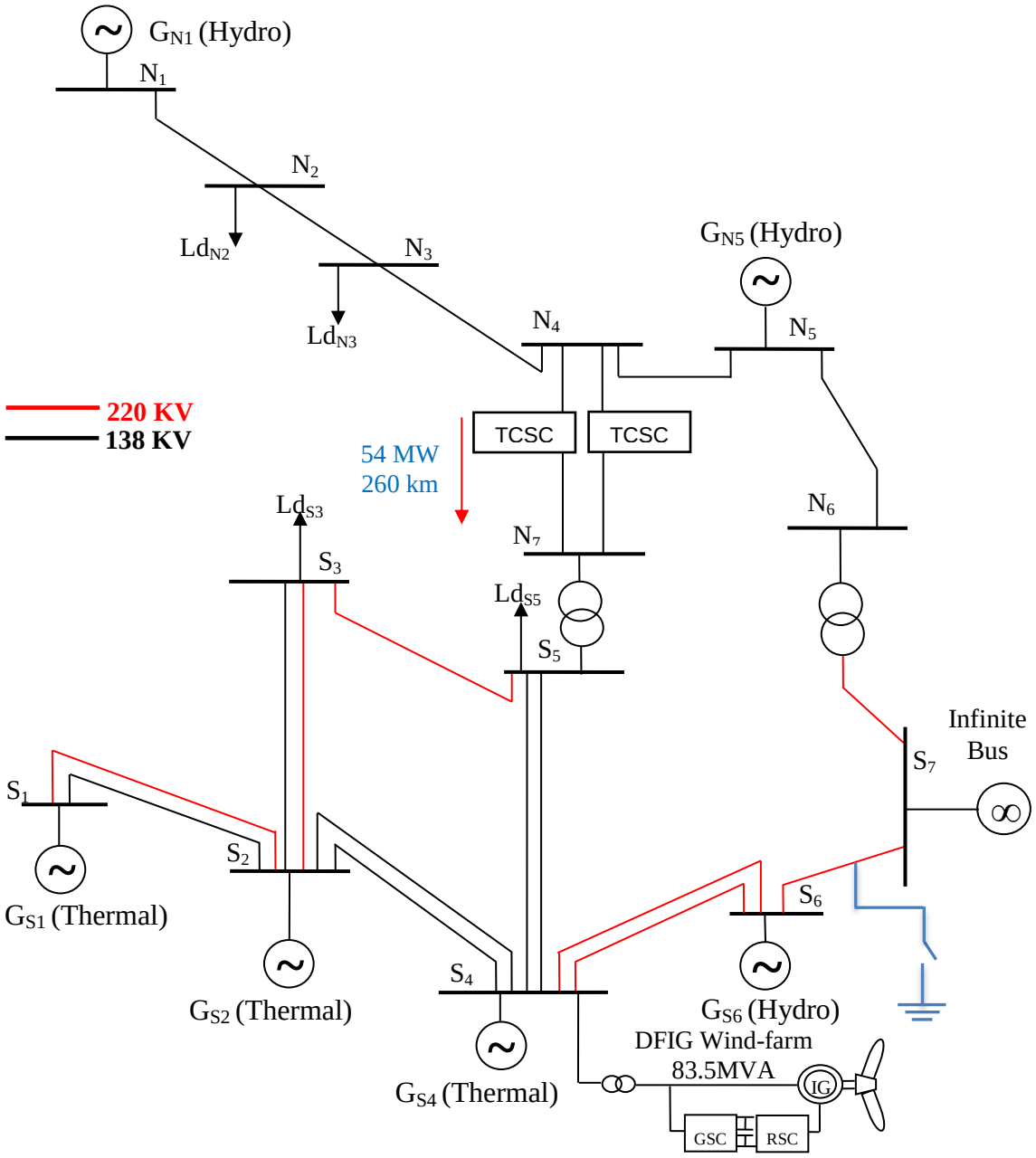

Figure 4.8: Case Study II: temporary three-phase fault with a duration of 0.05 seconds on the transmission line S_6-S_7 near bus S_6.

The following observations are made from Figures 4.9 to 4.12:

- The TCSC supplemental controller has a positive impact on the damping of the first and subsequent swings of the tie-line real power flow. However, the oscillations in the transmission line real power flows of $P_{S4\text{-}S5}$, $P_{S7\text{-}S6}$ and $P_{N6\text{-}S7}$, generator relative load angles

and speeds exhibit similar damping behavior in both cases of fixed capacitor compensation and TCSC compensation scheme.

- In the case of the TCSC compensation scheme, Figure 4.12 shows that the oscillations in the voltage of bus S_6 are damped relatively quicker than in the case of fixed capacitor compensation. The oscillations in the voltage of load-buses N_2, N_3, S_3 and S_5 also exhibit the same damping behavior in both cases of fixed capacitor compensation and TCSC compensation scheme.

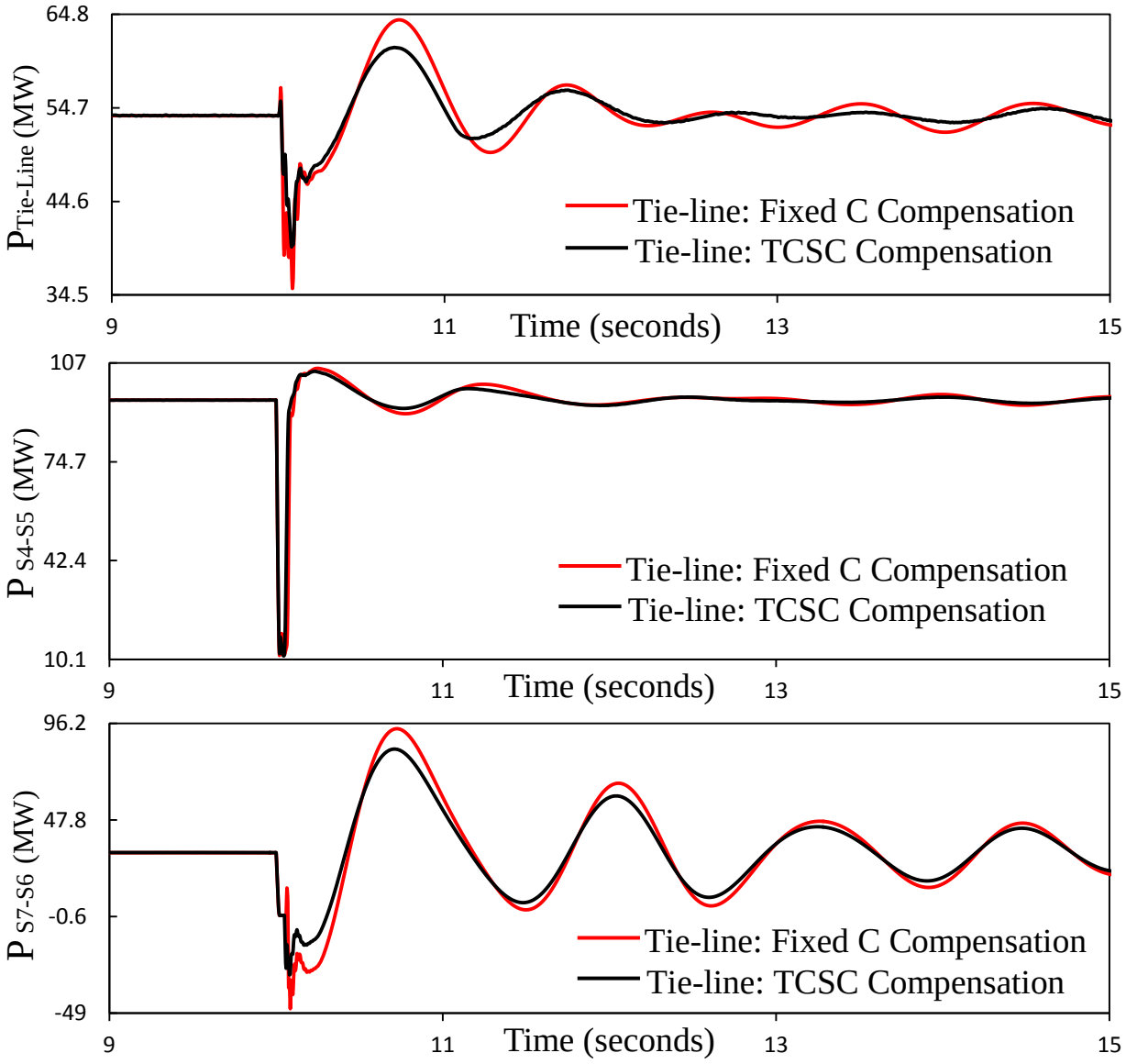

Figure 4.9: Real power flows on the tie-line and other transmission lines during and after clearing a temporary three-phase fault with a duration of 0.05 seconds on the transmission line S_6-S_7 (case study II).

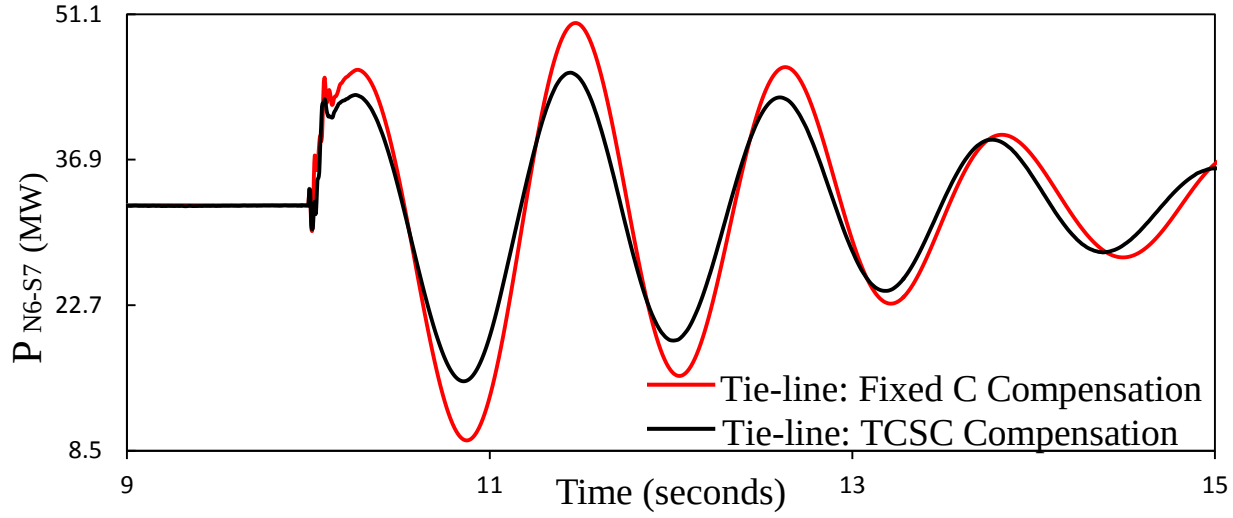

Figure 4.9: Continued.

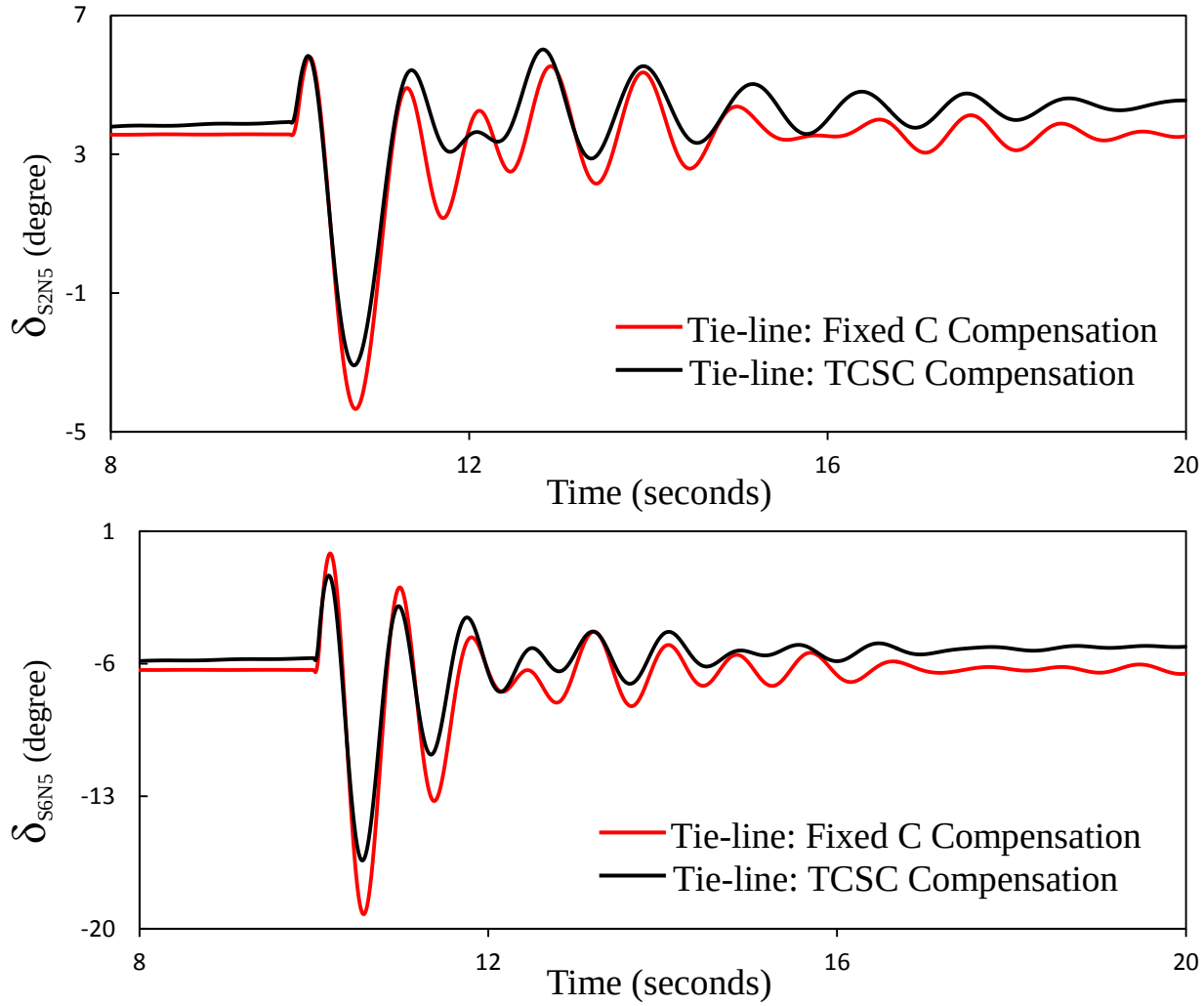

Figure 4.10: Generator load angles, measured with respect to generator G_{N5} load angle, during and after clearing a temporary three-phase fault with a duration of 0.05 seconds on the transmission line S_6-S_7 (case study II).

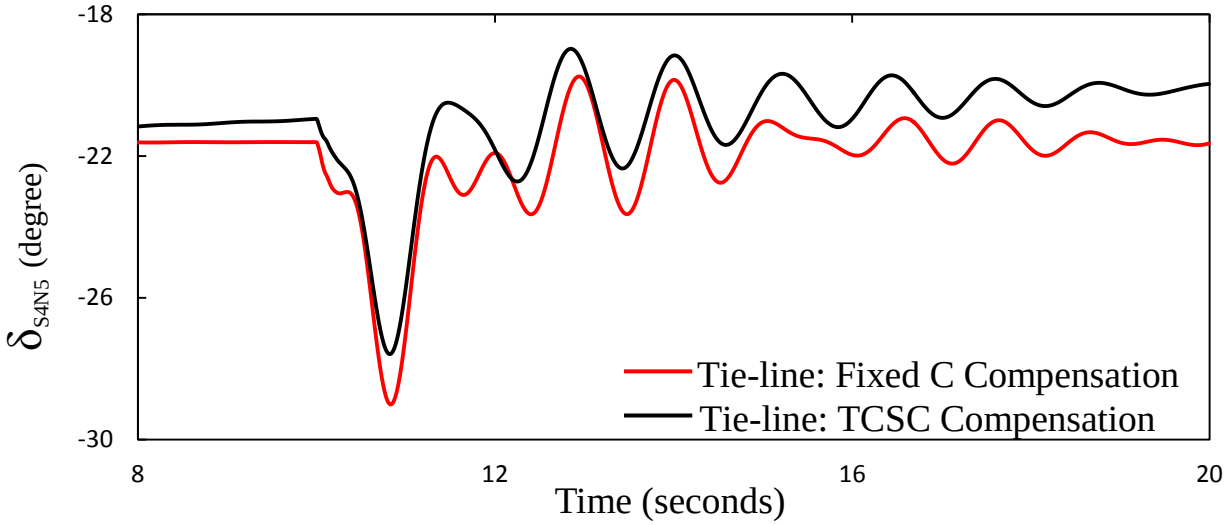

Figure 4.10: Continued.

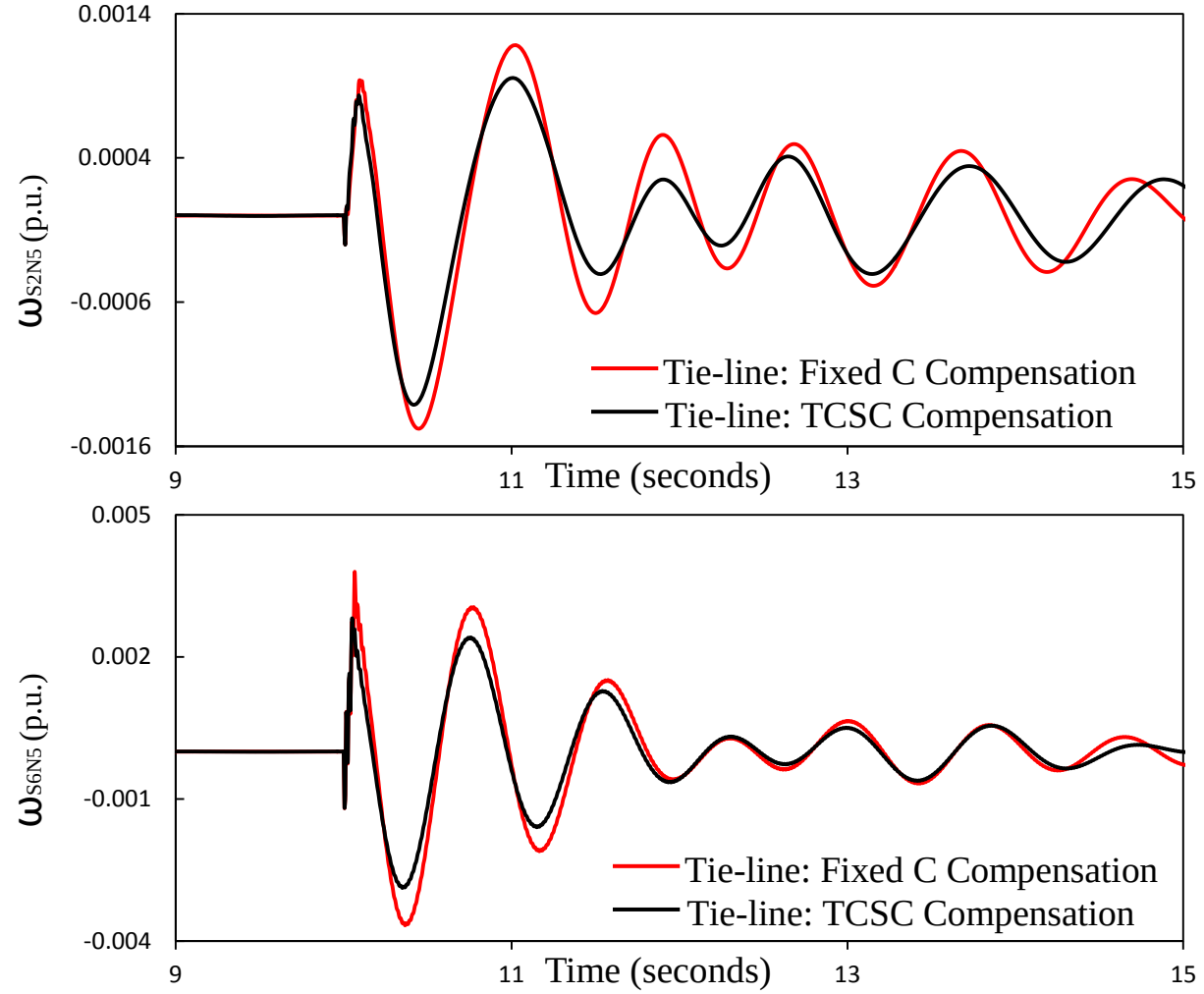

Figure 4.11: Generator speeds, measured with respect to generator N_5 speed, during and after clearing a temporary three-phase fault with a duration of 0.05 seconds on the transmission line S_6-S_7 (case study II).

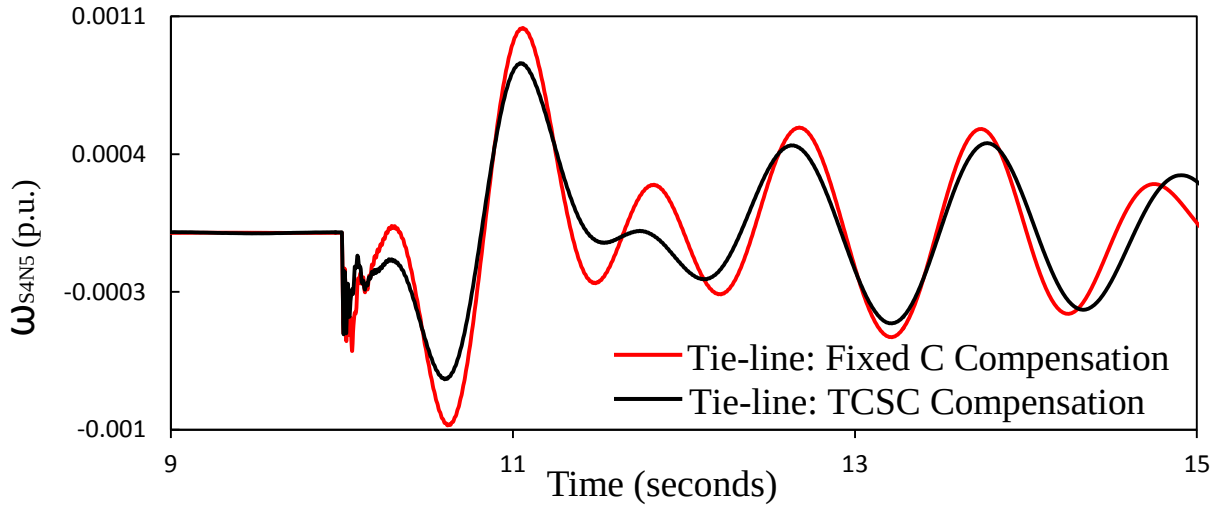

Figure 4.11: Continued.

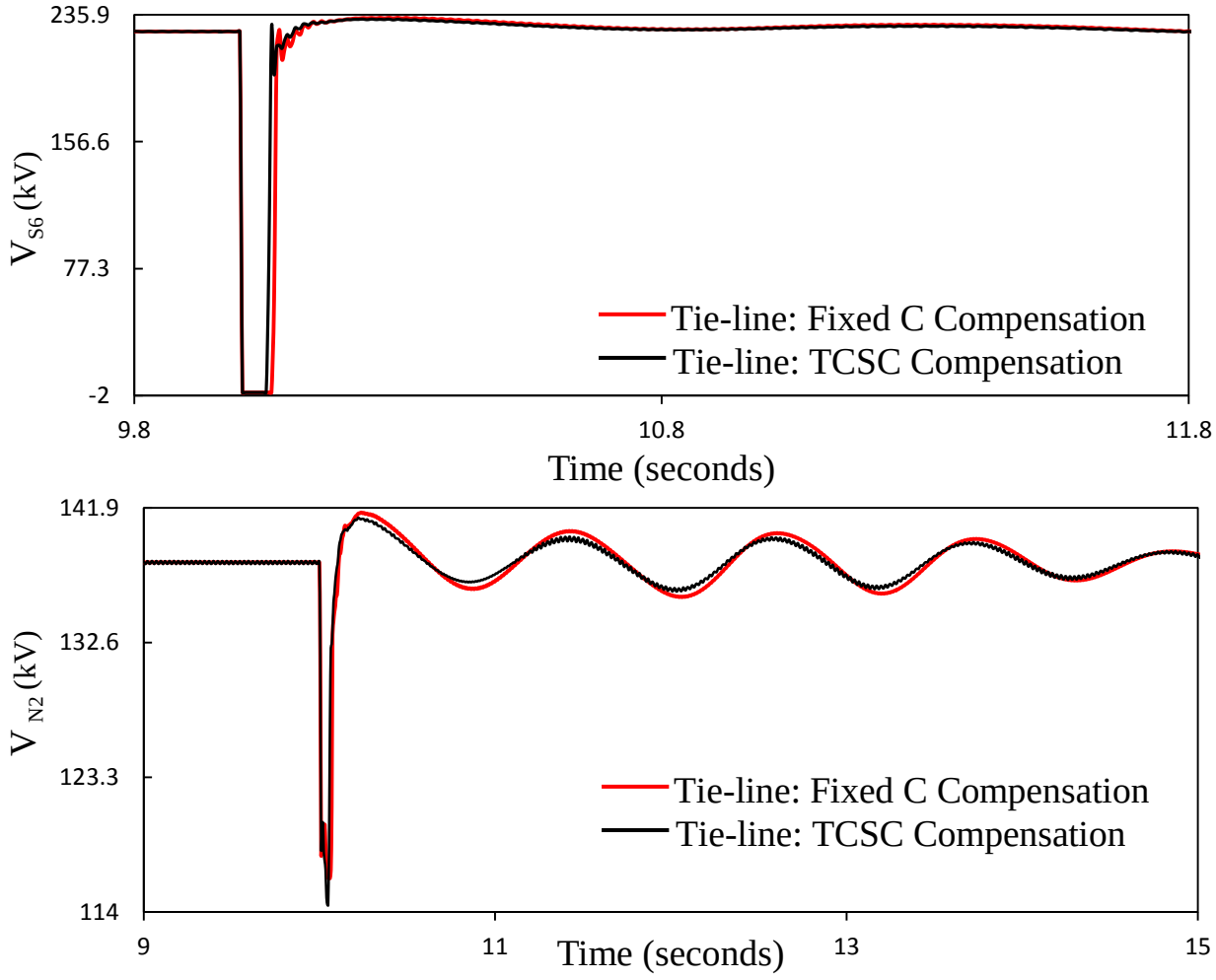

Figure 4.12: Bus voltage responses during and after clearing a temporary three-phase fault with a duration of 0.05 seconds on the transmission line S_6-S_7 (case study II).

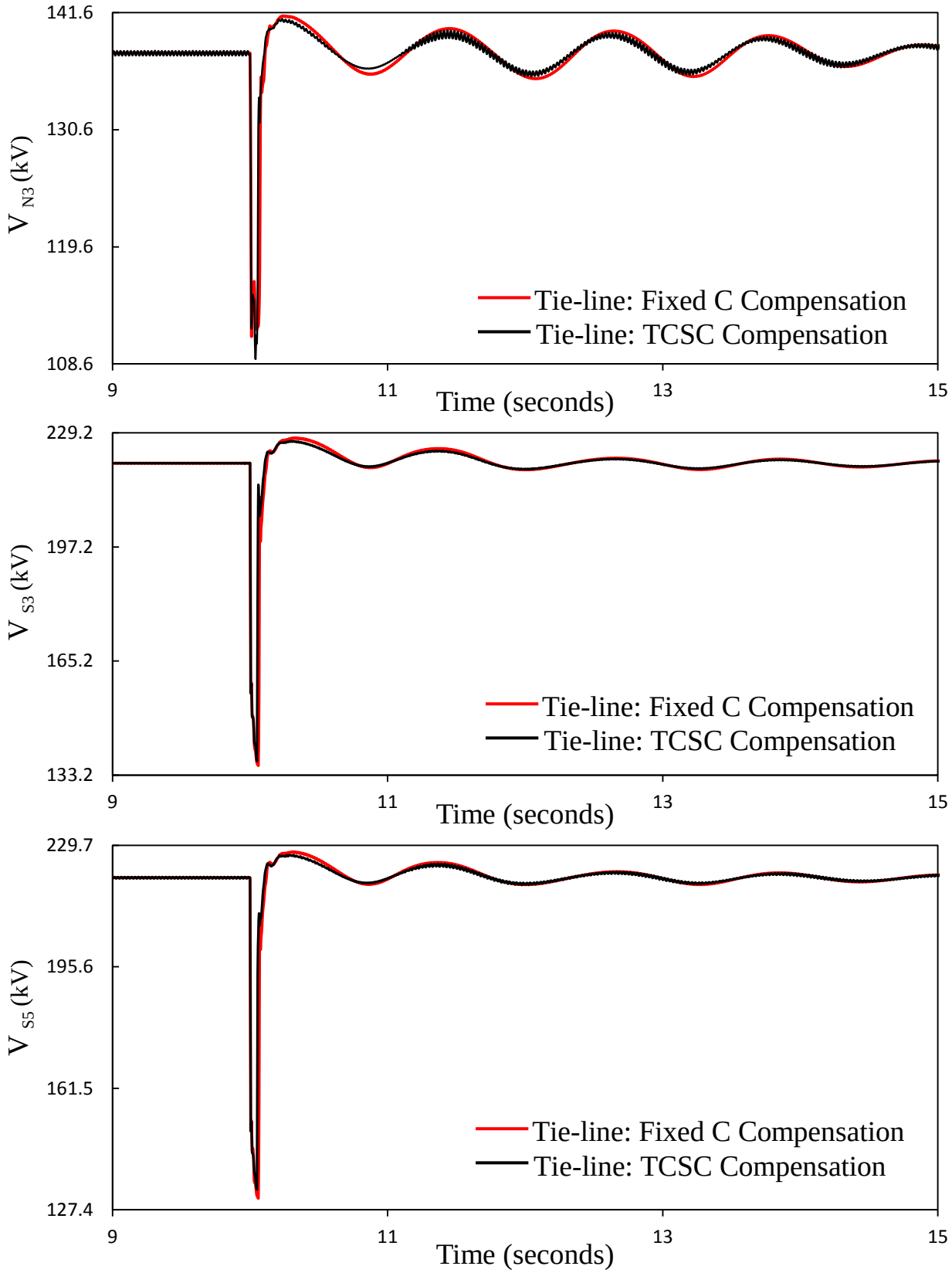

Figure 4.12: Continued.

4.5 Case Study III: Temporary Three-Phase Fault with a Duration of 0.05 Seconds at Bus S_7

The fault location is shown in Figure 4.13. In this case, generator G_{N5} load angle, measured with respect to generator G_{S4} load angle (δ_{N5S4}) is selected as the TCSC supplemental control stabilizing signal as it provides a noticeable improvement in the damping of the power system oscillations. Selected transmission line real power flows, generator load angles and speeds (measured with respect to generator G_{N5} load angle and speed) and system bus voltages during and after the fault clearing are illustrated in Figures 4.14 to 4.17 respectively. The transfer function of the TCSC supplemental control is given by

$$G_{\delta_{N5S4}}(S) = 0.11\frac{10}{(S+10)}\frac{0.8S}{(0.8S+1)}\frac{1+0.28S}{1+0.1S} \tag{4.3}$$

The following observations can be made from Figures 4.14 to 4.17:

- It can be observed from Figure 4.14 that the oscillations in tie-line real power flow as well as transmission line real power flows of $P_{S4\text{-}S5}$, $P_{S5\text{-}S3}$ and $P_{S7\text{-}S6}$ are not noticeably improved in the case of TCSC compensation scheme, compared with the case of fixed capacitor compensation. It is worth noting here that the oscillations in transmission line real power flows are not severe even in the case of fixed capacitor compensation (the highest value from peak to valley is approximately 9 MW), and they are also quickly damped after five seconds.

- Figure 4.15 shows that the oscillations in the generator relative load angles exhibit similar damping behavior in both cases of fixed capacitor compensation and TCSC compensation scheme.

- The TCSC supplemental controller provides significant improvement in damping the first and subsequent swings of the generator relative speeds, and provides better damping than in the case of fixed capacitor compensation.

- In the case of the TCSC compensation scheme, the oscillations in the voltage of buses N_6 and S_7 are faster and well damped than in the case of fixed capacitor compensation.

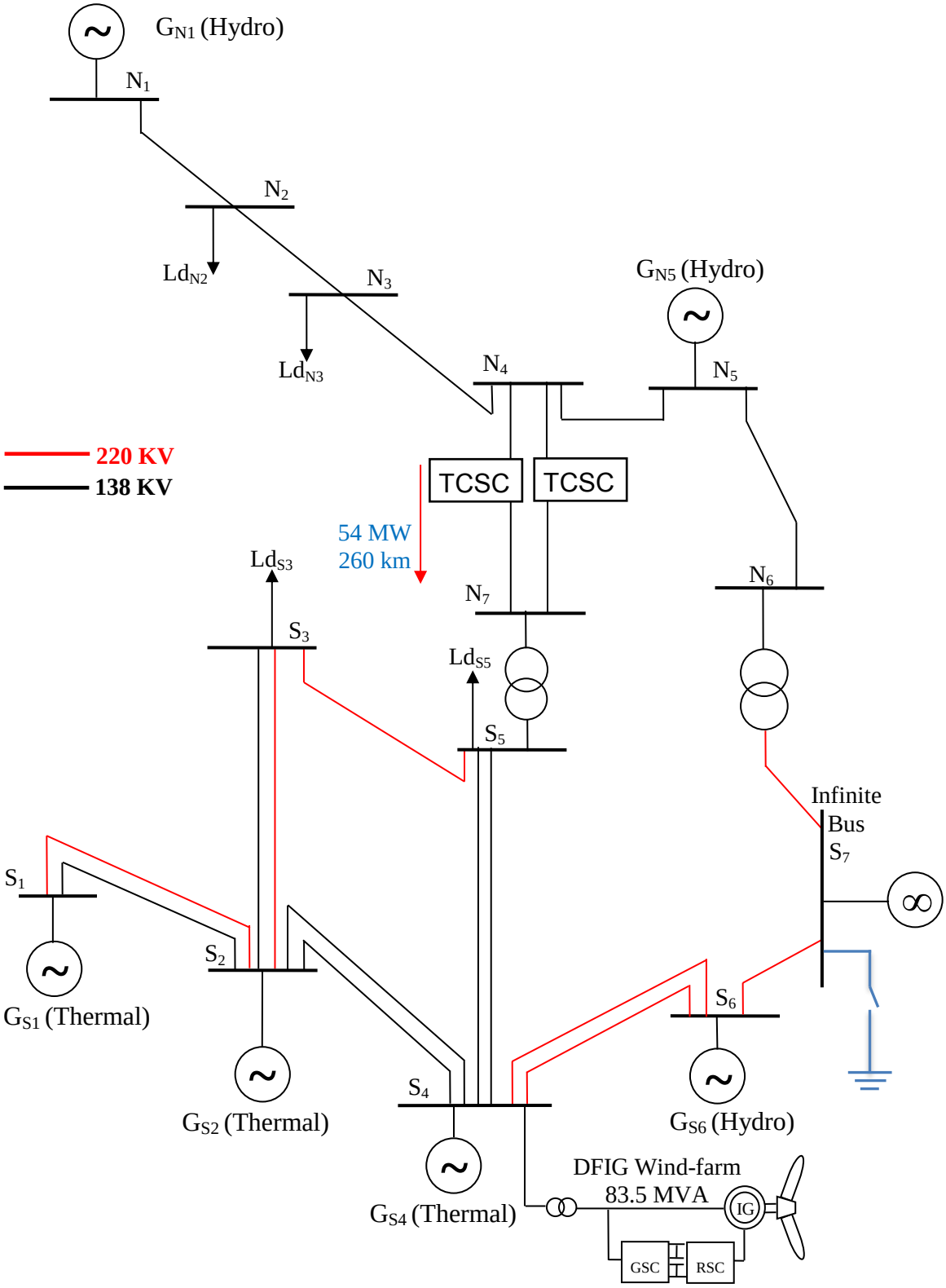

Figure 4.13: Case Study III: temporary three-phase fault with a duration of 0.05 seconds at bus S_7.

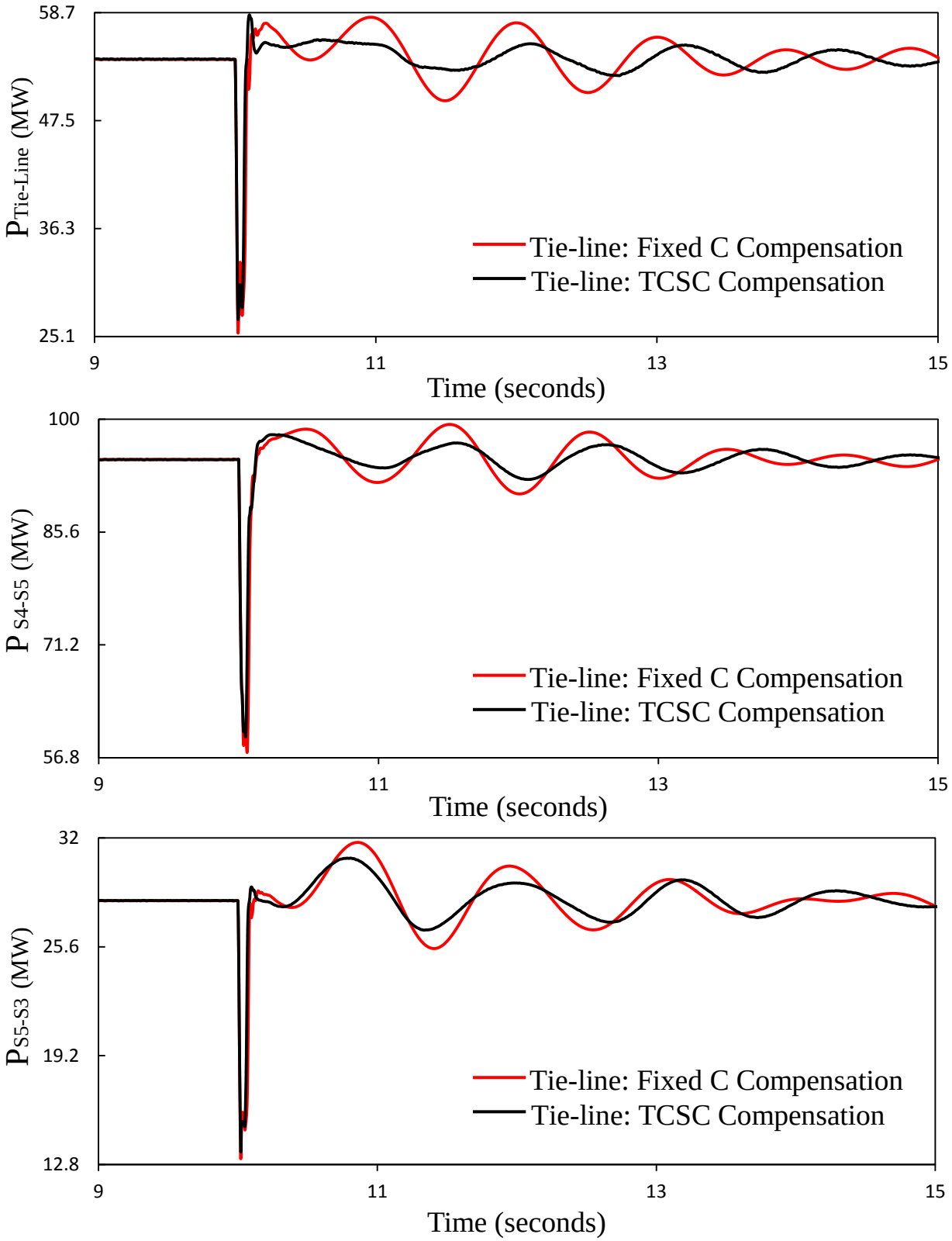

Figure 4.14: Real power flows on the tie-line and other transmission lines during and after clearing a temporary three-phase fault with a duration of 0.05 seconds at bus S_7 (case study III).

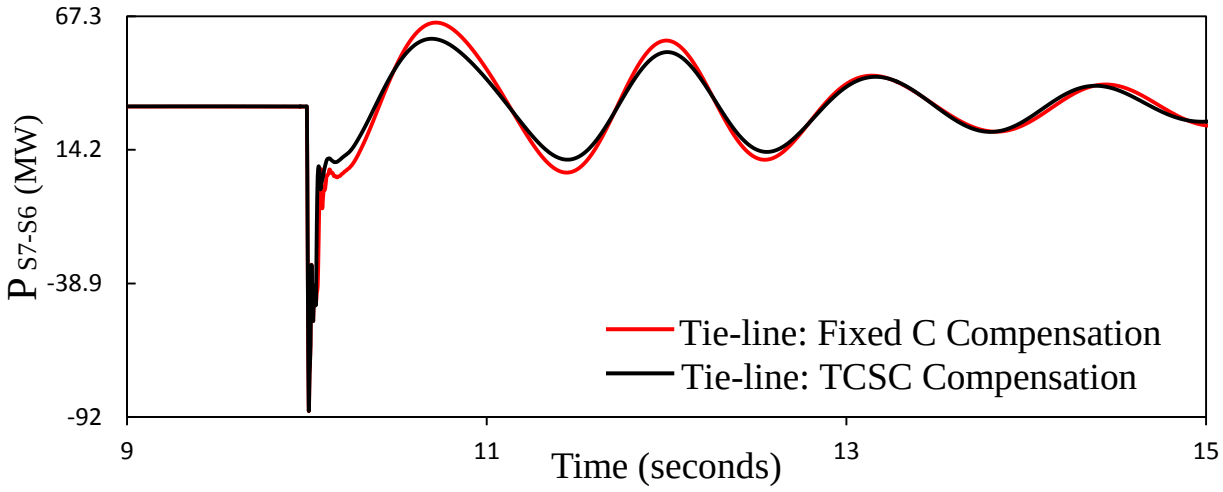

Figure 4.14: Continued.

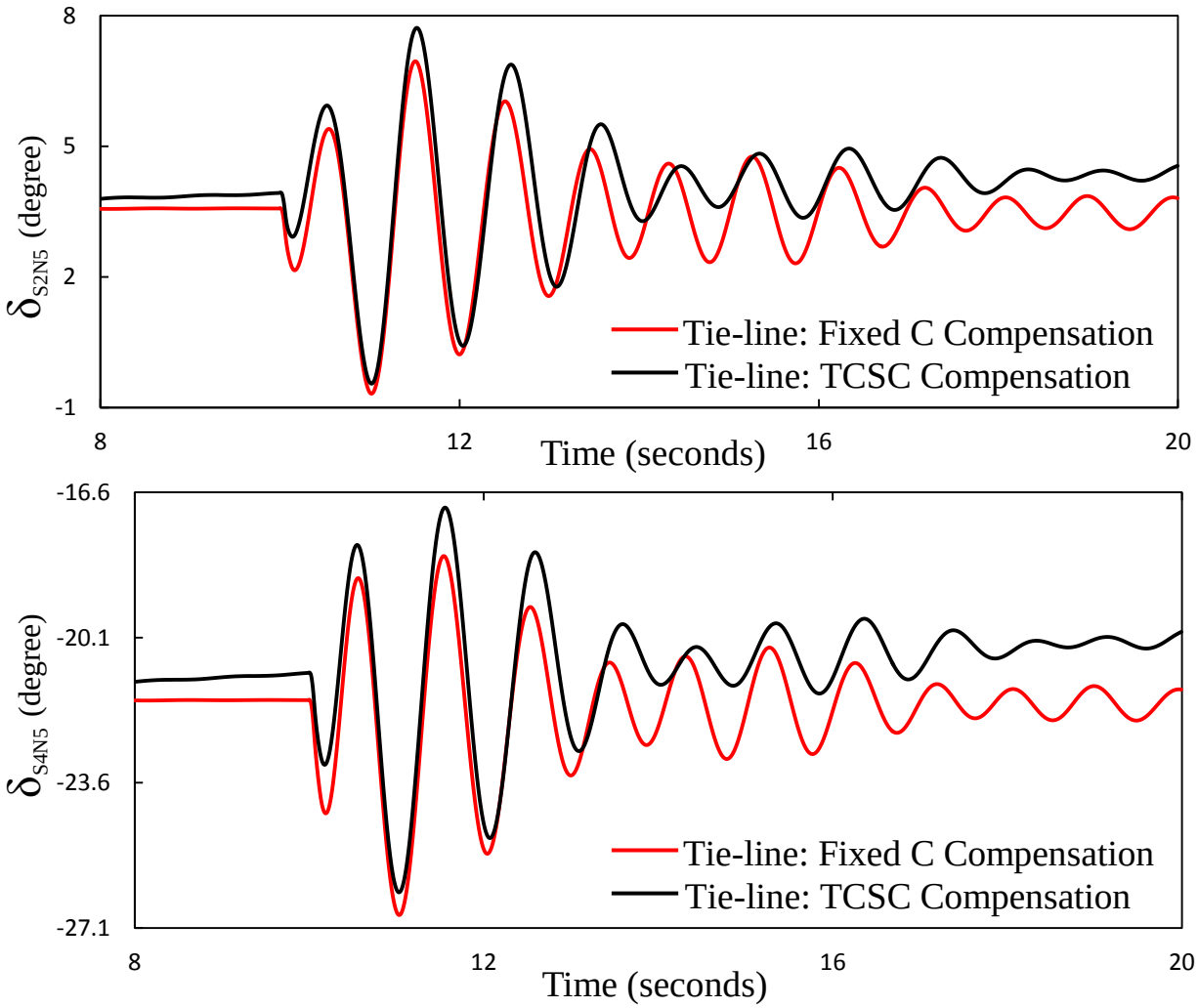

Figure 4.15: Generator load angles, measured with respect to generator G_{N5} load angle, during and after clearing a temporary three-phase fault with a duration of 0.05 seconds at bus S_7 (case study III).

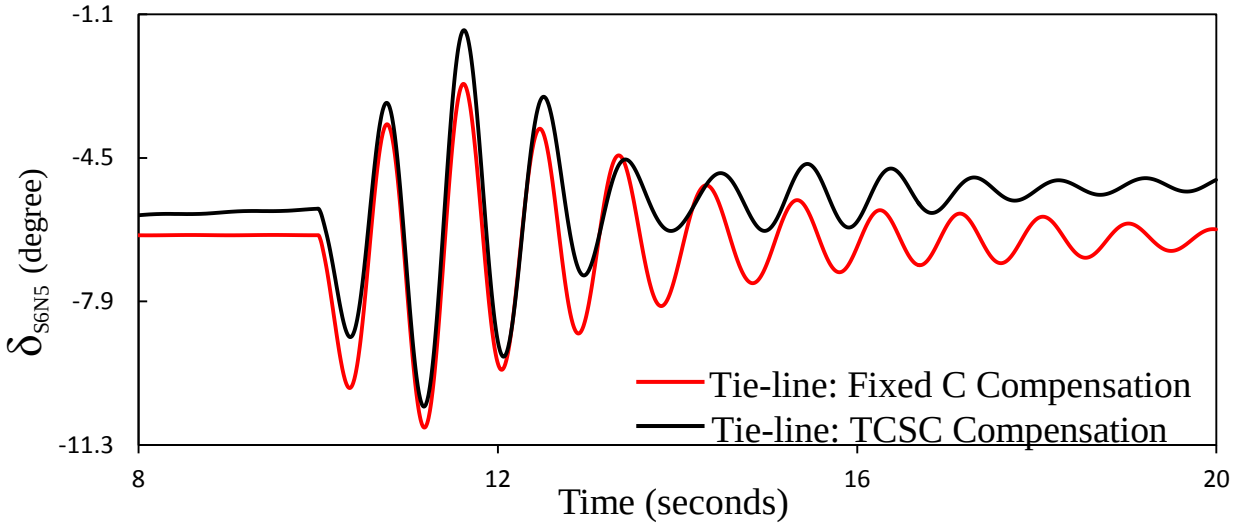

Figure 4.15: Continued.

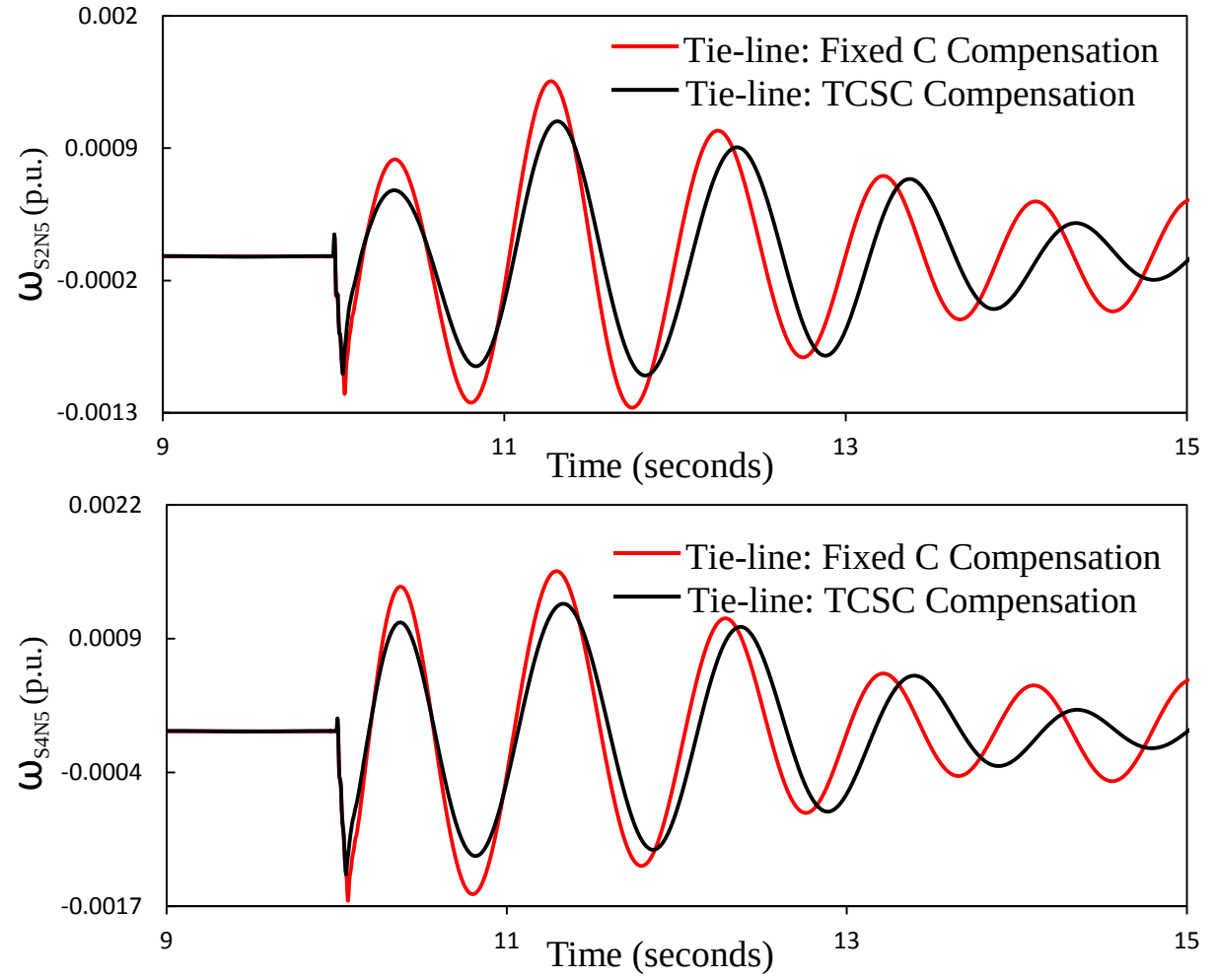

Figure 4.16: Generator speeds, measured with respect to generator G_{N5} speed, during and after clearing a temporary three-phase fault with a duration of 0.05 seconds at bus S_7 (case study III).

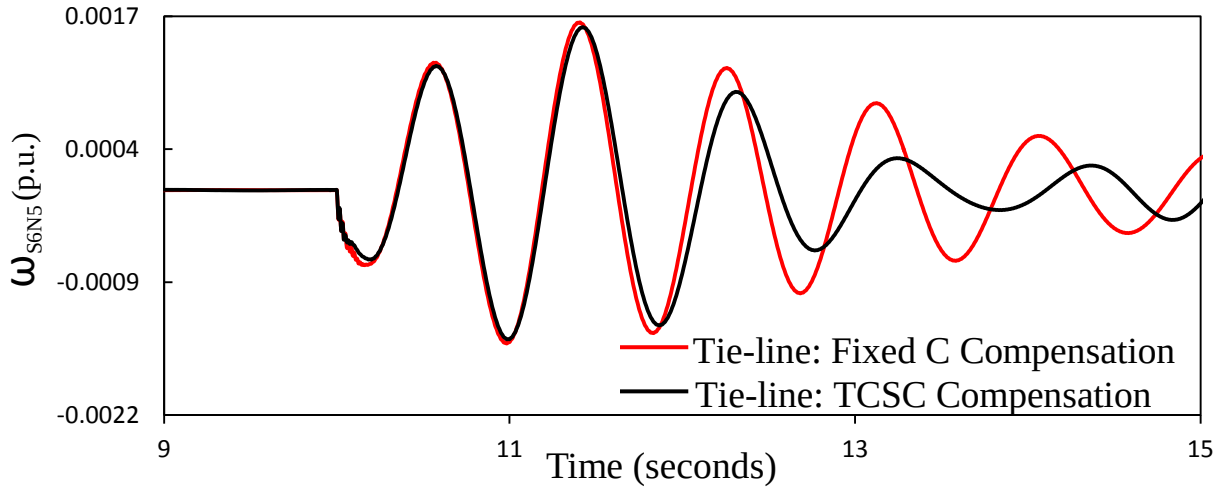

Figure 4.16: Continued.

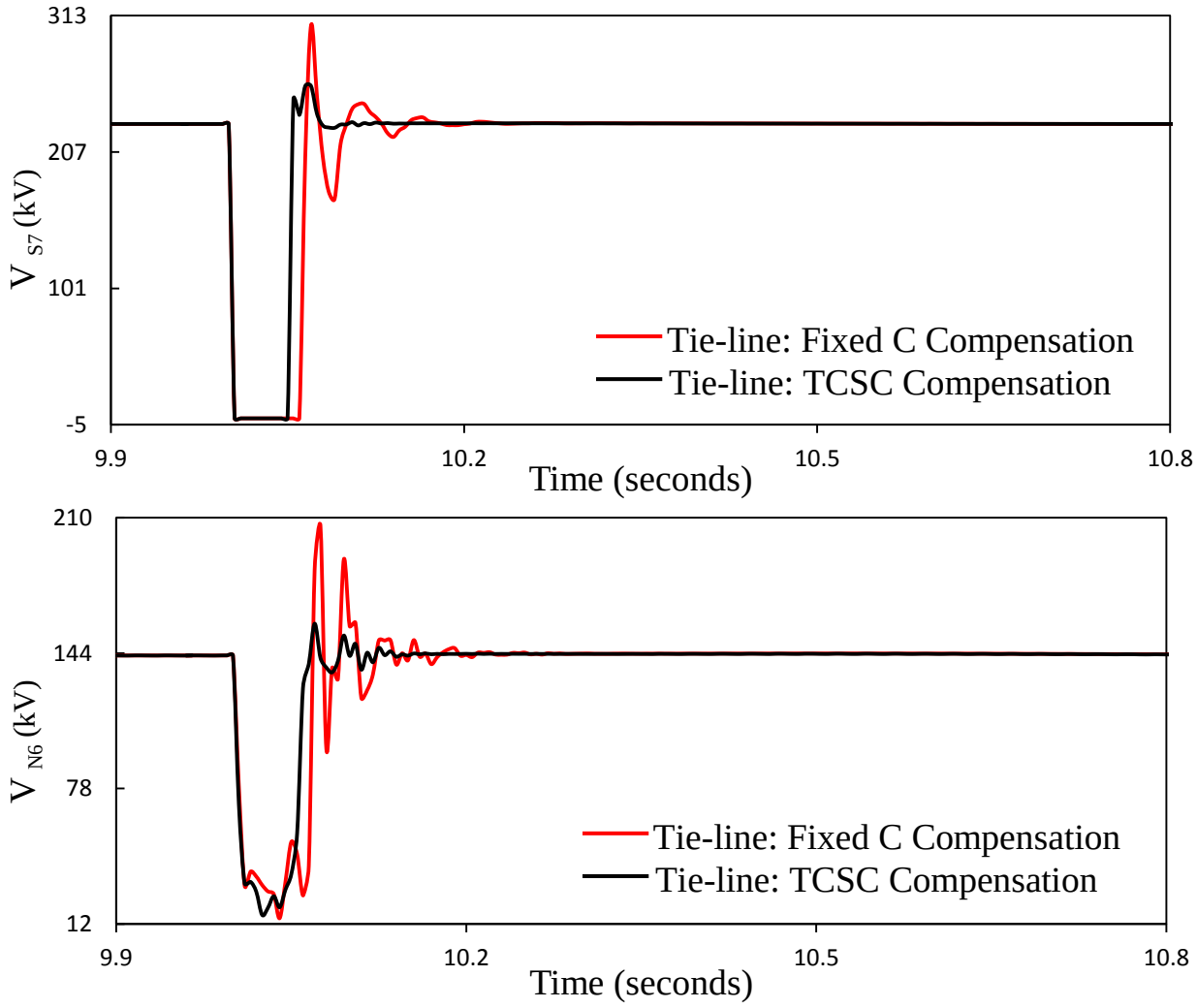

Figure 4.17: Bus voltage responses during and after clearing a temporary three-phase fault with a duration of 0.05 seconds at bus S_7 (case study III).

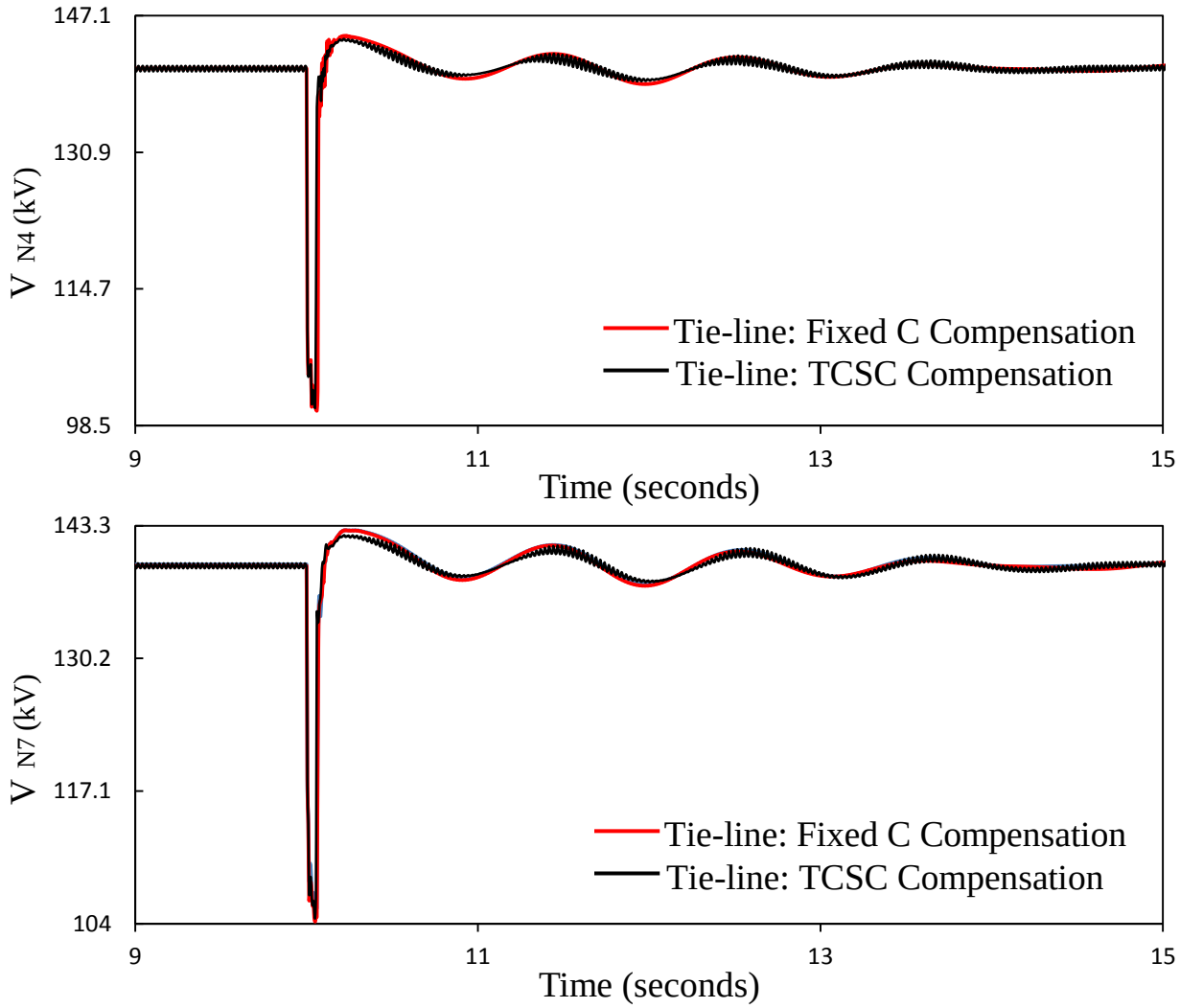

Figure 4.17: Continued.

4.6 Case Study IV: Three-Cycle, Three-Phase Fault at Bus S_7; SaskPower System Loses Its Connection with the Manitoba Grid

Transmission lines N_6-S_7, S_6-S_7, shown in Figure 4.18, represent respectively SaskPower North and South system connections to the Manitoba grid, which is represented in the studies conducted in this thesis by an infinite-bus. A fault on bus S_7 followed by tripping lines N_6-S_7 and S_6-S_7 leads to the SaskPower system losing its connection with the Manitoba grid. In this case, generator G_{N5} load angle, measured with respect to generator G_{S6} load angle (δ_{N5S6}) is selected as the TCSC supplemental control stabilizing signal as it provides a noticeable improvement in the damping of the power system oscillations. Selected transmission line real power flows, generator load angles and speeds (measured with respect to generator G_{N5} load

angle and speed) and system bus voltages during and after the fault clearing (line tripping) are illustrated in Figures 4.19 to 4.22 respectively. The transfer function of the TCSC supplemental control is given by

$$G_{\delta_{N5S6}}(S) = 0.12\,\frac{10}{(S+10)}\,\frac{S}{(S+1)}\,\frac{(1+0.1S)}{(1+0.5S)} \tag{4.4}$$

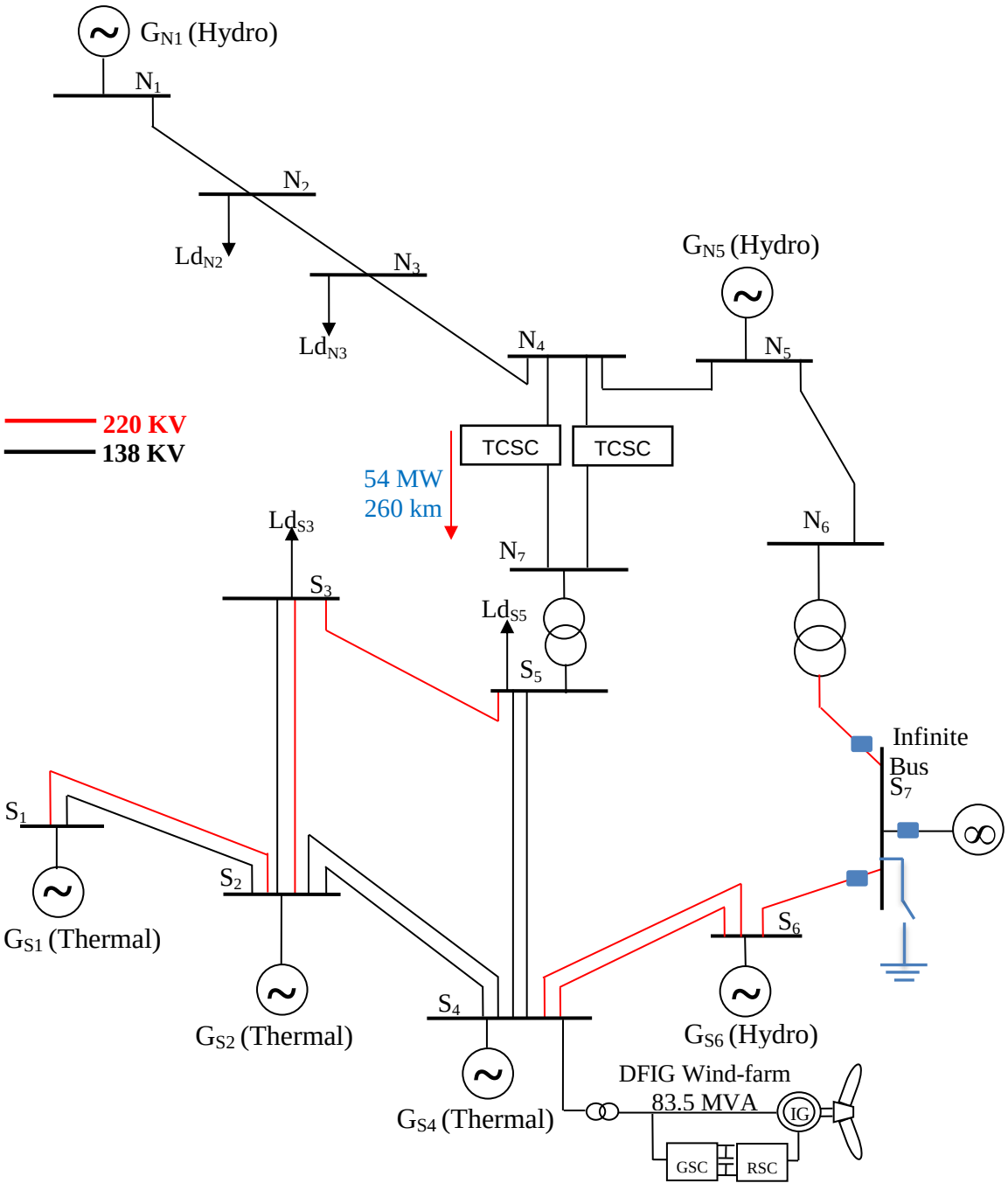

Figure 4.18: Case Study IV: three-cycle, three-phase fault at bus S_7; SaskPower system loses its connection with the Manitoba grid.

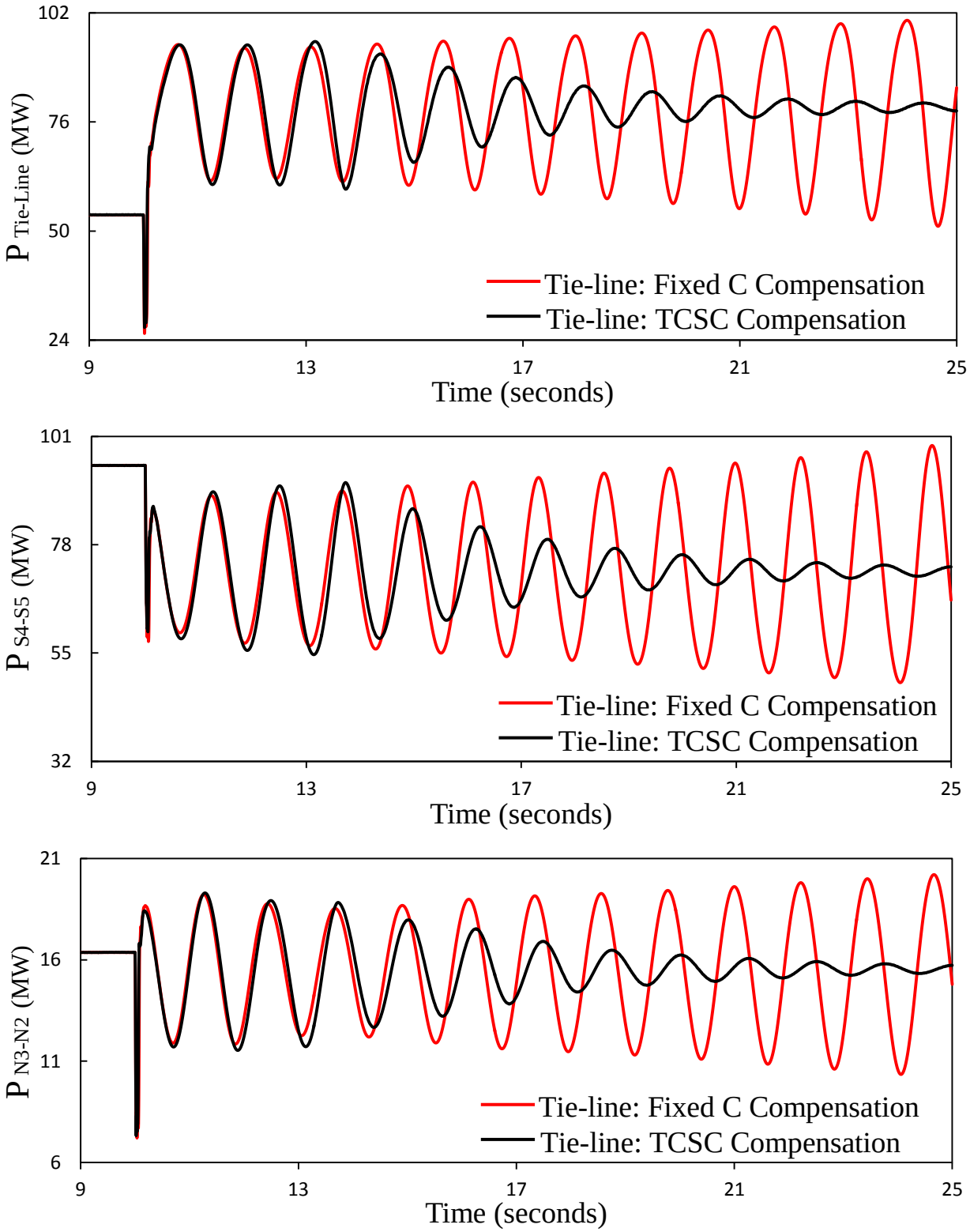

Figure 4.19: Real power flows on the tie-line and other transmission lines during and after clearing a three-cycle, three-phase fault on the Manitoba connection bus (case study IV).

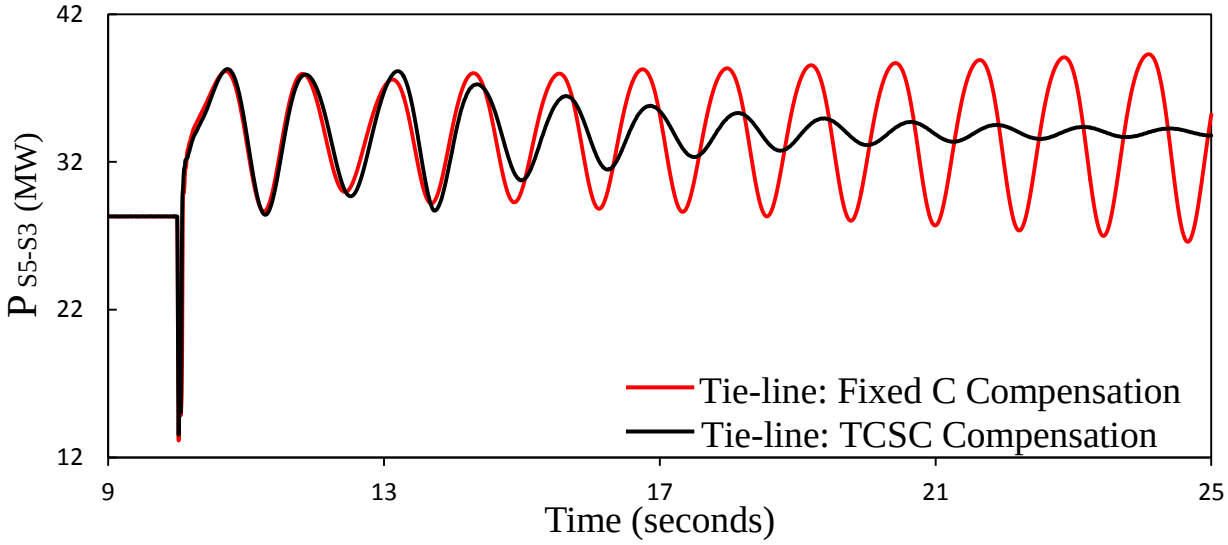

Figure 4.19: Continued.

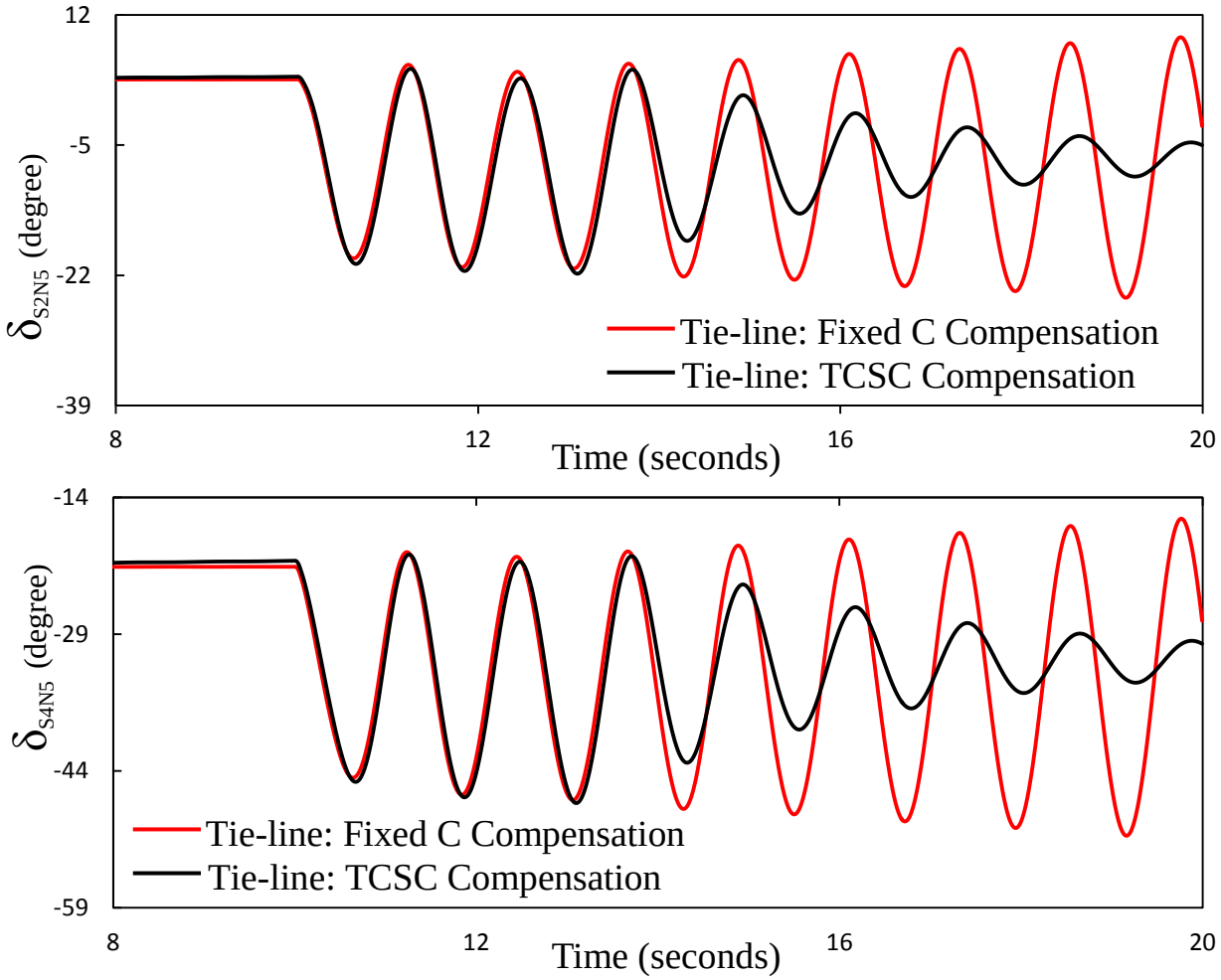

Figure 4.20: Generator load angles, measured with respect to generator G_{N5} load angle, during and after clearing a three-cycle, three-phase fault on the Manitoba connection bus (case study IV).

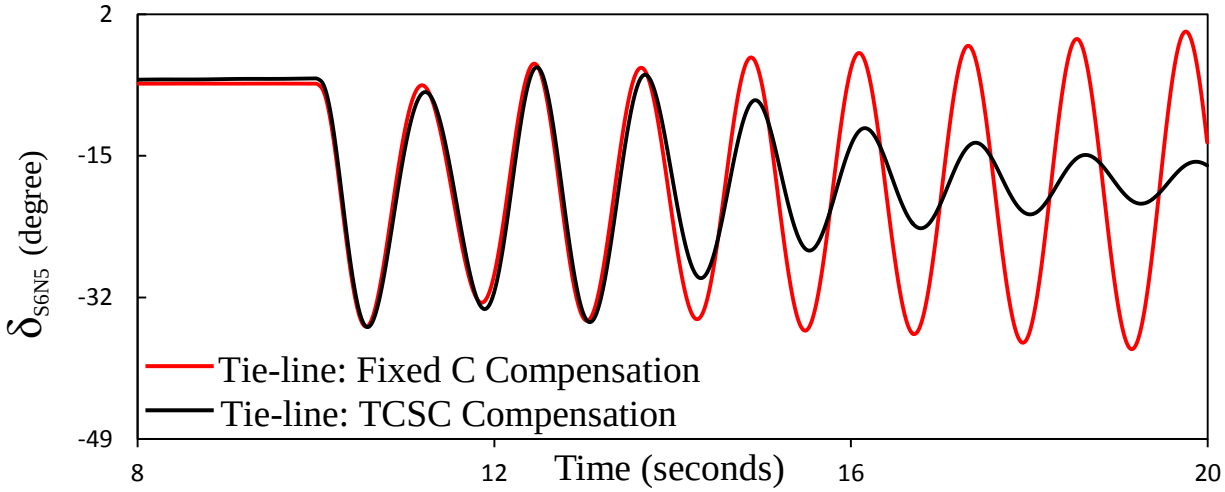

Figure 4.20: Continued.

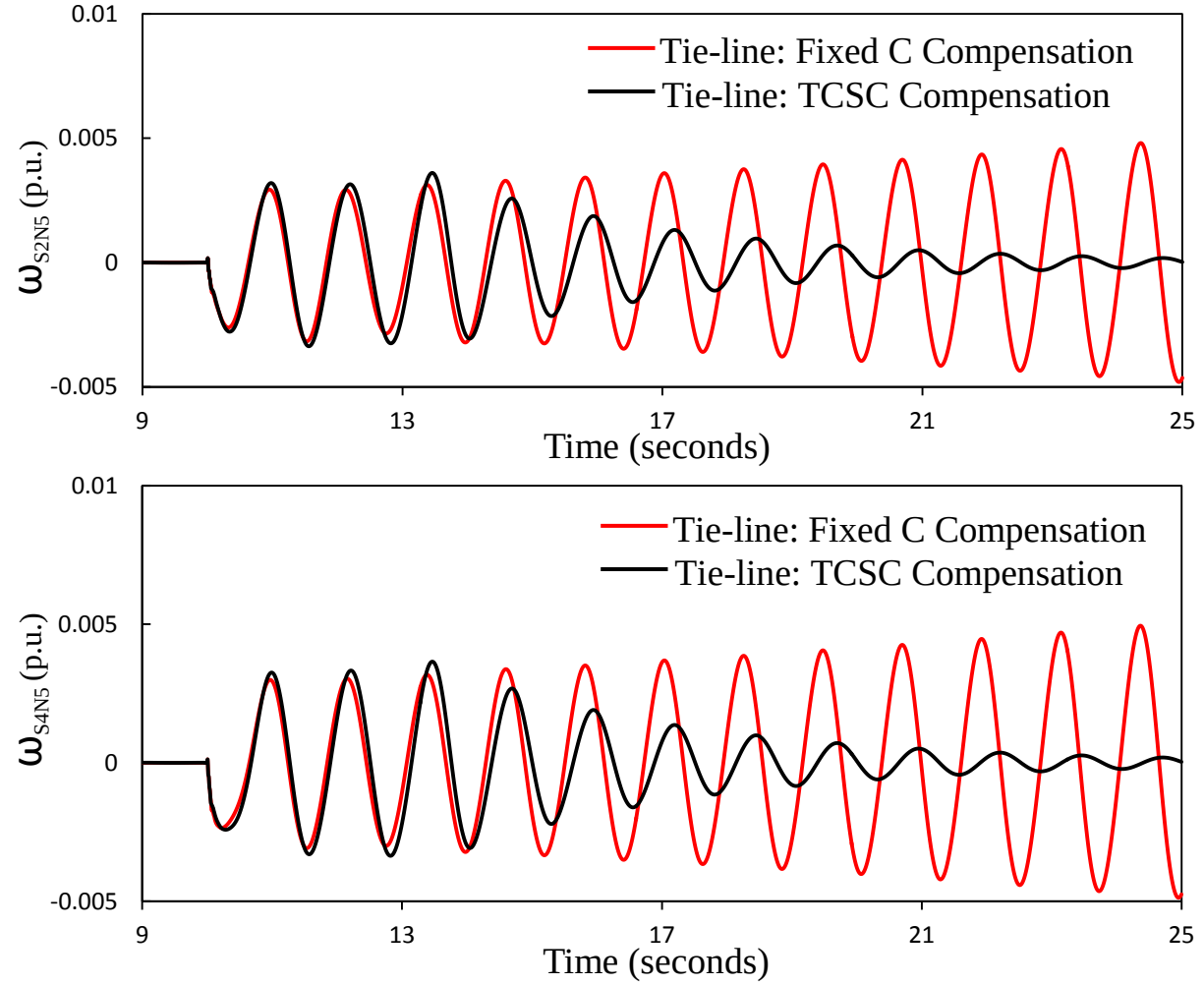

Figure 4.21: Generator speeds, measured with respect to generator G_{N5} speed, during and after clearing a three-cycle, three-phase fault on the Manitoba connection bus (case study IV).

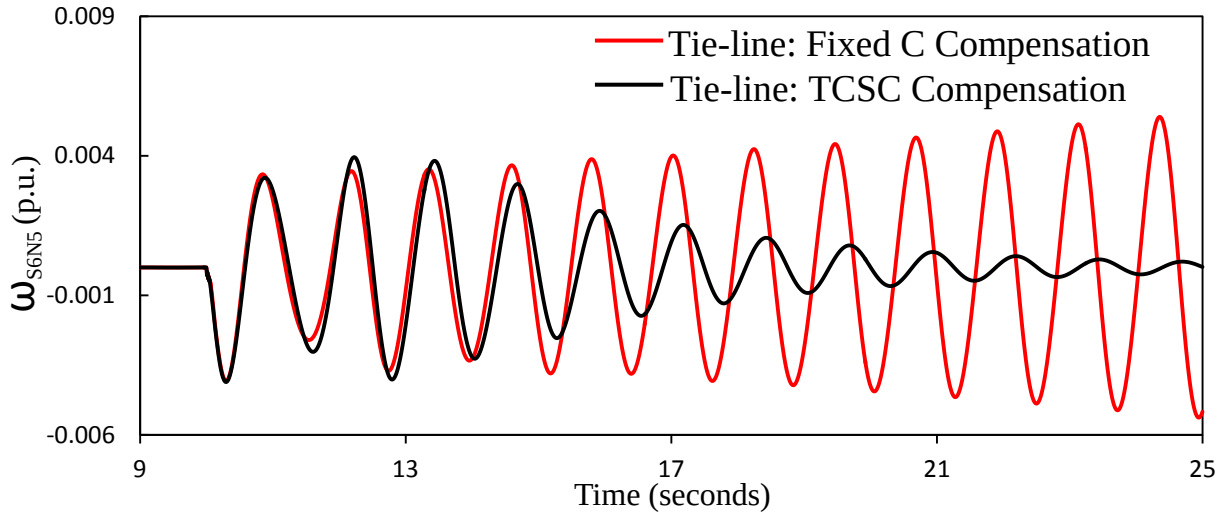

Figure 4.21: Continued.

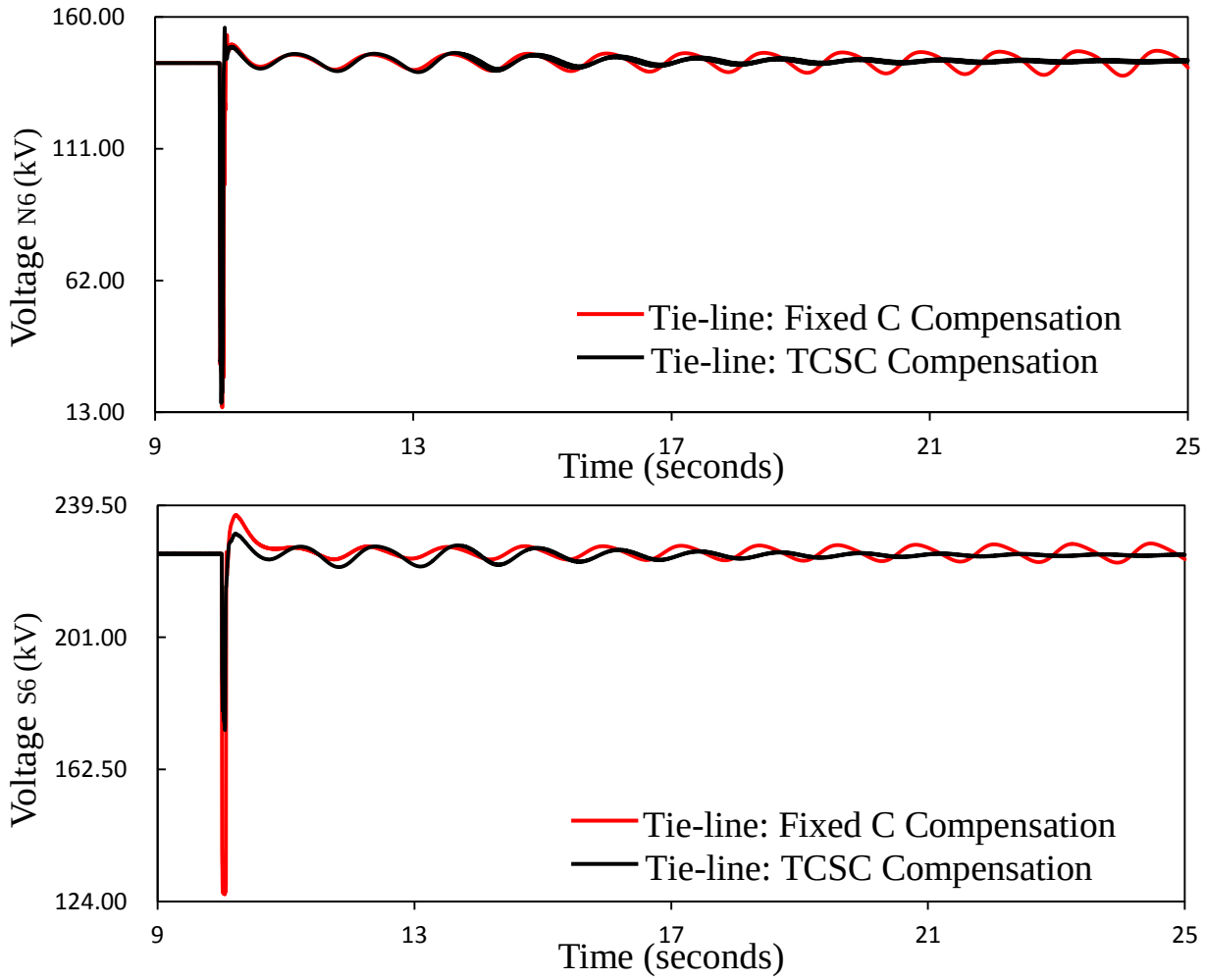

Figure 4.22: System bus voltages during and after clearing a three-cycle, three-phase fault on the Manitoba connection bus (case study IV).

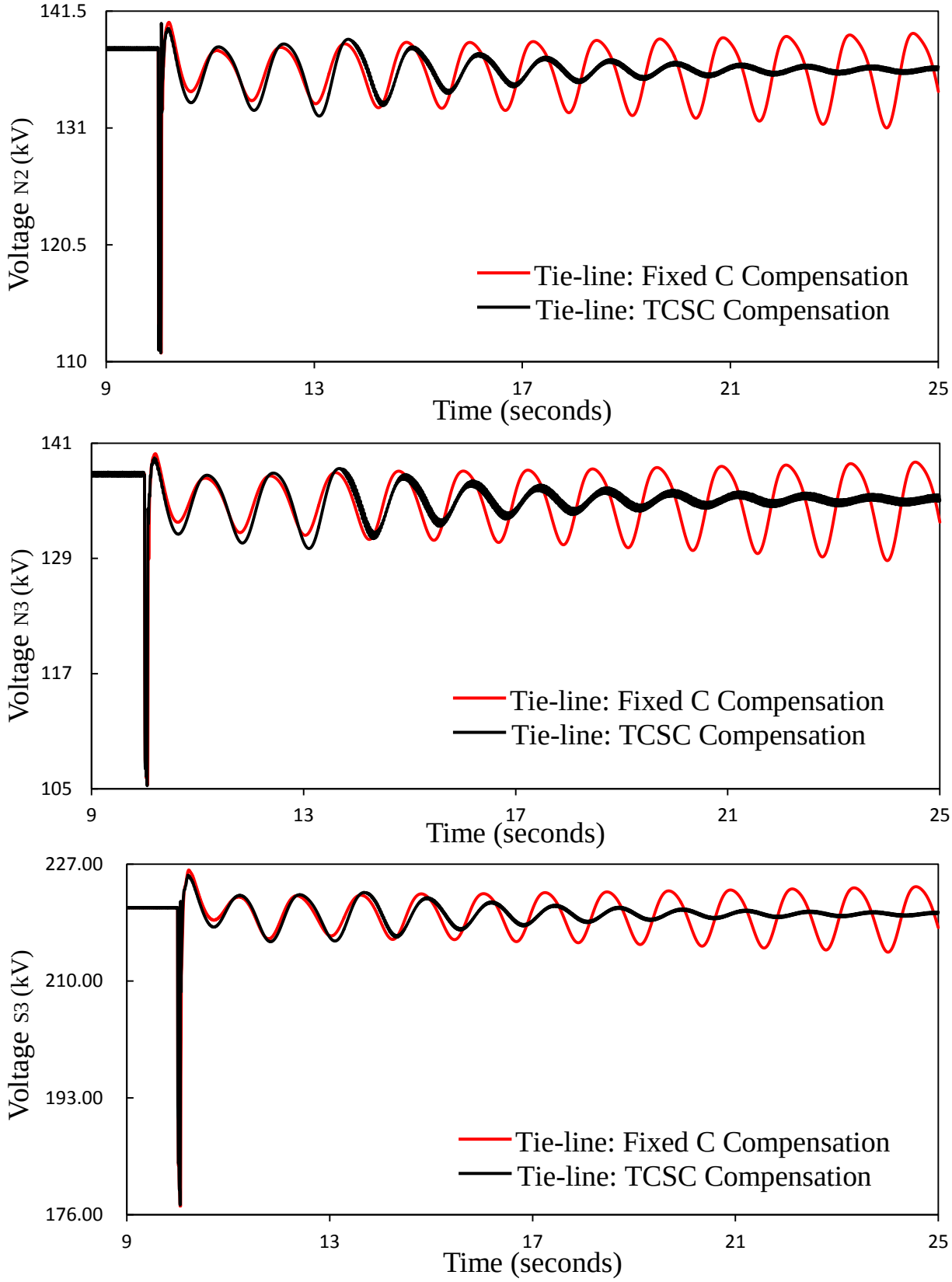

Figure 4.22: Continued.

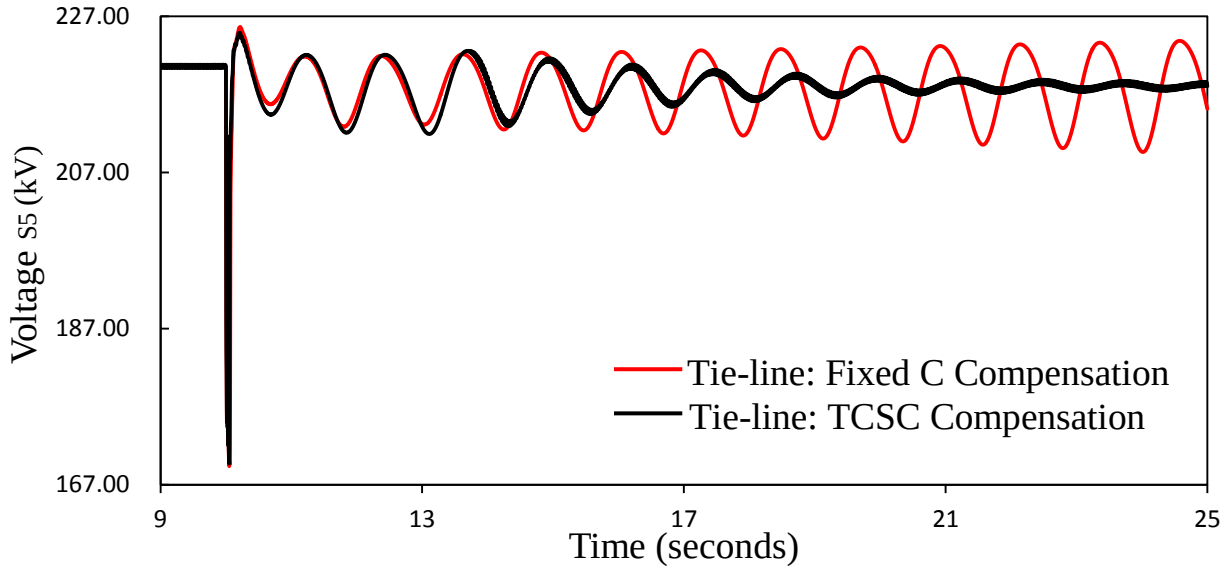

Figure 4.22: Continued.

The following observations are made from examing these figures:

- In the case of fixed capacitor compensation, the SaskPower integrated system loses its stability. Severe growing oscillations can be observed in transmission line real power flows, generator relative load angles and speeds and system bus voltages. On the contrary, in the case of the TCSC compensation scheme, SaskPower system stability is maintained after such a severe disturbance.

- As a result of losing the connection with Manitoba grid, more power is transmitted from the North system to the South system through the tie-line, which is evident from the increase in the real power flow through the tie-line as shown in Figure 4.19.

4.7 Case Study V: Three-Cycle, Three-Phase Fault on Transmission Line S_4-S_5 with Line Tripping

It can be seen from Figures 3.12 and 4.23, transmission line S_4-S_5 is a major line in SaskPower South system that delivers 97.15 MW to load Ld_{S5}. Selected transmission line real power flows, generator angles and speeds, and system bus voltages during and after fault clearing (line tripping) are illustrated in Figures 4.24 to 4.27 respectively. Generator G_{N5} load angle, measured with respect to generator G_{S4} load angle (δ_{N5S4}) is selected as the TCSC supplemental control stabilizing signal as it provides a noticeable improvement in the damping

of the power system oscillations. The transfer function of the TCSC supplemental control is given by

$$G_{\delta_{N5S4}}(S) = 0.125\frac{10}{(S+10)}\frac{S}{(S+1)} \tag{4.5}$$

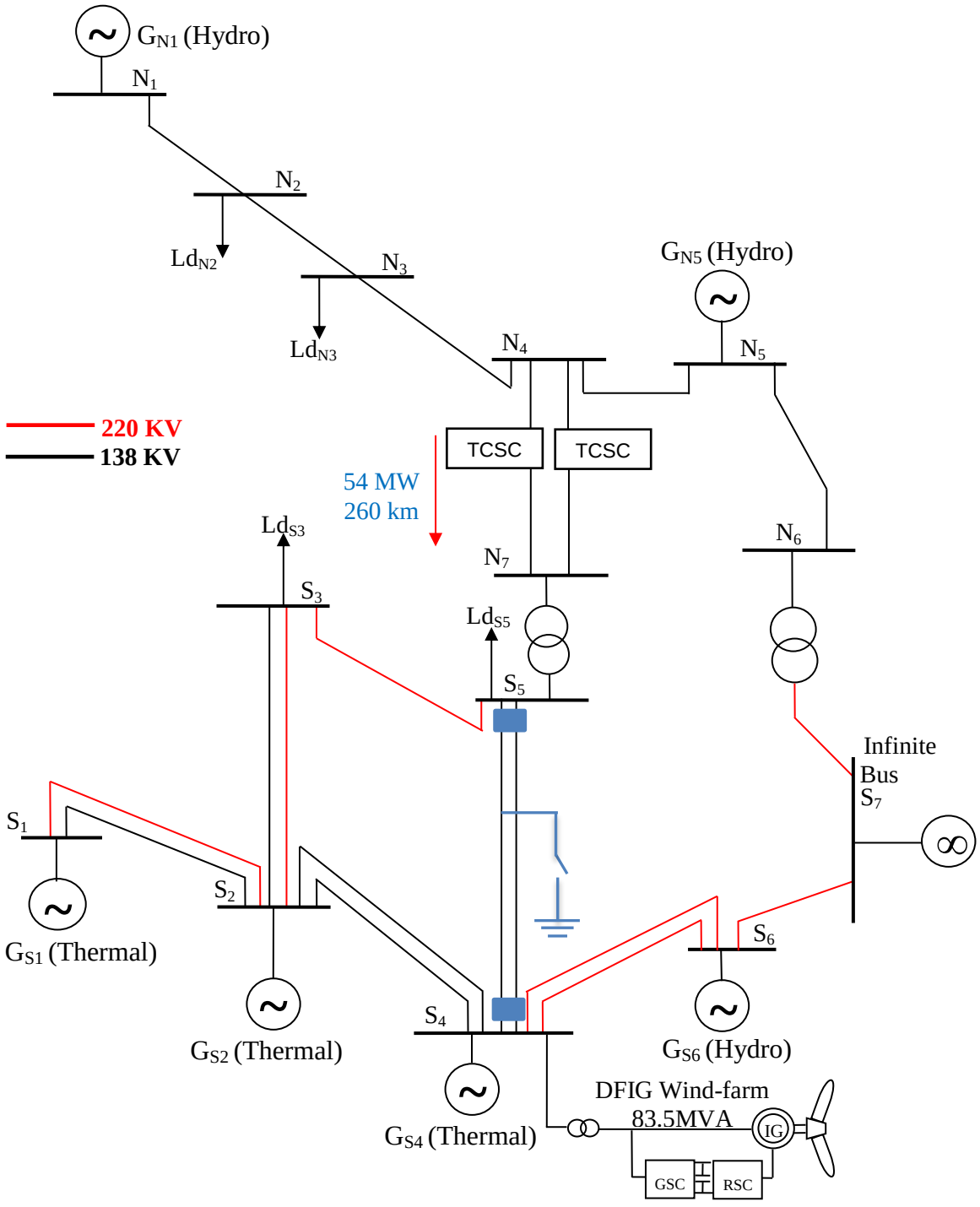

Figure 4.23: Case Study V: three-cycle, three-phase fault on transmission line S_5-S_4 with line tripping.

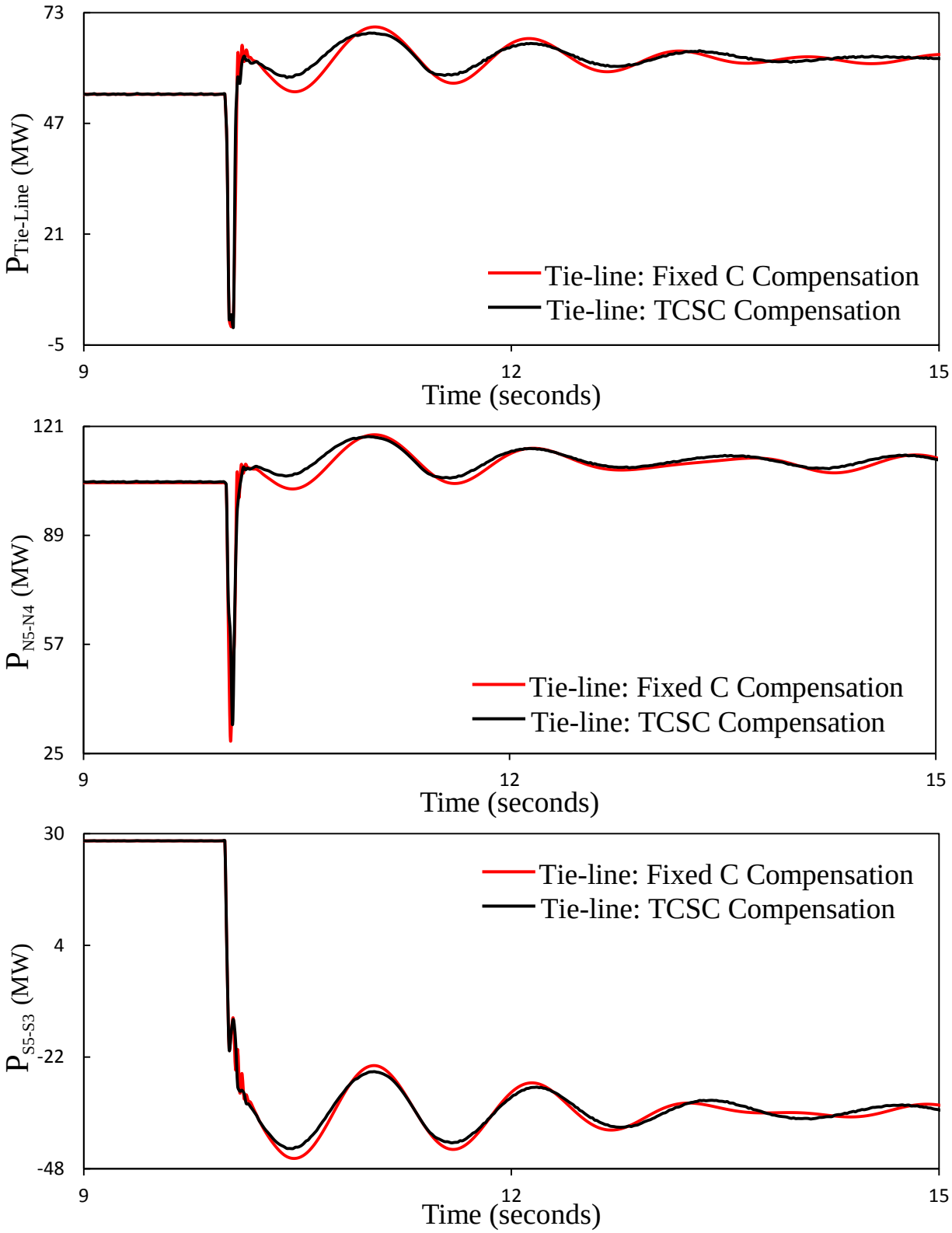

Figure 4.24: Transmission line real power flows during and after clearing a three-cycle, three-phase fault on transmission line S_5-S_4 (case study V).

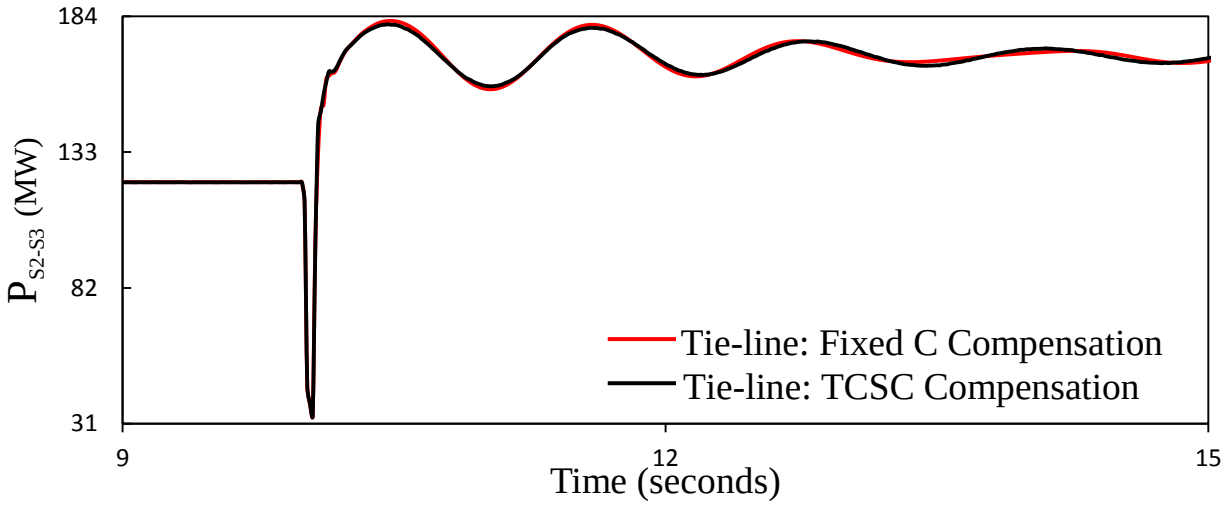

Figure 4.24: Continued.

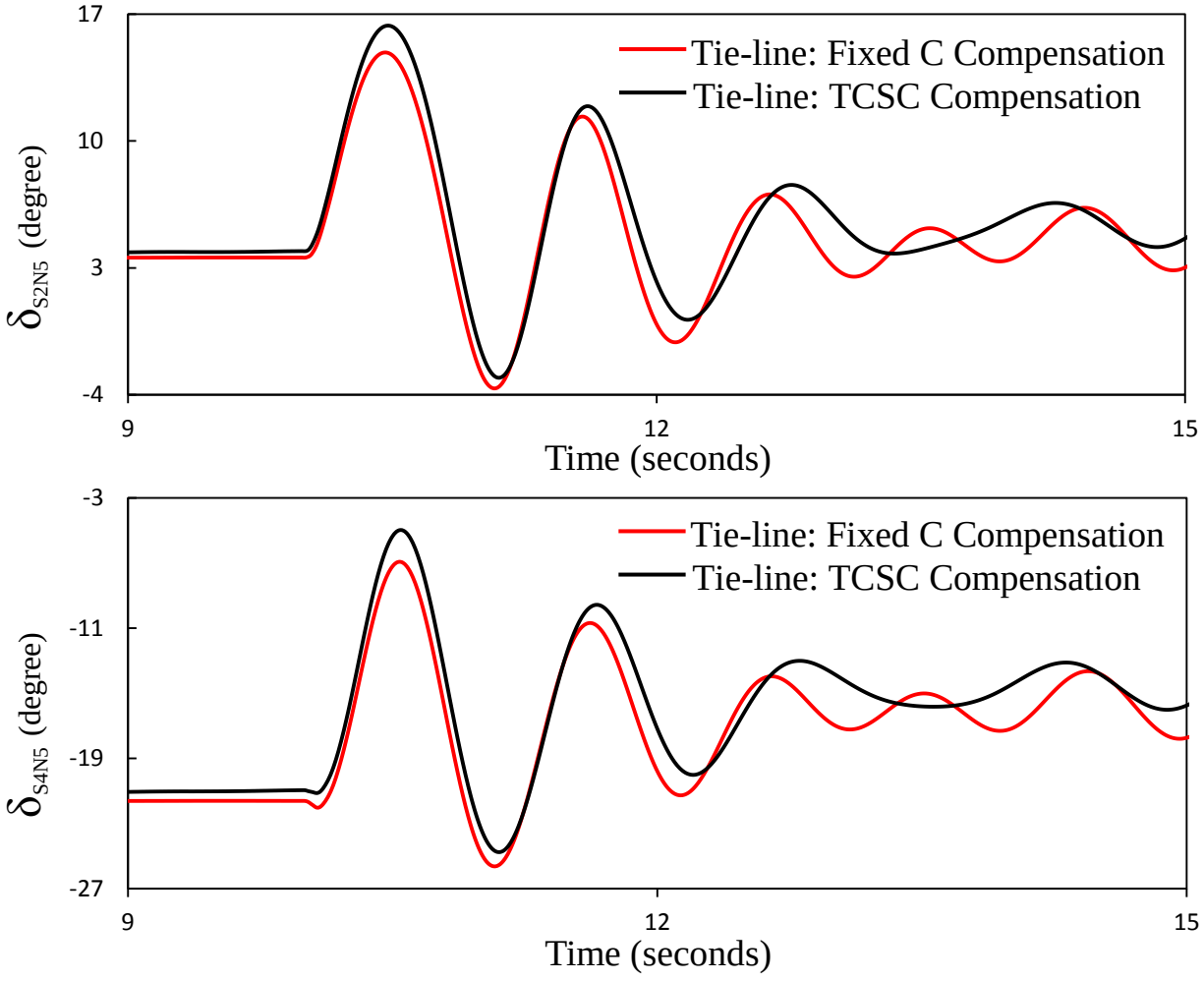

Figure 4.25: Generator load angles measured with respect to generator G_{N5} load angle, during and after clearing a three-cycle, three-phase fault on transmission line S_5-S_4 (case study V).

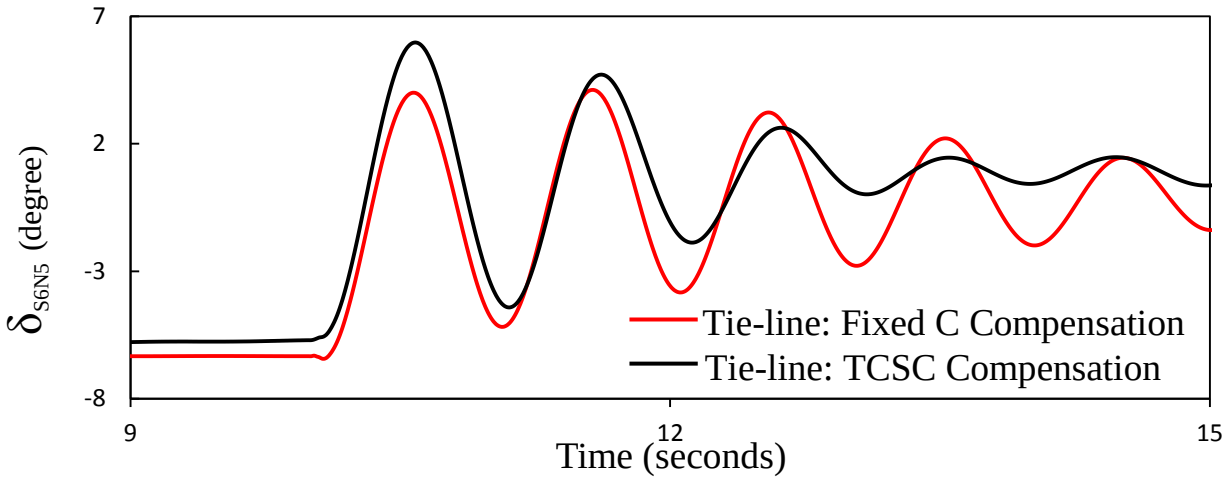

Figure 4.25: Continued.

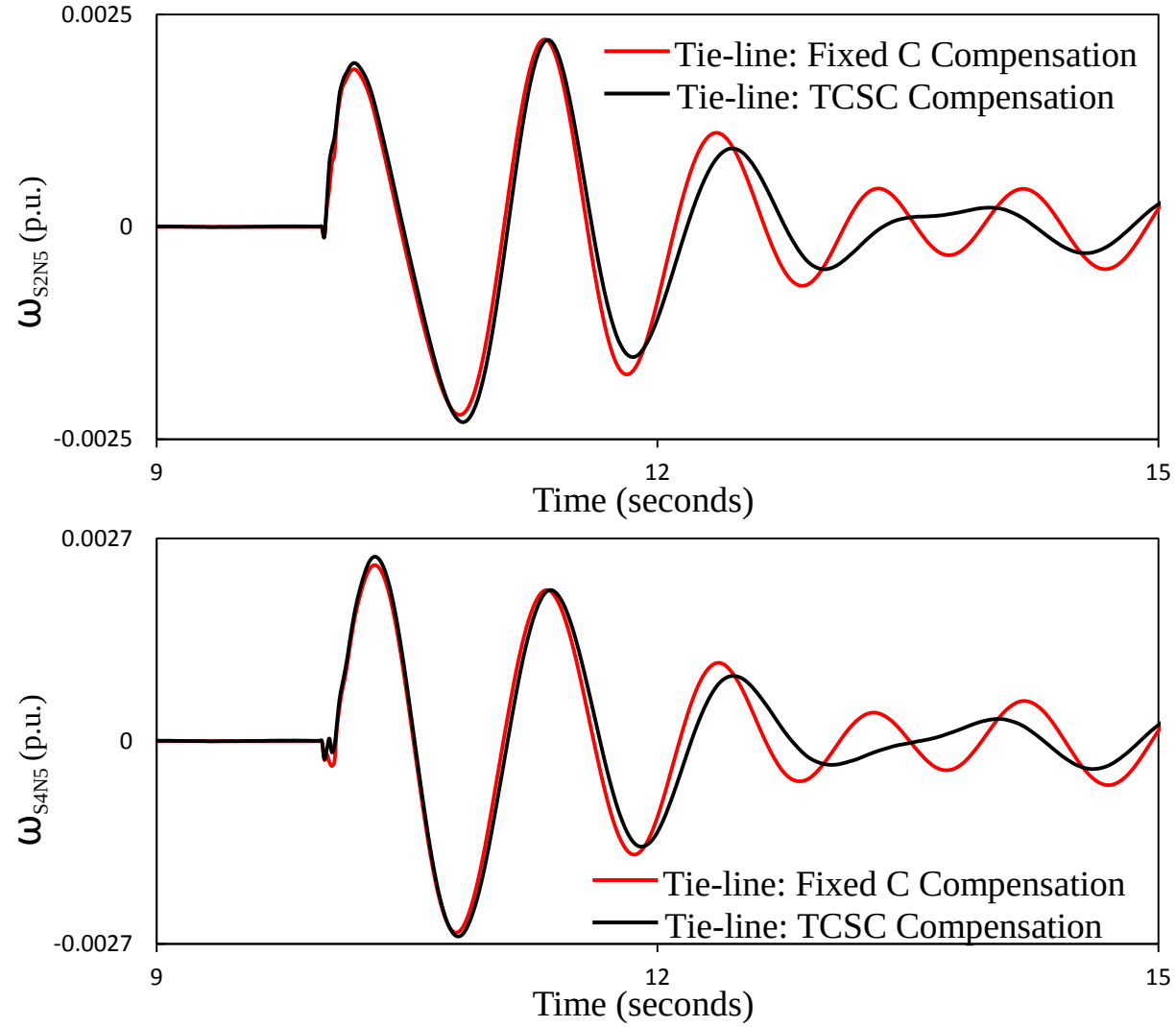

Figure 4.26: Generator speeds measured with respect to generator G_{N5} speed, during and after clearing a three-cycle, three-phase fault on transmission line S_5-S_4 (case study V).

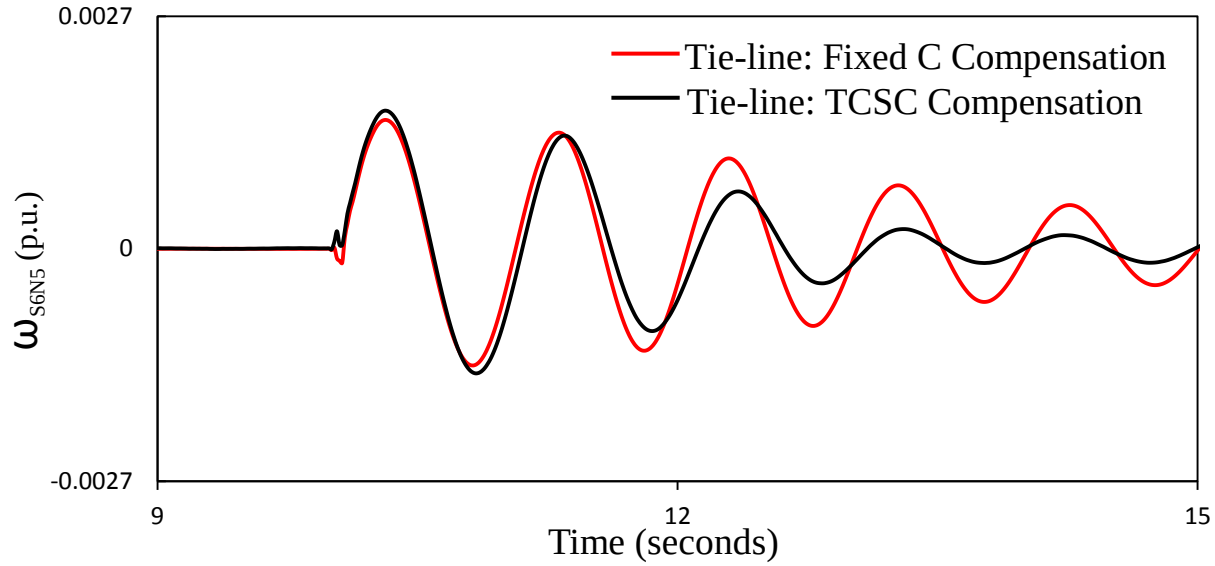

Figure 4.26: Continued.

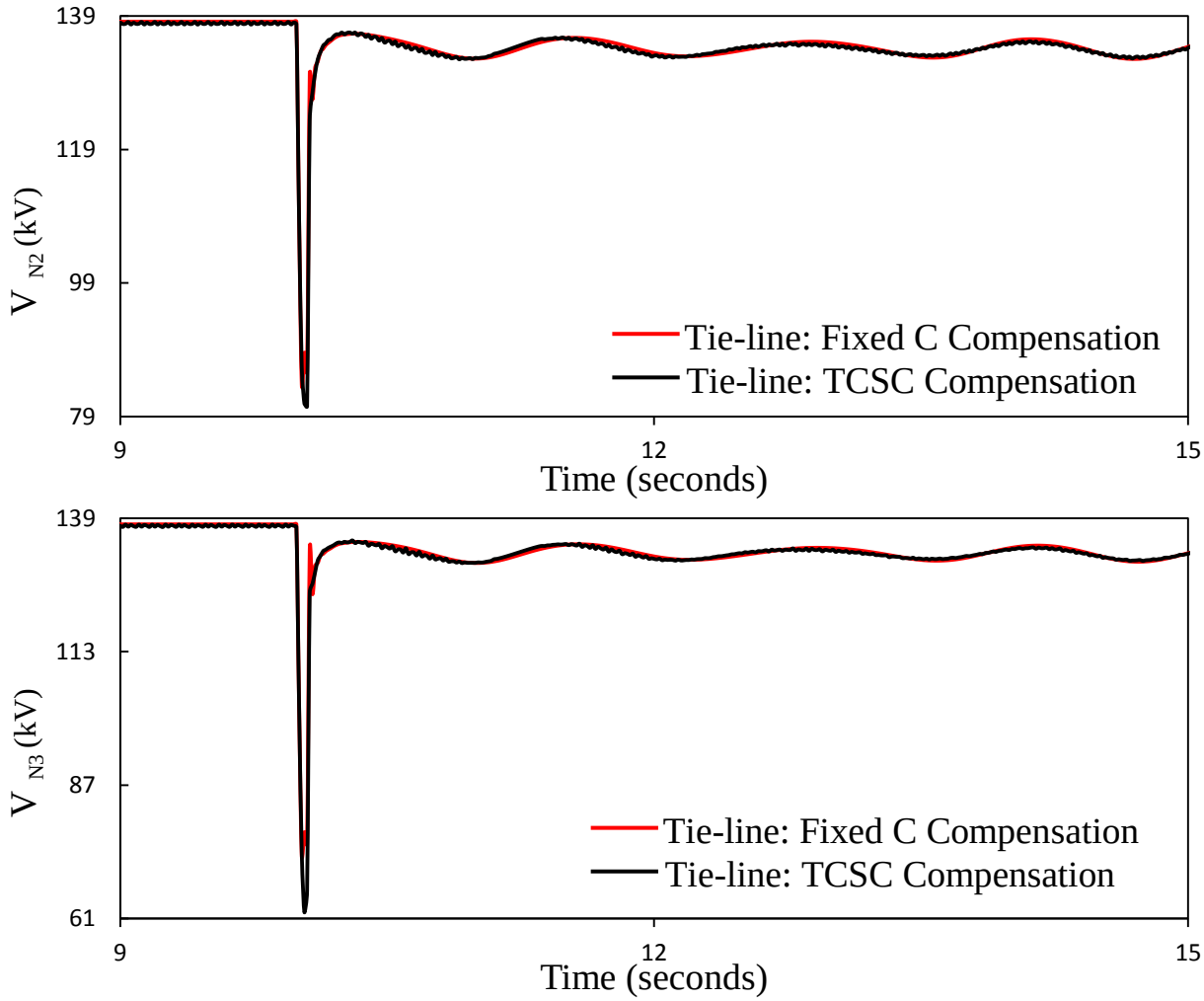

Figure 4.27: System bus voltages during and after clearing a three-cycle, three-phase fault on transmission line S_5-S_4 (case study V).

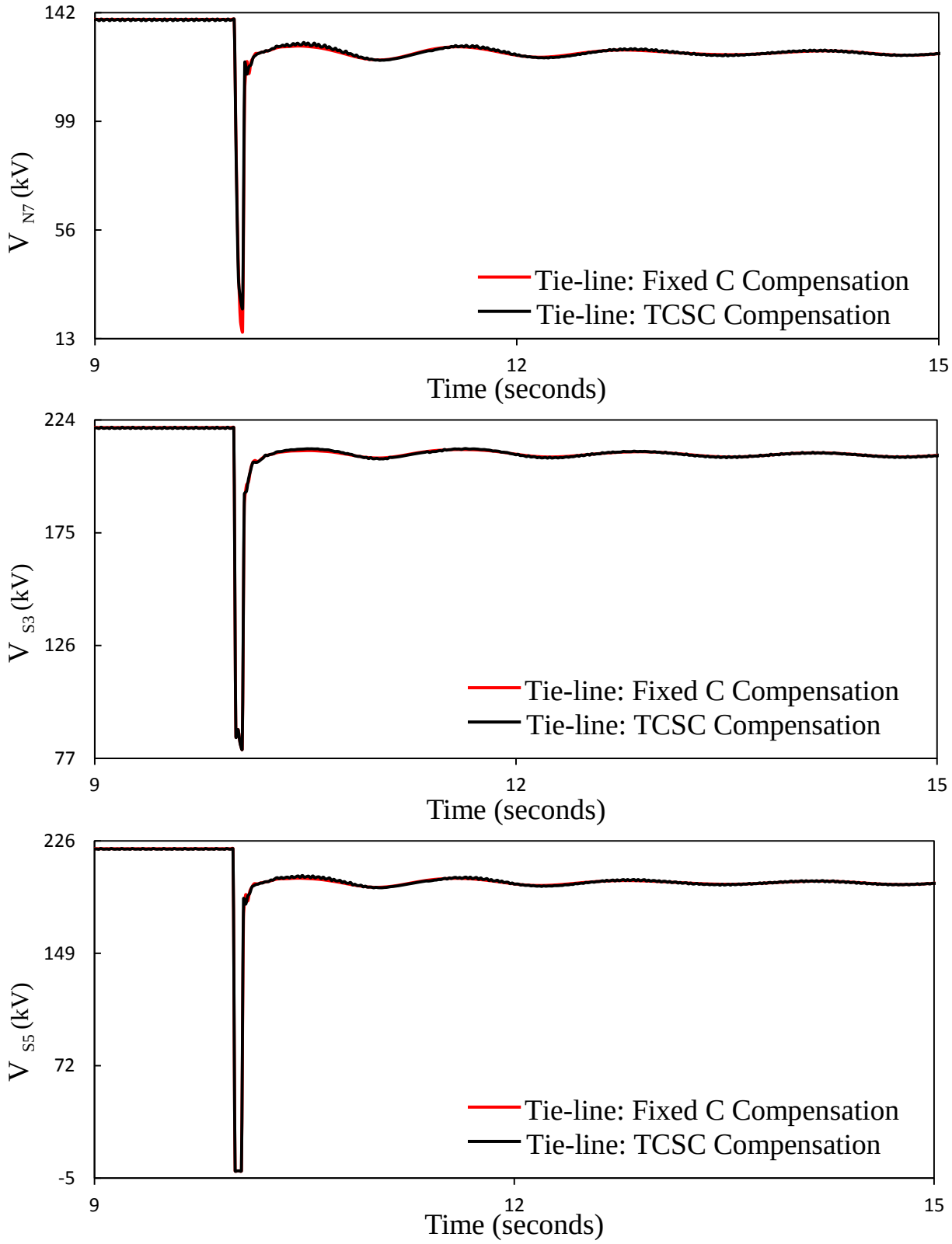

Figure 4.27: Continued.

The following observations can be made from these figures:

- As shown in Figure 3.12, load Ld_{S5} at bus S_5 is supplied by the power flow from transmission line S_4-S_5 and the TCSC-compensated tie-line. Transmission line S_5-S_3 delivers 27.41 MW from bus S_5 to load Ld_{S3}. After the fault clearing (tripping transmission line S_5-S_4), the real power flow on line S_3-S_5 is reversed, which is shown in Figure 4.24, in order to supply load Ld_{S5} at bus S_5, and more power on line S_2-S_3 is transmitted to compensate for the loss of the power transmitted on line S_4-S_5.

- In the case of the TCSC compensation scheme, Figure 4.24 shows that the first and subsequent swings are well-damped but the post-contingency oscillations are not significantly improved compared with the case of fixed capacitor compensation.

- It is evident that the post-contingency oscillations are well-damped in the generator relative load angles and speeds in the case of the TCSC supplemental compensation scheme.

4.8 Summary

In this chapter, the effectiveness of the hybrid three-phase TCSC compensation scheme in damping power system oscillations resulting from clearing system faults is investigated through several case studies of time-domain simulations. In this context, the TCSC supplemental controller structures and their stabilizing signals on the damping of power system oscillations with various fault locations and different types of faults are explored. The main conclusions drawn from the results of these studies are presented in the next chapter.

Chapter 5

SUMMARY AND CONCLUSIONS

5.1 Summary

Connecting the SaskPower North and South systems would bring sufficient technical and economic benefits. The interconnection would increase the power exchange between the North and the South systems as well as between the SaskPower and Manitoba grids. This tie-line would also improve the reliability of the entire SaskPower grid because it can prevent multiple outages through emergency power exchange.

The main objective of this research work was to investigate the dynamic performance of a proposed 260 km, 138 kV double-circuit tie-line incorporating a hybrid TCSC compensation scheme that would connect SaskPower North and South systems. The potential problems that might arise due to such an interconnection, namely power flow control and low-frequency oscillations should be studied and quantified and a proposed feasible solution should be established. In this context, the effectiveness of a proposed Power Oscillation Damping (POD) controller incorporated in hybrid TCSC compensation scheme in damping power system oscillations in the tie-line is investigated through several time-domain simulation studies on a test system that reasonably represent the SaskPower North system and the Northern part of its South system. Although SaskPower real system data were not used, it is believed that the observations and conclusions drawn from this research work should be very similar to those that would have been reached with real SaskPower system data. This is due to the fact that typical generator and transmission line data are used in the studies conducted in this thesis.

In Chapter 1, the fundamental benefits and the problems arising from grid interconnections are introduced. A brief introduction to the SaskPower North and South systems and the objectives of the research are also presented in this chapter.

In Chapter 2, the system used in the investigations conducted in this thesis is described and the detailed dynamic models of its individual components are also presented. At the end of this chapter, the results of the digital time-domain simulations of a case study using the system during a three-phase fault are presented.

In Chapter 3, a comprehensive description of the TCSC, its three modes of operation, as well as the analysis of its net reactance are presented. Modeling the hybrid TCSC compensation scheme in the ElectroMagnetic Transient Program (EMTP-RV) is also discussed in this chapter. The load flow profiles of the SaskPower North and South systems as well as the interconnected North and South systems (with an AC interconnection incorporating a hybrid TCSC compensation scheme) are examined and important conclusions are drawn.

In Chapter 4, the effectiveness of the supplemental controller of the hybrid TCSC compensation scheme in damping power system oscillations is demonstrated through time-domain simulation case studies.

5.2 Conclusions

The studies conducted in this thesis yield the following conclusions:

1. Either HVAC or HVDC tie-lines can be used to interconnect the SaskPower North and South systems. As AC is the dominant mode of generation, transmission, and distribution, an AC link is a more natural method to interconnect existing AC power systems. Moreover, the option of an AC link is technically feasible [8].

2. The inter-area low-frequency oscillations observed in the SaskPower integrated system have a frequency in the range of 0.65 to 0.9 Hz.

3. The low-frequency oscillations are well-damped in the case of a TCSC compensation scheme with the control design technique applied in the TCSC supplemental controller in this thesis, and by performing multiple time-domain simulations,.

4. Generator G_{S4} and generator G_{S6} load angles, measured with respect to generator G_{N5} load angle (δ_{N5S4} and δ_{N5S6}) are found to be appropriate stabilizing signals for the TCSC supplemental controller.

5. Adequate improvement in the damping power system oscillations is achieved in most of the case studies with the phase-compensation-type transfer functions for the TCSC supplemental controller,.

6. In the case study in which the SaskPower interconnected system loses connection with the Manitoba grid, the system stability is maintained with the tie-line incorporating the TCSC compensation scheme. On the contrary, the system loses stability with the interconnection compensated with fixed capacitor banks.

7. In severe cases (i.e., SaskPower North system loses connection with the Manitoba grid), system stability cannot be maintained even with the TCSC compensation scheme incorporated in the tie-line.

REFERENCES

[1] *Multi Dimensional Issues in International Electric Power Grid Interconnections.* Department of Economic and Social Affairs . Division of Sustainable Development. United Nations. New York. 2005

[2] M. Klein, G.J. Rogers and P. Kunder, "A Fundamental Study of Inter-Area Oscillations in Power System", IEEE Transactions on Power Systems, Vol. 6, No. 3, August 1991, pp. 914-921.

[3] S. Dodds, B. Railing, K. Akman, B. Jacobson, T. Worzyk and B. Nilsson, "HVDC VSC (HVDC light) transmission - operating experiences," CIGRE 2010, Paris, France, paper No. B4-203-2010.

[4] G. Asplund, K. Eriksson and K. Svensson, "HVDC Light-DC transmission based on voltage sourced converters," 1998, ABB Review, No. 1, pp. 4-9.

[5] E. Acha, *FACTS: modeling and simulation in power networks*, Chichester, Wiley, 2004.

[6] J. Arrillaga, *High voltage direct currect transmission*, 2nd edition, London, Institution of Electrical Engineers, 1998.

[7] F. Schettler, H. Huang and N. Christl, "HVDC transmission systems using voltage sourced converters- Design and application," Proceedings of the IEEE Power Engineering Society Transmission and Distribution Conference, Seattle, WA, United States, Institute of Electrical and Electronics Engineers Inc, 2000, Vol. 2, pp. 715-720.

[8] J. Wu, J. Wen, H. Sun and S. Cheng, "Feasibility Study of Segmenting Large Power System Interconnections With AC Link Using Energy Storage Technology," IEEE Transactions on Power Systems, Vol. 27, No. 3, August 2012, pp. 1245-1252.

[9] P.M. Anderson and R.G. Farmer, *Series Compensation of Power Systems*, PUBLH!, 1996.

[10] P. Kunder, *Power System Stability and Control*, New York, McGraw-Hill, 1994.

[11] R. Billinton, M. Fotuhi-Firuzabad and S.O. Faried, "Power System Reliability Enhancement using a Thyristor Controlled Series Capacitor," IEEE Transactions on Power Systems, Vol. 14, No. 1, February 1999, pp. 369-374.

[12] P.M. Anderson, B.L. Agrawal and J.E. Van Ness, *Subsynchronous Resonance in Power Systems*, IEEE Press, 1990.

[13] IEEE Subsynchronous Resonance Working Group, "Terms, definitions and symbols for subsynchronous oscillaitons [power systems]," *IEEE Transactions on Power Apparatus and Systems*, Vol. PAS-104, No. 6, June 1985, pp. 1325-1334.

[14] G.J. Rogers, *Power System Oscillation*, Massachusetts, Kluwer Academic Publishers, 2000, pp. 1-6.

[15] Y.H. Song and A.T. Johns, *Flexible AC Transmission Systems (FACTS)*, London, Institution of Electrical Engineers, 1999.

[16] N.G. Hingorani and L. Gyugyi, *Understanding FACTS: Concepts and Technology of Flexible AC Transmission Systems*, New York, IEEE Press, 2000.

[17] C. Gama, "Brazilian North-South Interconnection Control-Application and Operating Experience with a TCSC," Proceedings of the 1999 IEEE PES Summer meeting, Edmonton, Alberta, Canada, July 18-22, 1999, Vol. 2, pp. 1103-1108.

[18] C. Gama and L. Angquist, "Commissioning and Operative Experience of TCSC for Damping Power Oscillation in the Brazilian North-South Interconnection," CIGRE, Session 2000, Paris, France, paper No. 14-104.

[19] H.A. Othman and L. Angquist, "Analytical Modeling of Thyristor-Controlled Series Capacitors for SSR Studies," IEEE Transactions on Power Systems, Vol. 11, No. 1, February 1996, pp. 119-127.

[20] B.K. Perkins and M.R. Iravani, "Dynamic Modeling of a TCSC with Application to SSR Analysis," IEEE Transactions on Power Systems, Vol. 12, No. 4, pp. 1619-1625, 1997.

[21] R.J. Piwko, C.W. Wegner, S.J. Kinney and J.D. Eden, "Subsynchronous Resonance Performance Tests of the Slatt Thyristor-Controlled Series Capacitor," IEEE Transactions on Power Delivery, Vol. 11, No. 2, April 1996, pp. 1112-1119.

[22] W. Zhu, R. Spee, R.R. Mohler, G.C. Alexander, W.A. Mittelstadt and D. Maratukulam, "An EMTP Study of SSR Mitigation Using the Thyristor-Controlled Series Capacitor," IEEE Transactions on Power Delivery, Vol. 10, No. 3, July 1995, pp. 1479-1485.

[23] N. Kakimoto and A. Phongphanphanee, "Subsynchronous Resonance Damping Control of Thyristor-Controlled Series Capacitor," IEEE Transaction on Power Delivery, Vol. 18, No. 3, July 2003, pp. 1051-1059.

[24] R. Rajaraman, I. Dobson, R.H. Lasseter and Y. Shern, "Computing the Damping of Subsynchronous Oscillations due to a Thyristor Controlled Series Capacitor," IEEE Transactions on Power Delivery, Vol. 11, No. 2, April 1996, pp. 1120-1127.

[25] P. Mattavelli, A.M. Stankovic and G.C. Verghese, "SSR Analysis with Dynamic Phasor Model of Thyristor-Controlled Series Capacitor," IEEE Transactions on Power Systems, Vol. 14, No. 1, February 1999, pp. 200-208.

[26] A. Daneshpooy and A.M. Gole, "Frequency Response of the Thyristor Controlled Series Capacitor," IEEE Transactions on Power Delivery, Vols. 16, No. 1, January 2001, pp. 53-58.

[27] J.F. Hauer, W.A. Mittelstadt, R.J. Piwko, B.L. Damsky and J.D. Eden, "Modulation and SSR Tests Performed on the BPA 500 kV Thyristor Controlled Series Capacitor Unit at Slatt Substation," IEEE Transactions on Power Systems, Vol. 11, No. 2, May 1996, pp. 801-806.

[28] P.S. Dolan, J.R. Smith and W.A. Mittelstadt, "A Study of TCSC Optimal Damping Control Parameters for Different Operating Conditions," IEEE Transactions on Power Systems, Vol. 10, No. 4, November 1995, pp. 1972-1978.

[29] J. Urbanek, R.J. Piwko, E.V. Larsen, B.L. Damsky, B.C. Furumasu and W.A. Mittelstadt, "Thyristor Controlled Series Compensation Prototype Installation at the Slatt 500 kV Substation," IEEE Transactions on Power Delivery, Vol. 8, No. 3, July 1993, pp. 1460-1469.

[30] S. Nyati, C.A. Wegner, R.W. Delmerico, R.J. Piwko, D.H. Baker and A. Edris, "Effectiveness of Thyristor Controlled Series Capacitor in Enhancing Power System Dynamics: An Analog Simulator Study," IEEE Transactions on Power Delivery, Vol. 9, No. 2, April 1994, pp. 1018-1027.

[31] Y.Y. Hsu and T.S. Luor, "Damping of Power System Oscillations Using Adaptive Thyristor-Controlled Series Compensators Tuned by Artificial Neural Networks," IEE Proceedings, Generation, Transmission and Distribution, Vol. 146, No. 2, March 1999, pp. 137-142.

[32] X.X. Zhou and J. Liang, "Nonlinear Adaptive Control of TCSC to Improve the Performance of Power Systems," IEE Proceedings, Generation, Transmission and Distribution, Vol. 146, No. 3, May 1999, pp. 301-305.

[33] S. Pan, "Damping Power System Oscillations Using a Phase Imbalanced Hybrid Series Capacitive Compensation Scheme," M.Sc. Thesis, Department of Electrical and Computer Engineering, University of Saskatchewan, Saskatoon, October 2010.

[34] Y. Yu, *Electric Power System Dynamics*, New York, Academic Press, 1983.

[35] O.I. Elgerd, *Electrical Energy Systems Theory*, McGraw-Hill, 1971.

[36] L. Wang and K-H Wang, "Dynamic Stability Analysis of a DFIG-Based Offshore Wind Farm Connected to a Power Grid Through an HVDC Link," IEEE Transactions on Power Systems, Vol. 26, No. 3, August 2011, pp. 1501-1510.

[37] Y. Lei, A. Mullane, G. Lightbody and R. Yacamini, "Modeling of the Wind Turbine with a Double Fed Induction Generator for Grid Integration Studies," IEEE Transactions on Energy Conversion, Vol. 21, No. 1, March 2006, pp. 257-264.

[38] C. Zhu, L. Fan and M. Hu, "Control and Analysis of DFIG-Based Wind Turbines in a Series Compensated Network for SSR Damping," 2010 IEEE Power and Energy Society General Meeting, Minneapolis, MN, July 25-29, 2010, Digital Object Identifier: 10.1109/PES.2010.5590091.

[39] W. Qiao, "Dynamic Modeling and Control of Doubly Fed Induction Generators Driven by Wind Turbines," IEEE Power Systems Conference and Exposition, PSCE '09, Seattle, WA, March 2009, pp. 1-8.

[40] L. Fan, R. Kavasseri, Z. Lee Miao and C. Zhu, "Modeling of DFIG-Based Wind Farms for SSR Analysis," IEEE Transactions on Power Delivery, Vol. 25, No. 4, October 2010, pp. 2073-2082.

[41] J. Zhang, "Power System Dynamic Enhancement Using Phase Imbalance Series Capacitive Compensation and Doubly Fed Induction Generator-Based Wind Farms," M.Sc. Thesis, Department of Electrical and Computer Engineering, University of Saskatchewan, Sasktoon, April 2013.

[42] M.A. Poller, "Doubly-fed induction machine models for stability assessment of wind farms," in *Power Technology Conference*, Bologna, Italy, June 23-26, 2003, pp. 1-6.

[43] A.D. Hansen and G. Michalke, "Multi-pole permanent magnet synchronous generator wind turbine's grid support capability in uninterrupted operation during grid faults," *IET Renewable Power Generation*, Vol. 3, Issue 3, September 2009.

[44] M. Lindholm, "Doubly fed drivers for variable speed wind turbines-- a 40 kW laboratory setup," PhD thesis, Technical University of Denmark, Kongens Lyngby, Denmark, 2004.

[45] L. Xu, L. Yao and C. Sasse, "Grid Integration of Large DFIG-Based Wind Farms Using VSC Transmission," *IEEE Transactions on Power Systems*, Vol. 22, No. 3, August 2007, pp. 976-984.

[46] W. Qiao, G. Harley and G.K. Venayamoorthy, "Coordinated Reactive Power Control of a Large Wind Farm and a STATCOM Using Heuristic Dynamic Programming," *IEEE Transactions on Energy Conversion*, Vol. 24, No. 2, June 2009, pp. 493-503.

[47] A.D. Hansen, G. Michalke, P. Sorensen, T. Lund and F. Iov, "Co-ordinated Voltage Control of DFIG Wind Turbines in Uninterrupted Operation during Grid Faults," *Wind Energy*, Vol. 10, No. 1, January/February 2007, pp. 51-68.

[48] P.M. Anderson and A.A. Fouad, *Power System Control and Stability*, IEEE Press, 1994.

[49] K. Kabiri, S. Henschel and H.W. Dommel, "Resistive Behavior of Thyristor-Controlled Series Capacitors at Subsynchronous Frequencies," IEEE Transactions on Power Delivery, Vol. 19, No. 1, January 2004, pp. 374-379.

[50] R.M. Mathur and R.K. Varma, *Thyristor-Based FACTS Controller for Electrical Transmission System*, Piscataway, NJ, IEEE, 2002.

[51] H. Xie and L. Ängquist, "Synchronous Voltage Reversal control of TCSC-impact on SSR conditions," Proceedings of the Nordic Workshop on Power and Industrial Electronics (NORPIE), 2004.

[52] L. Ängquist, "Synchronous Voltage Reversal Control of Thyristor Controlled Series Capacitor," Royal Institute of Technology, TRITA-ETS-2002-07, ISSN 1650-674X.

[53] L. Ängquist and C. Gama, "Damping Algorithm based on Phasor Estimation," Proceedings of the IEEE Power Engineering Socirty Winter Meeting, Columbus, Ohio, January 28-February 1, 2001, Vol. 3, pp. 1160-1165.

[54] D. Rai, S.O. Faried, G. Ramakrishna and A. Edris, "Damping Inter-Area Oscillations using Phase Imbalanced Series Compensation Schemes," IEEE Transactions on Power Systems, Vol. 26, No. 3, August 2011, pp. 1753-1761.

[55] D. Rai, "Power System Dynamics Enhancement Through FACTS Devices and Adaptive Control," Ph. D. Thesis, Department of Electrical and Computer Engineering, University of Saskatchewan, Saskatoon, 2012.

[56] A.M. Gole, S. Filizadeh, R.W. Menzies and P.L. Wilson, "Optimization-enabled Electromagnetic Transient Simulation," IEEE Transactions on Power Delivery, Vol. 20, No. 1, January 2005, pp. 512-518.

[57] A.M. Gole, S. Filizadeh and P.L. Wilson, "Inclusion of Robustness into Design using Optimizaiton-enabled Transient Simulation," IEEE Transactions on Power Delivery, Vol. 20, No. 3, July 2005, pp. 1991-1997.

[58] R. Grünbaum and Jacques Pernot, "Thyristor Controlled Series Compensation: A State of the Art Approach for Optimization of Transmission over Power Links," ABB online website: [http://www05.abb.com/global/scot/scot221.nsf/veritydisplay/d578889d05b3ba01c1256fda003b4cff/$File/SEE_FIILE2001_TCSC.pdf].

[59] N. Yang, Q. Liu and J. McCalley, "TCSC Controller Design for Interarea Oscillations," IEEE Transactions on Power Systems, Vol. 13, No. 4, November 1998, pp. 1304-1309.

[60] X. Chen, N. Pahalawaththa, U. Annakkage and C. Kumbe, "Output Feedback TCSC Controllers to Improve Damping of Meshed Multi-Machine Power Systems," IEE Proceedings, Generation, Transmission and Distribution, Vol. 44, No. 3, May 1997, pp. 243-248.

[61] J. Machowski, S. Robak and J. Bialek, "Damping of Power Swings by Optimal Control of Series Compensators," Proceedings of the 10th International Conference on Power System Automation and Control *PSAC'97*, Bled, Slovenia, October 1-3, 1997, pp. 39-44.

[62] J.F. Hauer, M.K. Donnelly, W.A. Mittelstadt, W. Litzenberger and D.J. Maratukulam, "Information Functions and Architecture for Networked Monitoring of Wide Area Power System Dynamics: Experience with the Evolving Western System Dynamic Information Network," Proceedings of the Sixth Symposium of Specialists on Electric Operational and Expansion Planning (VI SEPOPE), Bahia, Brazil, May 24-29, 1998.

[63] B. Bhargava and A. Salazar, "Use of Synchronized Phasor Measurement System for Monitoring Power System Stability and System Dynamics in Real-Time," Proceedings of the 2008 IEEE PES GM, Pittsburgh, PA, July 20-24, 2008, pp. 1-8.

[64] H. Ni, G.T. Heydt and L. Mili, "Power System Stability Agents using Robust Wide Area Control," IEEE Transactions on Power Systems, Vol. 17, No. 4, November 2002, pp. 1123-1131.

[65] X. Xie, J. Xiao, C. Lu and Y. Han, "Wide-Area Stability Control for Damping Interarea Oscillations of Interconnected Power Systems," IEE Proceedings, Generation, Transmission and Distribution, Vol. 153, No. 5, September 2006, pp. 507-514.

[66] C.W. Taylor, D.E. Erickson, K.E. Martin, R.E. Wilson and V. Venkatasubramanian, "WACS-Wide-Area Stability and Voltage Control System: R&D and Online Demonstration," Proceedings of IEEE, Vol. 93, No. 5, May 2005, pp. 892-906.

[67] X. Zhou and J. Liang, "Overview of Control Scheme for TCSC to Enhance the Stability of Power Systems," IEE Proceedings, Generation, Transmission and Distribution, Vol. 146, No. 2, March 1999, pp. 125-130.

APPENDIX A

DATA OF THE MODELED SYSTEM

A.1 Synchronous Generators

Table A. 1: Synchronous generator data.

	G_{N1}	G_{N5}	G_{S1}	G_{S2}	G_{S4}	G_{S6}
Rating, MVA	25	231.6	192	147.1	192	231.6
Rated voltage, kV	13.2	13.8	18	15.5	18	13.8
Armature resistance, r_a, p.u.	0.005	0.005	0.002	0.002	0.002	0.005
Leakage reactance, x_l, p.u.	0.18	0.18	0.184	0.184	0.184	0.18
Direct-axis synchronous reactance, x_d, p.u.	1.18	1.18	2.03	2.03	2.03	1.18
Quadrature-axis synchronous reactance, x_q, p.u.	0.78	0.78	1.97	1.97	1.97	0.78
Direct-axis transient reactance, $x_d^{'}$, p.u.	0.295	0.295	0.309	0.309	0.309	0.295
Quadrature-axis transient reactance, $x_q^{'}$, p.u.	0.2868	0.2868	0.471	0.471	0.471	0.2868
Direct-axis subtransient reactance, $x_d^{''}$, p.u.	0.2362	0.2362	0.225	0.225	0.225	0.2362
Quadrature-axis subtransient reactance, $x_q^{''}$, p.u.	N/A	N/A	0.225	0.225	0.225	N/A
Direct-axis transient open-circuit time constant, $T^{'}_{d0}$, s	3.996	3.996	7.32	7.32	7.32	3.996
Quadrature-axis transient open-circuit time constant, $T^{'}_{q0}$, s	0.0484	0.0484	0.67	0.67	0.67	0.0484
Direct-axis subtransient open-circuit time constant, $T^{''}_{d0}$, s	0.02972	0.02972	0.022	0.022	0.022	0.02972
Quadrature-axis subtransient open-circuit time constant, $T^{''}_{q0}$, s	N/A	N/A	0.032	0.032	0.032	N/A
Zero-sequence reactance, x_0, p.u.	0.18	0.18	0.184	0.184	0.184	0.18
Inertia constant, H, s	4.5	3.5	4.15	4.15	4.15	3.5

A.2 Transformers

Table A. 2: Transformer data.

	T_{N1}	T_{N5}	T_{S1}	T_{S2}	T_{S4}	T_{S6}	$T_{WindFarm}$
Rating, MVA	25	250	200	150	200	250	82.5
Rated voltage, kV	13.2/138	13.8/138	18/220	15.5/220	18/220	13.8/220	34.5/220
Resistance, r_T, p.u.	0.002	0.002	0.002	0.002	0.002	0.002	0.005
Leakage reactance, x_T, p.u.	0.12	0.12	0.12	0.12	0.12	0.12	0.12

A.3 Transmission Lines

Table A. 3: Transmission line data.

	138 kV Voltage Level	220 kV Voltage Level
$R_{T.L.}$, Ω/km	0.13047	0.093
$L_{T.L.}$, Ω/km	0.4847	0.501144
$C_{T.L.}$, µS/km	3.3679	3.338448

A.4 System Loads

Table A. 4: System load data.

	System Loads, MVA
Ld_{N2}	32+ *j* 24
Ld_{N3}	28+ *j* 21
Ld_{S1}	115+ *j* 86
Ld_{S2}	50+ *j* 37
Ld_{S3}	150+ *j* 50
Ld_{S4}	85+ *j* 64
Ld_{S5}	120+ *j* 60
Ld_{S6}	55+ *j* 41

A.5 Excitation Systems

Table A. 5: Excitation system data.

$K_A = 2$	$K_E = 1.0$
$K_{FE} = 0.03$	$T_A = 0.04$ s
$T_{FE} = 1.0$ s	$T_E = 0.01$ s
Lim_max = 5 p.u.	*Lim_min* = -5 p.u.

A.6 Three-Phase TCSC Data

Table A. 6: TCSC data.

$K_P = 0.5$	$K_I = 5$
$C_{TCSC} = 125.5\ \mu F$	$L_{TCSC} = 8.97\ mH$